



Title	Highly reliable Cu particles sinter joining for die-attach of next generation power devices
Author(s)	高, 悦
Citation	大阪大学, 2019, 博士論文
Version Type	VoR
URL	<a href="https://doi.org/10.18910/73557">https://doi.org/10.18910/73557</a>
rights	
Note	

*The University of Osaka Institutional Knowledge Archive : OUKA*

<https://ir.library.osaka-u.ac.jp/>

The University of Osaka

Doctoral Dissertation

**Highly reliable Cu particles sinter joining for die-attach of next generation power devices**

**Yue Gao**

July 2019

Department of Adaptive Machine Systems  
Graduate school of Engineering,  
Osaka University,



# **Highly reliable Cu particles sinter joining for die-attach of next generation power devices**

## **Abstract**

Next generation power devices based on wide gap band (WBG) semiconductor materials, such as SiC, GaN, GaO, diamond and soon, have attract much attention because their excellent endurance performance for high working temperature, high current density, high voltage and high operating frequency. In order to realize the promising performance of WBG devices, the assembly and package technology of these chips in devices are also crucial. Among of that, the die-attach materials, which directly bond the WBG chips to substrates, largely determine the servicing performance and long-term reliability of these power devices. The die-attach materials with high operating temperature, high conductivity and high reliability are required in these WBG devices. Metallic particle pastes are considered as the most suitable solution, especially, copper (Cu) particles paste has attracted intensive attention due to its high temperature stability and excellent conductivity with reasonable cost. However, to achieved high reliable sintered Cu joint, high sintering temperature, high assisting pressure and reductive gas protection are necessary. Those complicated sintering condition limited the wide application of Cu sinter joining. Thus, this work aims to achieve highly reliable sintered Cu joints in a relative mild sintering condition. The main topics of this thesis including the improvement in Cu particle synthesis, modification in Cu paste fabrication, and evaluation of the reliability. At first, a simple and large-scale polyol method was utilized to synthesize bimodal Cu particles under air atmosphere. The size, size distribution, and morphology of Cu particles were controlled by the reaction parameters, such as Cu source and additives. Insoluble Cu source was certified to be suitable for the formation of bimodal Cu particles. The insoluble Cu source provided a slow and steady Cu ions supplement for the formation of fresh Cu nuclei. And then the fresh Cu nuclei continuously modified the nucleation and growth of the following Cu particles. In addition, sodium sulfide (Na<sub>2</sub>S) additive had also

controlled the size of Cu particles due to its reduction capability, which accelerated the formation of Cu particles. These results indicate that the Cu source and additives can optimize the particles size and size distribution in the polyol process and open a new way for the formation of metallic particles. However, in this part, the good bonding strength was only achieved in formic acid atmosphere which was not suitable for industrial application.

To endow the Cu paste with the sinterability even at inert atmosphere, reductant additive were added into Cu paste. The shear test results show that the ascorbic acid (AA) as reductant additive could realize the steady sintered Cu joints at 300 °C with inert N<sub>2</sub> protection. AA could endow the Cu paste with self-reduction and self-protection characteristics. The self-reduction characteristic is due to the reduction process of AA, as it reduces the Cu oxide layer on the metal Cu even at room temperature. The self-protection characteristic is due to the decomposition of AA, which prevents further oxidation during the sintering process. These characteristics are beneficial for the sintering of Cu particles and for enhancing the bonding strength of joints. High shear strength of 27.8 MPa were achieved by the improved Cu paste.

The next step was reliability evaluation of sintered Cu joints, Thermal storage test was performance on the sintered Cu joints. In both high temperature storage test and high humidity test, the sintered Cu joints shows good stability in shear strength. However, the Cu oxides was also observed in the aged Cu joints. Those Cu oxides was proved to contribute to the bonding performance. The thermal shock reliability of sintered Cu joints on SiC power device application was also investigated. Silicon carbide (SiC) dummy chips were bonded to DBC substrate and thermal shock test from -40 °C to 250 °C were performed both in the ambient atmosphere and in vacuum. Then, the SiC MOSFETs bonded by sintered Cu joints were evaluated by power cycle test from 25 °C to 200 °C and the thermal conductivity was evaluated by T3ster equipment. The results showed the sintered Cu exhibited extremely high reliability during the thermal shock aging test in ambient atmosphere although inferior reliability was observed in vacuum. This

phenomenon was investigated and explained. And the power cycle test showed no obvious deterioration occurred, which proved the good reliability of sintered Cu joints.



# Table of Contents

<b>Abstract</b> .....	I
<b>Table of Contents</b> .....	V
<b>List of Figures</b> .....	IX
<b>List of Tables</b> .....	XIII
<b>Chapter 1 Research background</b> .....	1
<b>1.1 Development and challenge of power device</b> .....	3
1.1.1 Traditional Si power device .....	3
1.1.2 Wide band gap power device .....	6
1.1.3 Packaging challenge of WBG power device and die-attach materials .....	9
<b>1.2 Overview of die-attach technology for high-temperature application</b> .....	12
1.2.1 High-temperature lead-free solders .....	12
1.2.2 Transient liquid phase bonding process .....	14
1.2.3 Ag stress-migration bonding .....	16
1.2.4 Ag particle sinter joining .....	18
1.2.5 Cu particle sinter joining .....	20
<b>1.3 Motivation of present research</b> .....	23
1.3.1 Preparation of Cu particles .....	24
1.3.2 Development and challenges of sinter Cu joining technology .....	25
<b>1.4 Purpose and scope of the present study</b> .....	27
<b>References</b> .....	29
<b>Chapter 2 One-step synthesis of bimodal Cu particles</b> .....	37
<b>2.1 Introduction</b> .....	39
<b>2.2 Experiments</b> .....	40
2.2.1 Cu particles preparation .....	40

2.2.2	Characterization of Cu particles .....	41
2.2.3	Fabrication and evaluation of Cu joints.....	42
<b>2.3</b>	<b>Results and discussion.....</b>	<b>42</b>
2.3.1	The effect of soluble/insoluble Cu salt on Cu particles.....	42
2.3.2	The effect of Na <sub>2</sub> S agent.....	47
2.3.3	Bonding property of bimodal Cu particles pastes .....	51
<b>2.4</b>	<b>Conclusion.....</b>	<b>55</b>
	<b>Reference.....</b>	<b>57</b>
	<b>Supplementary Materials .....</b>	<b>60</b>
<b>Chapter 3</b>	<b>Realization of high-strength Cu sinter joining by ascorbic acid-treated Cu particle paste.....</b>	<b>63</b>
<b>3.1</b>	<b>Introduction .....</b>	<b>65</b>
<b>3.2</b>	<b>Experimental.....</b>	<b>67</b>
3.2.1	Improve Cu paste with reductant additive .....	67
3.2.2	Fabrication of sintered Cu joints .....	67
3.2.3	Characterization and evaluation .....	67
<b>3.3</b>	<b>Results and discussion.....</b>	<b>68</b>
3.3.1	Shear strength result of sintered Cu joints.....	68
3.3.2	The effect of AA additive .....	69
3.3.3	Development on Cu paste with AA-treated solvent .....	80
<b>3.4</b>	<b>Conclusions .....</b>	<b>82</b>
	<b>References.....</b>	<b>84</b>
<b>Chapter 4</b>	<b>Reliability analysis of Cu sinter joining .....</b>	<b>89</b>
<b>4.1</b>	<b>Introduction .....</b>	<b>91</b>
<b>4.2</b>	<b>Experimental.....</b>	<b>92</b>
4.2.1	Fabrication of bonded sample.....	92

4.2.2	Thermal/humidity storage test .....	92
4.2.3	Thermal shock test and power cycle test .....	92
4.2.4	Characterization and evaluation .....	92
<b>4.3</b>	<b>Results and discussion</b> .....	<b>93</b>
4.3.1	Bondability of sintered Cu joints on different structures .....	93
4.3.2	Thermal storage test and humidity storage test .....	94
4.3.3	Thermal shock test .....	99
4.3.4	Power cycle test .....	107
<b>4.4</b>	<b>Conclusion</b> .....	<b>108</b>
	<b>References</b> .....	<b>109</b>
<b>Chapter 5</b>	<b>Conclusions</b> .....	<b>111</b>
	<b>Research achievements</b> .....	<b>116</b>
	<b>Acknowledgement</b> .....	<b>121</b>



## List of Figures

Fig. 1. 1 The operating range and application of various power devices (Applied materials)	5
Fig. 1. 2 The properties comparison of Si, SiC and GaN	8
Fig. 1. 3 The relationship between junction temperature and breakdown voltage of various semiconductor (simulation)	9
Fig. 1. 4 the structure of tradition IGBT module and common failure in packaging.	10
Fig. 1. 5 TLP process (left) and the Cu-Sn TLP bonding process (right) during the bonding time of (a) 10 min; (b) 40 min; (c) 60 min; (d) 90 min; (e) 240 min; and (f) 480 min	15
Fig. 1. 6 Multilayer foil as interlayer (a) [48] and power-based TLP process (b)	16
Fig. 1. 7 Schematic image of Ag stress-migration bonding process	17
Fig. 1. 8 The deposited surface at initial state (a) and after heating process (b). (c) showed cross-sectional SEM micrograph of hillock growth on Ag films and (d) showed the nearly perfect bonded joints obtained by Ag migration bonding	18
Fig. 1. 9 Comparison of soldering and metallic particles sintering	19
Fig. 1. 10 Schematic diagram of Ag nano-volcanic eruption (left) and the corresponding TEM micrographs (right)	20
Fig. 1. 11 die-attach based on Cu particles sinter joining	21
Fig. 1. 12 Synthesized Cu particles by various method.	25
Fig. 2. 1 FE-SEM micrographs, size distribution and corresponding XRD patterns (e) of Sample I (a, c, e) and Sample II (b, d, e), the insert images in 1c and id indicate the size distribution measured by DLS of the supernatant of Sample I and Sample II.	44
Fig. 2. 2 Color change of reaction solution (a), UV-Vis absorption spectra (b) and XRD patterns (c) during synthesis process of Sample I.	45
Fig. 2. 3 Color change of reaction solution (a), UV-Vis absorption spectra (b) and XRD patterns (c) during synthesis process of Sample II.	46

Fig. 2. 4 FE-SEM micrographs of Sample III (a) and Sample IV (b) and corresponding XRD pattern (c).	48
Fig. 2. 5 FE-SEM micrographs, size distribution and corresponding XRD patterns (e) of Sample V (a, c, e) and Sample VI (b, d, e).	49
Fig. 2. 6 Color change of reaction solution (a), UV-Vis absorption spectra (b) and XRD patterns (c) during synthesis process of Sample VI.	50
Fig. 2. 7 The shear strength of the Cu joints sintered in N <sub>2</sub> (a) and in formic acid (b).	52
Fig. 2. 8 FE-SEM micrographs of Cu joints fracture surface obtained by Sample I (a) II (b), V (c) and VI (d).	53
Fig. 2. 9 XRD patterns of sample II (a) and VI (b) aged in air. (Inset: enlarge part of 30-40° range)	55
Fig. 3. 1 Shear strength of sintered Cu joints obtained by Cu paste using various additives	69
Fig. 3. 2 XRD and XPS patterns of as-synthesized Cu particles before (a,c) and after AA treatment (b,d). Insert images in a and b are enlarged part at range of 35°-40°.	70
Fig. 3. 3 TEM micrographs of Cu particles before (a,c) and after AA treated (b,d) in both low (a,b) and high (c,d) magnification.	71
Fig. 3. 4 TG-DTA plots of pure AA (a), EG-0wt.% AA paste (b) and EG-10wt.% AA paste (c).	73
Fig. 3. 5 XRD patterns of EG-Cu paste (a, b) and EG-AA-Cu paste (c, d). Note that (b) and (d) were enlarged parts in 35°- 40° of (a) and (c), respectively.	74
Fig. 3. 6 Variation in shear strength of sintered Cu-Cu joints by Cu paste with different AA contents at different sintering temperatures.	76
Fig. 3. 7 Fracture surfaces of sintered Cu-Cu joints at 300°C by using EG-0wt.% AA paste (a), EG-5wt.% AA paste (b), EG-10wt.% AA paste (c), and EG-15wt.% AA paste (d). The arrows indicate the tensile deformation.	77
Fig. 3. 8 Cross-section images of sintered Cu-Cu joints by using the EG-0wt.% AA paste (a-d) and the EG-10wt.% AA paste (e-h) at sintering temperature of 200 °C (a,e), 250 °C (b,f), 300 °C (c,g) and 350 °C (d,h).	79

Fig. 3. 9 The promotion mechanism of AA in Cu pastes.	80
Fig. 3. 10 Shear strength of sintered Cu joints obtained by Cu paste using various solvent and AA additive	82
Fig. 4. 1 Shear strength of sintered Cu joints between different chips and substrate	94
Fig. 4. 2 Shear strength of sintered Cu joints during various storage test	95
Fig. 4. 3 the fracture (a-d) and cross-section SEM observation of joints at the initial state (a,e) and stored at 200 °C in air (b,d), at 200 °C in vacuum (c,g) and 85 °C/85 RH (d,h) for 1000h	96
Fig. 4. 4 XRD pattern of intered Cu joints at as-bonded state, after 1000 h in thermal storage test and humidity storage test	97
Fig. 4. 5 O element content in sintered Cu joints during thermal storage test and humidity storage test	98
Fig. 4. 6 Cross-section observation on center (a) and edge (b) part of the as-bonded specimens, (c) and (d) are the high-resolution images of the corresponding parts in (a) and (b).	99
Fig. 4. 7 The shear strength evolution of SiC-DBC specimens were tested in ambient and vacuum	100
Fig. 4. 8 Cross-section observation on center part of specimens accomplished with thermal shock test of 100 cycles (a), 500 (b) and 1000 (c) in ambient, d, e and f were the high-resolution images of a, b and c, respectively.	101
Fig. 4. 9 Cross-section observation on edge of specimens after thermal shock test of 100 cycles, 500 cycles and 1000 cycles in ambient, d, e and f, which show the defects, are the high-resolution images of the corresponding parts in c.	101
Fig. 4. 10 Cross-section observation on the center of specimens after thermal shock test of 1000 cycles in vacuum, b and c are the high-resolution images of the corresponding parts in a.	103
Fig. 4. 11 Cross-section observation on the edge of specimens after thermal shock test of 1000 cycles in vacuum, b, c and d are the high-resolution images of the corresponding parts in a.	104

Fig. 4. 12 EDX analysis on the cross-section of specimens of as-bonded state (a), after 1000 cycles in ambient (b) and vacuum (c), d and e were point analysis spectra of b and c respectively	105
Fig. 4. 13 XRD patterns of sintered Cu joints at as-bonded state, after 1000 cycle in ambient and vacuum	106
Fig. 4. 14 power cycle test of SiC MOSFET with DBC substrate (a), and T3ster result of samples before and after power cycles test of 1000 cycles	108

## **List of Tables**

Table 1. 1 Relative properties of various semiconductors	7
Table 1. 2 Mechanical properties of common materials in die-attach	11
Table 1. 3 Solidus and liquidus temperature of common materials in die-attach	13
Table 1. 4 Summary of various die-attach materials	23
Table 1. 5 Recent strength results of the sintered Cu joints and their sintering conditions	26
Table 2. 1 Reagent of synthesis groups	41
Table 2. 2 Summary of particles size and the radius ratio between small and big particles	54



# **Chapter 1**

## **Research background**



## **1.1 Development and challenge of power device**

### **1.1.1 Traditional Si power device**

For the time being, around 40% of the worldwide energy is consumed as electric power, which drives modern life as well as industry and transportation. The intense requirement of electric power stimulates the continuous technology development in electric generation, storage, distribution, and management [1]. Electric power systems, which is able to regulate electricity flow in power generation-storage-distribution, has been regarded as one of the great inventions in the modern world. Among of the systems, solid-state power semiconductor devices work as controller of electric systems and regulate at least 50% of the electricity in the world [2]. Thus, how to improve the regulating efficient to reduce the power loss of the power devices is one of the main concerns for researchers.

The first solid-state power semiconductor device with copper oxide for rectifiers appeared in 1927, which was used in early battery chargers and power supplies for radio equipment. Then, Germanium (Ge) was used to fabricate bipolar transistor. Those Ge transistors supported the power devices with relative low responding frequency (100 kHz) and low operating temperature (85 °C). The widely used silicon (Si) semiconductor devices appeared in the 1950s, starting a generation of power devices with better responding frequency and higher operating temperature (150 °C) [3]. The generation of Si semiconductor lasts for over half the century. During the time, various Si-based power devices were developed. The representative power devices include thyristor, power Metal-Oxide-Semiconductor Field-Effect Transistor (MOSFET), and Insulated Gate Bipolar Transistor (IGBT).

Bipolar power thyristors which can regulate current between blocking states and on-states by using an independent terminal were first developed in the 1950s [4, 5]. At the early stage, the endurance current was around 100 A and the permitting voltage is about several hundred. For time being, the tolerant current and voltage have been enlarged toward 5000 A and 8000 V respectively for a single device. Nowadays, thyristors have

been widely used in regulating ultra-high electrical power such as variable speed motor drives, high power inverter and traction. They can also be used in power distribution systems such as high-voltage direct current (HVDC) transmission networks.

In the 1970s, power metallic oxide semiconductor field effect transistor (power MOSFET) based on Si was created as a new class of power devices [6]. Comparing with thyristors, power MOSFET sacrifices the ability to endure high voltage and high current, but provides excellent switching speed, high resistance toward overload/noise and high reliability in devices opened new applications in high frequency (10-50kHz) with low operating voltages (<200 V) working condition. Today, these Si-based power MOSFETs have exhibited extensive use in the most power system, DC to DC converters, and low voltage motor controllers.

Thanks to the deep study in the metallic oxide semiconductor (MOS) and bipolar physics, the insulated gate bipolar transistor (IGBT) was created and were immediately regarded as a successful innovation in power devices in 1980s [7]. IGBT consists of four alternating layers (P-N-P-N) that are controlled by a MOS gate structure without regenerative action. This structure is simple but combines the rapid gate-drive characteristics of MOSFETs with the high-current and low-saturation-voltage capability of bipolar transistors, which endue IGBT with high power density, considerable ruggedness and reasonable switching speed. IGBT predominant power switch technology in medium- to high-power applications like switched-mode power supplies, traction motor control and induction heating for medium and high power applications. Fig 1.1 shows the various applications of current power devices according to working frequency and operating power. Thyristors are available to individually control power up to 10 MW but only in a low frequency. These devices are suitable for HVDC power transmission. When the working voltage is in the range of 1 kW to 1 MW and operating frequency is in the range of 1 kHz to 100 kHz, the IGBT module is an ideal choice. When the required power is low (up to 1 kV and 100 A) and operating frequency is high (up to 1MHz), power MOSFET is much more effective with the assistance of appropriate control system.

Beyond thyristors, IGBT and power MOSFET, other power devices which are continuously designed to meet the various working condition. These power devices collaborate in various systems and support our current electrical society.

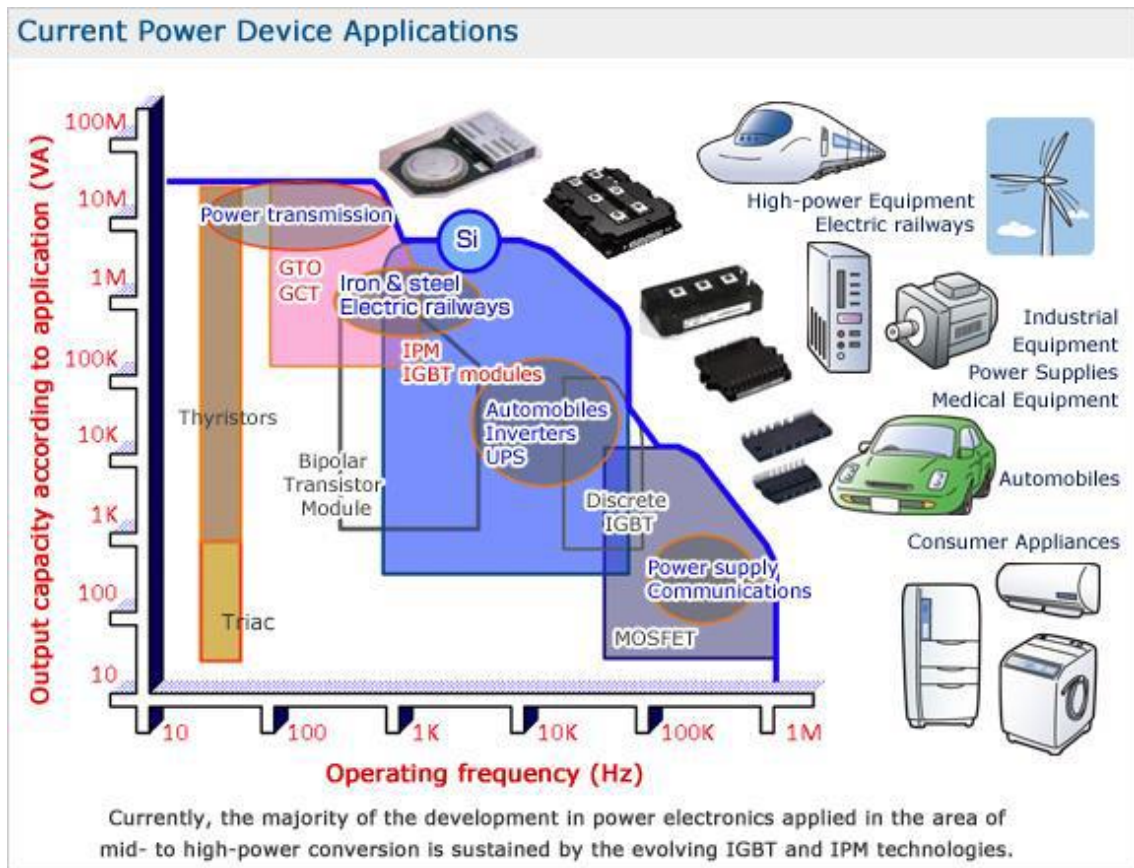


Fig. 1. 1 The operating range and application of various power devices (Applied materials)

In the foreseeable future, the demand for electrical power will continuously increase. Thus, innovation in power devices become much urgent i.e. semiconductor materials, devices designs, packaging technologies and so on. Improvement of the performance include higher working voltage and current, higher switch frequency, higher working temperature, higher reliability as well as higher converter efficient [8, 9].

### 1.1.2 Wide band gap power device

The electrical current switching capability of power devices mainly depends on a p-n junction structure, which is determined by kinds of semiconductor materials, can be achieved by doping different element. This structure allows the current flow only from the one side and block the electrons from the other side [10]. However, this character is limited by intrinsic carrier concentration of semiconductor. As intrinsic carrier concentration overrides doping concentration, the doping will lose its switching function and the p-n joints will act like a resistor. The intrinsic carrier concentration ( $n_i$ ) is related with the band gap of semiconductor by the following equation.

$$n_i = \sqrt{N_c N_v} \cdot e^{(-E_g/2kT)} \quad (1.1)$$

where  $N_c$  is the effective density of states in the conduction band;  $N_v$  is the effective density of states in the valence band;  $E_g$  is bandgap energy;  $k$  is Boltzmann's constant;  $T$  is thermodynamic temperature. From the equation, the  $n_i$  is largely influenced by the band gap energy as well as the temperature. For Si power devices, due to the narrow band gap energy of 1.12 eV, the  $n_i$  decreases rapidly when the temperature rises. Hence, the Si power devices are very difficult to be used over 200 °C combining complicated and heavy cooling system. Therefore, the novel semiconductor power devices with better thermal reliability at high temperature are in great need for various industries application, such as the automotive, down-hole oil, gas industries for well logging, aircraft, space exploration, nuclear environment, and radars [11].

Table 1. 1 Relative properties of various semiconductors [12]

Property	Si	GaAs	6H-SiC	4H-SiC	GaN	Diamond
Bandgap, $E_g$ (eV)	1.12	1.43	3.03	3.26	3.45	5.45
Dielectric constant, $\epsilon_r^1$	11.9	13.1	9.66	10.1	9	5.5
Electric Breakdown Field, $E_c$ (kV/cm)	300	400	2500	2200	2000	10000
Electron Mobility, $\mu_n$ ( $\text{cm}^2/\text{V}\cdot\text{s}$ )	1500	8500	500 80	1000	1250	2200
Hole Mobility, $\mu_p$ ( $\text{cm}^2/\text{V}\cdot\text{s}$ )	600	400	101	115	850	850
Thermal Conductivity, $\lambda$ (W/cm·K)	1.5	0.46	4.9	4.9	1.3	22
Saturated Electron Drift Velocity, $v_{sat}$ ( $\times 10^7$ cm/s)	1	1	2	2	2.2	2.7

<sup>1</sup>  $\epsilon = \epsilon_r \cdot \epsilon_0$  where  $\epsilon_0 = 8.85 \times 10^{-12}$  F/m

As mentioned above, the  $n_i$  is largely influenced by the band gap energy as well as the temperature. With narrow band gap energy, the  $n_i$  decreases rapidly with rising temperature. In order to improve the  $n_i$ , wide band gap (WBG) semiconductors is the best choice and are regarded as promising materials substituting to Si for next generation power devices. The WBG semiconductor also shows the higher critical field, the higher saturation velocity, and the lower intrinsic carrier density (Table 1.1). These properties endow WBG power devices higher junction temperature, higher switching frequency, higher working voltage, higher power capability, the lower conduction drop, and the better radiation hardness [12, 13]. The representative WBG power devices of silicon carbide (SiC) or gallium nitride (GaN) are compared to traditional Si devices and summarized in Fig. 1.2. It is obvious that SiC/GaN semiconductors are superior Si in every aspects.

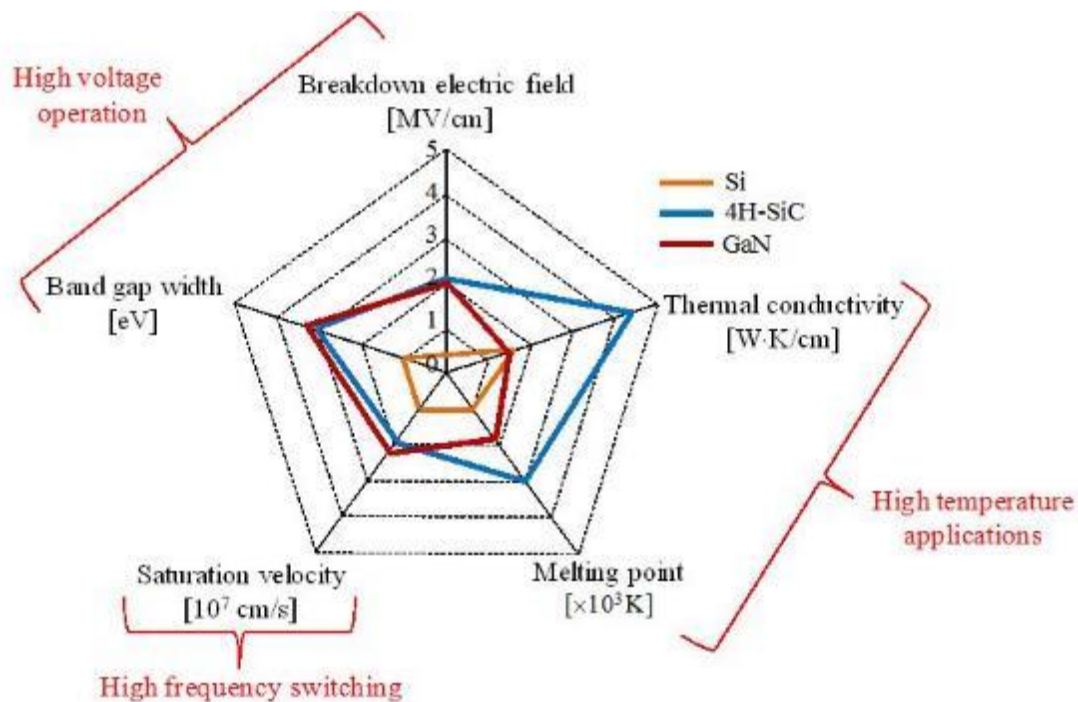


Fig. 1. 2 The properties comparison of Si, SiC and GaN [14]

Fig. 1.3 shows the relationship between junction temperature and breakdown voltage with various semiconductors. It is obvious that all the semiconductors have lower block voltage ability when temperature rising. However, the WBG semiconductors have an obvious advantage in blocking voltage both in low temperature and at high temperature. Si devices can only block a few hundred volts at 200 °C, and if it was applied to IGBT with operating condition of 6.5 kV, the operating temperature is limited to even lower than 125 °C. This weak point not only hinders Si power devices for high temperature but also requires a high-power cooling system. On the other hand, WBG semiconductors possess higher block voltage and higher temperature endurance. Thus, power devices with WBG semiconductors can operate at very high voltage over 100 kV even at a high temperature above 400 °C. Moreover, their high breakdown voltage capability also enables devices to be operated at high power density with a small size. WBG power devices, therefore, have been well studied [15-17]. Recently, some WBG devices have become commercially available.

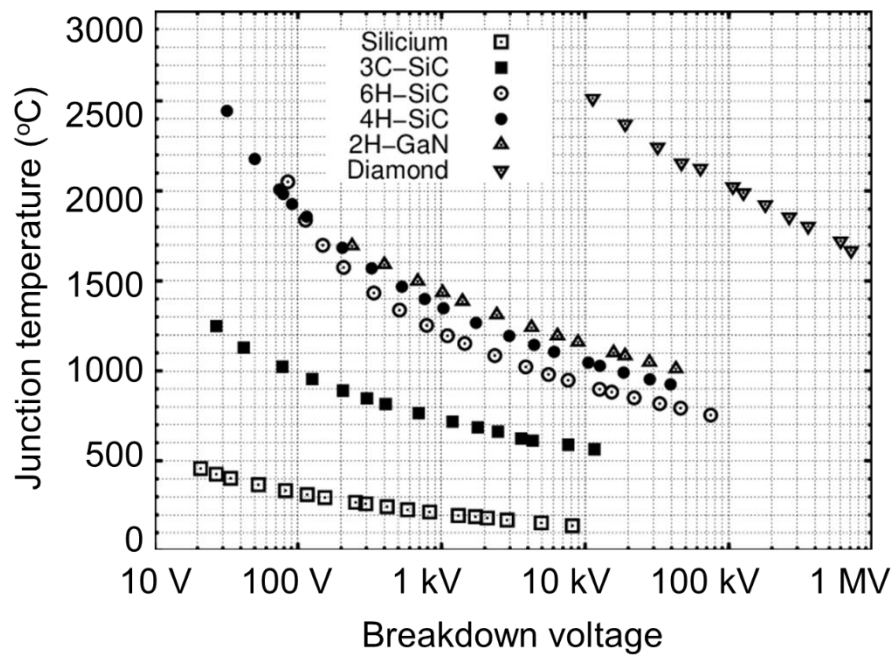


Fig. 1. 3 The relationship between junction temperature and breakdown voltage of various semiconductor (simulation) [18].

### 1.1.3 Packaging challenge of WBG power device and die-attach materials

Packaging technologies is an important part of power device integration. It not only influence operating temperature but also decides device reliability [19, 20]. For example, in a typical IGBT module (Fig. 1.4), it includes a heat sink, a substrate, terminal leads and IGBT die, as well as interconnections including wire bonding, die-attach and substrate attach. Failures of an IGBT often occur in its interconnections parts (Fig. 1.4), which include cracking in a die-attach layer, fracture in a substrate attach layer and peel-off of wire bonds.

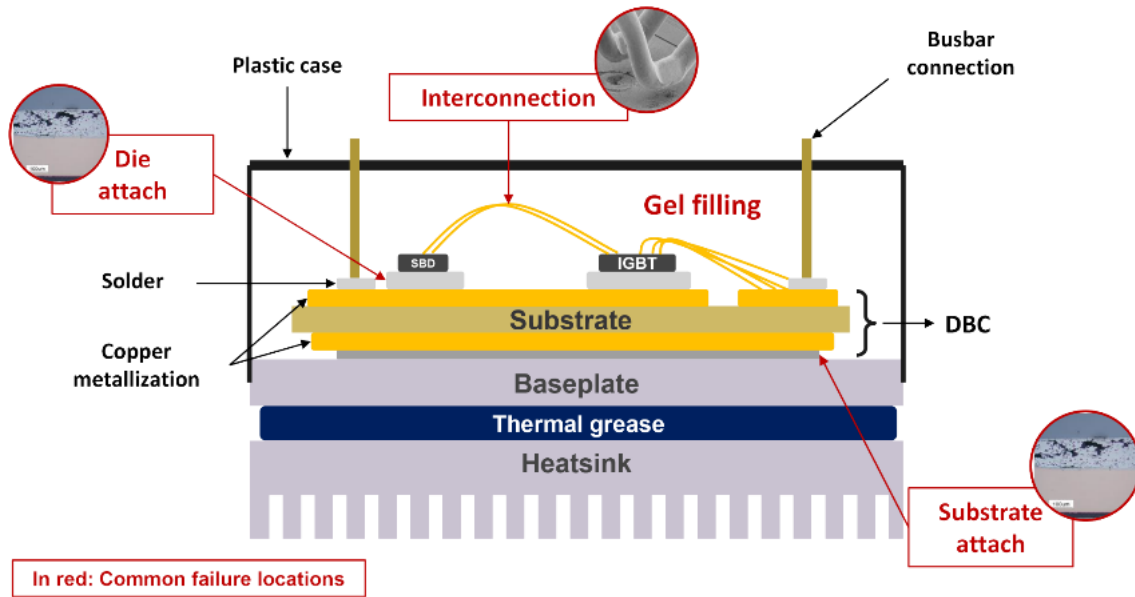


Fig. 1. 4 the structure of tradition IGBT module and common failure in packaging.

Failures of a die-attach is one of the main issues for packaging due to severe thermal/power cycling [21]. In operation, massive heat from its junction increases device temperature. Due to different coefficients of thermal expansion (CTE) between semiconductor dies and substrates, severe stress sometimes causes cracking in the die-attach layer. Table 1.2 lists selected thermal and mechanical properties of typical materials that are used in die-attach structure, such as ceramic substrates, substrate metallizations, semiconductor dies, and die-attach materials.

Table 1. 2 Mechanical properties of common materials in die-attach [22-27]

Component	Materials	Coefficient of thermal expansion (ppm/K)	Thermal conductivity ( $Wcm^{-1}K^{-1}$ )	Young module (GPa)
Die	Si	2.6	1.5	150
	SiC	3.8	5.0	410
	GaN	6.2	1.3	320
Bonding layer	Pb-5Sn	29	0.35	20
	Sn-3Ag-0.5Cu	24	0.59	51
	Sintered Ag	1.9	2.4	9
	Cu <sub>3</sub> Sn	19	0.7	108
DBA/DBC substrate	Al	17	2.05	68
	Cu	16.5	4.0	110
	Al <sub>2</sub> O <sub>3</sub>	6.5	0.3	310
	AlN	4.5	2.9	310
	Si <sub>3</sub> N <sub>4</sub>	2.6	0.9	314

The difference of coefficients of thermal expansion between semiconductor dies and substrates is huge, which even slight temperature change will lead to considerable stress in the die-attach layer. Thus, ideal die-attach materials should meet several requirements. Firstly, high bondability, i.e., strong initial bonding strength would take advantage during the thermal cycles and could endure more stress. Secondly, it must provide high reliability even at elevated temperature. Die-attach materials should be stable at high temperatures to avoid any defect formation caused by the formation of brittle intermetallic compounds (IMCs) [28]. Thirdly, it must ensure high electrical conductivity as well as high thermal conductivity [24]. Good electrical conductivity can swiftly transfer heat generated at a chip junction, which is beneficial to lower temperature of entire device and to decrease internal stress. Additional benefits will be realized by selection of specific material. For example, the self-healing properties, which can heal defects at in operation temperature,

can be added [29]. A microporous structure of a die-attach layer can relieve thermal stresses caused by thermal expansion mismatch. The problem such as electromigration also should be taken into consideration [30].

## **1.2 Overview of die-attach technology for high-temperature application**

The conventional high temperature die-attach material is Pb alloy solders, containing 85-95wt.% of Pb. However, due to its high risk on health and environment, these high-Pb solders has been replaced by Pb-free solders since 2016 by the restriction of hazardous substances (RoHS) and ELV [31]. Thus, many candidates of high-lead solders. Some of the promising replacements including high-temperature Pb-free alloys, transient liquid phase (TLP) bonding, Ag stress-migration bonding (SMB) and low temperature sinter bonding technology. In this section, the currently available candidates are briefly summarized.

### **1.2.1 High-temperature lead-free solders**

Over hundreds of alloys proposed as high-temperature lead-free solder. The basic binary alloys include Au-based alloys such as Au-Sn [32, 33], Au-Ge [34] and the other alloy such as Zn-Al [35, 36], Zn-Sn [37], Bi-Ag [38] and Sn-Sb [39]. The solidus/liquidus temperatures of some of them are listed in Table 1.3.

Table 1. 3 Solidus and liquidus temperature of common materials in die-attach [40]

Alloys	Composition (wt. %)	Solidus Temperature (°C)	Liquidus Temperature (°C)
<b>High-Pb Alloy System</b>			
Pb-Sn	Sn-65Pb	183	248
	Sn-70Pb	183	258
	Sn-80Pb	183	279
	Sn-90Pb	268	301
	Sn-95Pb	300	314
	Sn-98Pb	316	322
Pb-Ag	Pb-2.5Ag	304	304
	Pb-1.5Ag-1Sn	309	309
<b>Sn-Sb Alloy System</b>			
Sn-Sb	Sn-5Sb	235	240
	Sn-25Ag-10Sb (J-alloy)	228	395
<b>Au Alloy System</b>			
Au-Sn	Au-20Sn	280 (eutectic)	
Au-Si	Au-3.15Si	363 (eutectic)	
Au-Ge	Au-12Ge	356 (eutectic)	
<b>Bi Alloy System</b>			
Bi-Ag	Bi-2.5Ag	263 (eutectic)	
	Bi-11Ag	263	360
<b>Cu Alloy System</b>			
Cu-Sn	Sn-(1-4)Cu	227	~400
	Sn-Cu particles composites	~230	
<b>Zn Alloy System</b>			
Zn-Al	Zn-(4-6)Al(- Ga, Ge, Mg, Cu)	300~340	
	Zn-Sn	Zn-(10-30)Sn	199

Au-based alloys have a long history and is regarded as one of the best lead-free solders in performance. Au-20Sn alloy has the solidus and liquidus point of 280 °C and its soldering process temperature is around 300 °C, which is similar to that of high-lead solder. Au-20Sn solder has several advantages such as high yield strength, good wettability and low viscosity, and fluxless soldering as compared to the other alloys [41]. However, Au-Sn alloy still faces the problem of reliability because its hardness due to intermetallic compounds (IMC) deteriorating in thermal cycles. Au-Ge alloy shows a higher bonding strength and high reliability [34]. Unlike Au-Sn alloy, it does not form the

intermetallic compounds (IMC). Thus, Au-Ge soldering layer exhibits excellent reliability even in thermal cycling environment. However, Au-Ge alloy has a higher soldering temperature (380 °C). Of course, the high cost of Au-based alloys always prevents their widespread usage. Also, Au-based solders have high Young's modulus [42], which is not suitable due to introducing high stress concentration and increase a risk of failure.

As affordable Pb-free solders alternative, high temperature solders are Zn-Al, Zn-Sn, Bi-Ag and Sn-Sb. They, however, have their individual problems. For example, Zn-based alloy (Zn-Al, Zn-Sn) are low cost and easy to be fabricated, and has a high reliability because no IMC is formed. However, since Zn is quite active and Zn-based solders are easily oxidized in soldering. While Sn-Sb alloy has good creep properties and good reliability, melting reaction occurs relatively low temperature around 250 °C. Bi-based solders have a low thermal conductivity i.e. poor heat dissipation capability. In addition, Bi-based alloys have poor wettability on metallization layers. These drawbacks inhibit their wide adoption in traditional Si power devices as well as WBG power device.

### **1.2.2 Transient liquid phase bonding process**

Transient liquid phase bonding process (TLP) bonding was firstly established for Ni-based super alloy and has been widely used in industry. The process utilizes the partial melting reaction at mating dissimilar metal interface. For, soldering typical combinations of metals are (Au, Ag)-(In, Sn) and (Cu, Ni, Co)-Sn. TLP bonding layer is usually composed by IMCs [43, 44]. During TLP bonding process, metal with low melting point firstly melts and reacts with the counter metals by eutectic reaction. When TLP process finishes, a joint layer composed of IMCs with some residual metal, which possesses high melting point. [45, 46].

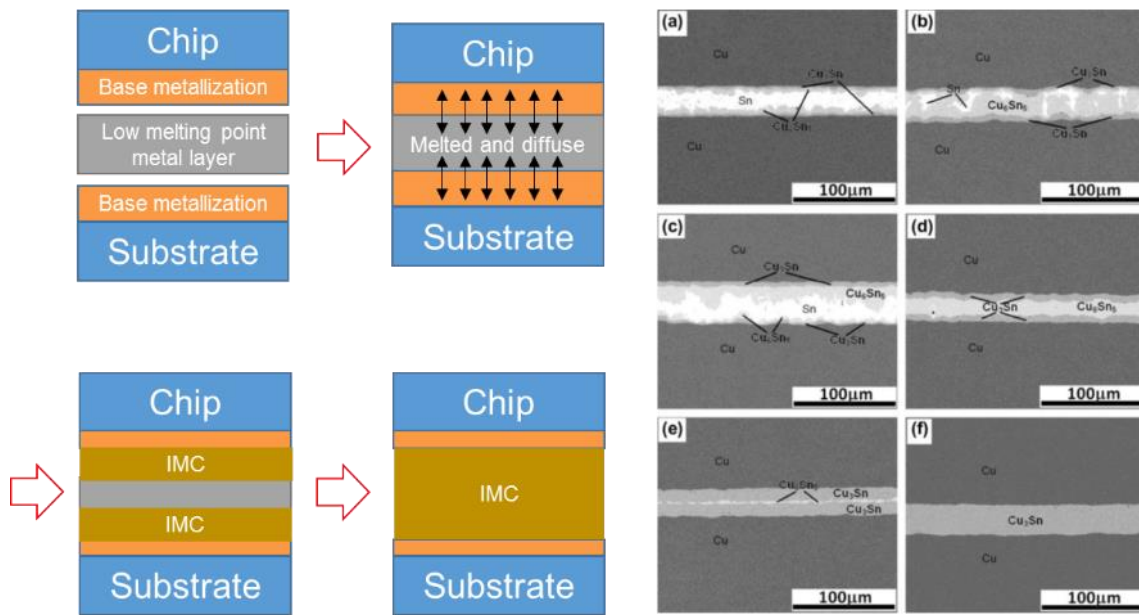


Fig. 1.5 TLP process (left) and the Cu-Sn TLP bonding process (right) during the bonding time of (a) 10 min; (b) 40 min; (c) 60 min; (d) 90 min; (e) 240 min; and (f) 480 min [47]

One of the representative TLP process was described in Fig. 1.5. A Sn interlayer of low melting point was placed between Cu metallization. When temperature raised to 250 °C. Sn interlayer melts followed by wetting on Cu metallizations and forming IMCs continuously, resulting in final formation of IMC ( $\text{Cu}_3\text{Sn}$ ) as a bonding layer. The melting temperature of IMCs formed in various TLP process is proved to far higher than the bonding temperature of 250°C. [48-51].

One of the fatal disadvantages of TLP process is the time cost. For example, the Cu/Sn/Cu system needs 480 min at 340 °C to achieve a complete IMC layer formation because IMC only grows at the interface between interlayer and metallization [47]. The other problem is the brittleness of IMCs, which easily cause defects formation. Bosco et al [52] reported that the strength of the joints produced by TLP bonding in the Cu/Sn system was high but with lower toughness than pure Cu. Placing high melting point metal into interlayer such as multilayer foil as interlayer (Fig. 1.6 a) or power-based TLP process (Fig. 1.6 b) could accelerate the bonding process. This system also cannot avoid

the brittle property of IMCs.

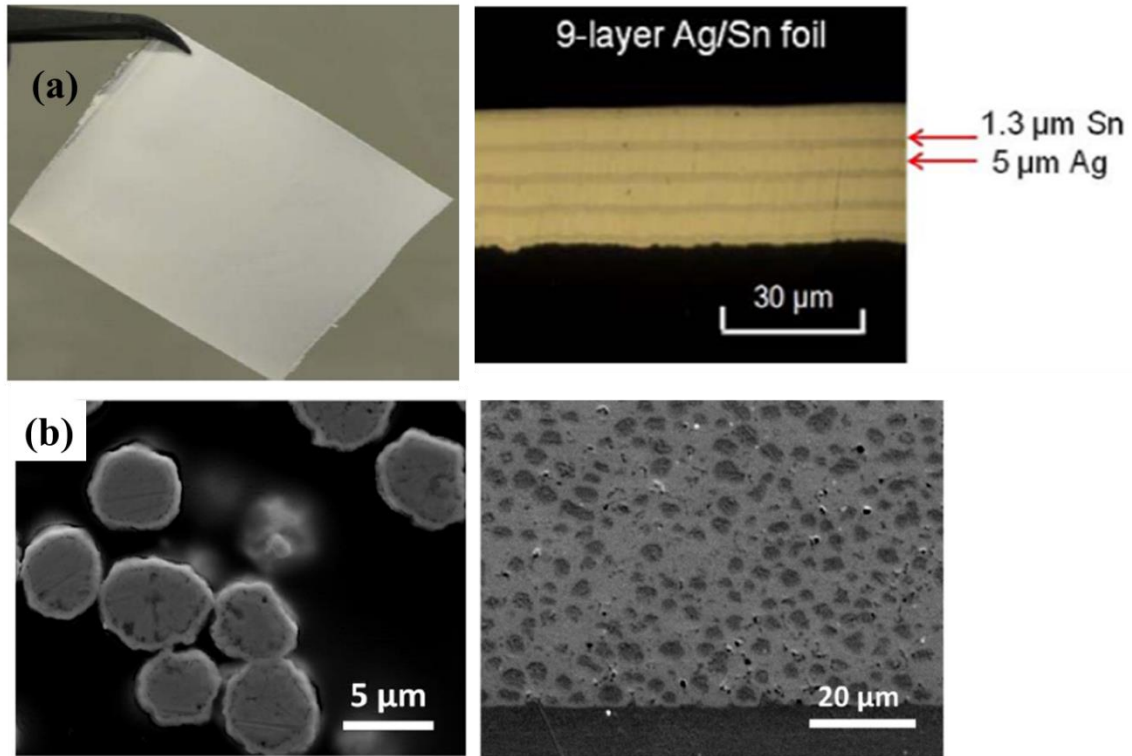


Fig. 1. 6 Multilayer foil as interlayer (a) [48] and power-based TLP process (b) [52]

### 1.2.3 Ag stress-migration bonding

Ag stress-migration bonding can be categorized direct bonding techniques which are pursued by the industrial world for decades. The principle of Ag stress-migration bonding is based on the phenomenon of Ag hillock formation and growth [53]. Hillocks, commonly observed in metal films, is formed by relaxation of the residual stress induced by thermal expansion mismatch between a film and a substrate. For example, during annealing a Ag film on a Si substrate, Ag atoms move along grain boundaries towards the film surface to form Ag hillocks. The height of those hillocks could reach to hundreds of nanometers or several micrometers [54].

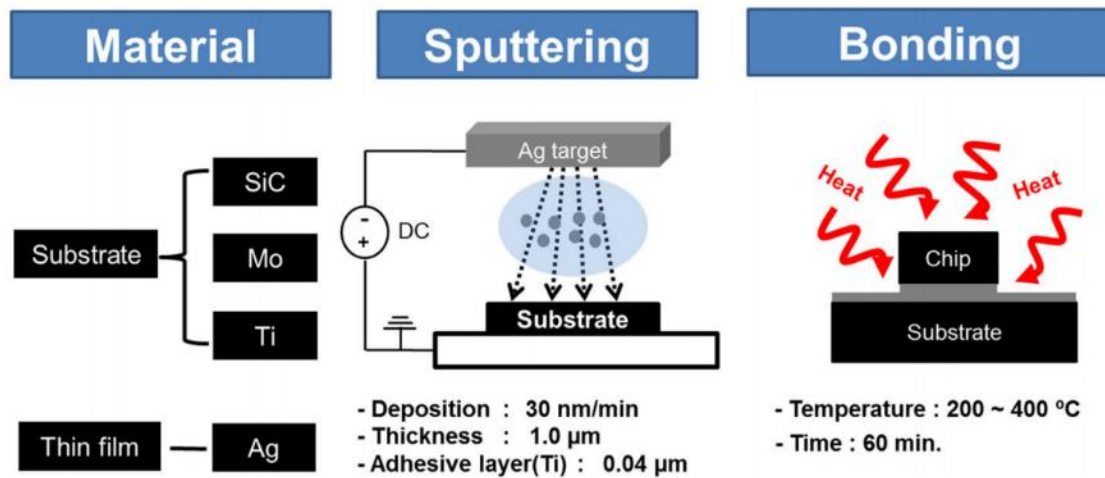


Fig. 1. 7 Schematic image of Ag stress-migration bonding process [55]

The Ag stress-migration bonding process is shown in Fig. 1.7. Ag metallization layer is deposited on surfaces of a substrate and a semiconductor chip. Hillocks were formed during heat treatment both sides. The formation of hillocks can fill the gap between a chip and a substrate, producing a “perfect” bonding layer with high bonding strength. In addition, the bonding layer does not have any IMC, providing a prospective availability for next generation die-attachment.

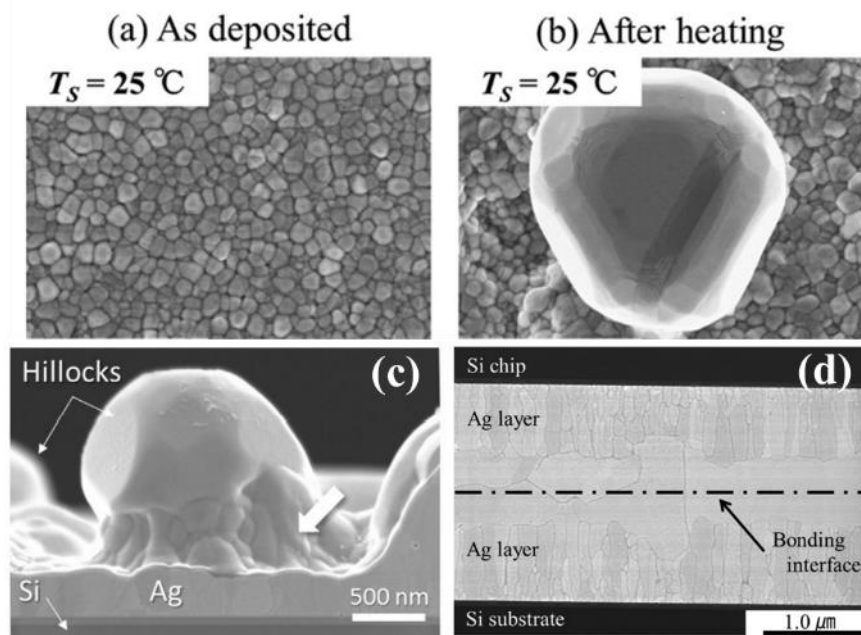


Fig. 1. 8 The deposited surface at initial state (a) and after heating process (b). (c) showed cross-sectional SEM micrograph of hillock growth on Ag films and (d) showed the nearly perfect bonded joints obtained by Ag migration bonding[53, 56]

#### 1.2.4 Ag particle sinter joining

As aforementioned, a bonding layer only consists of pure metal is preferred. Thus, a metallic particle sinter joining technology is another method to obtain such a reliable bonding layer (Fig. 1.8) [57, 58]. Sintering is the process of compacting and forming a solid mass of material by its particles without melting. Metal atoms diffuse among particles in heat with or without applied pressure, bridging particles together and creating one solid piece [59]. This process can occur below melting points of materials. Moreover, sintering temperature can be further decreased by decreasing particles size from micro to nano scale which can drastically increase their specific surface energy [60]. After sintering process, a metal bonding layer has high melting point and acquires high resistance toward thermal fatigue without any IMC.

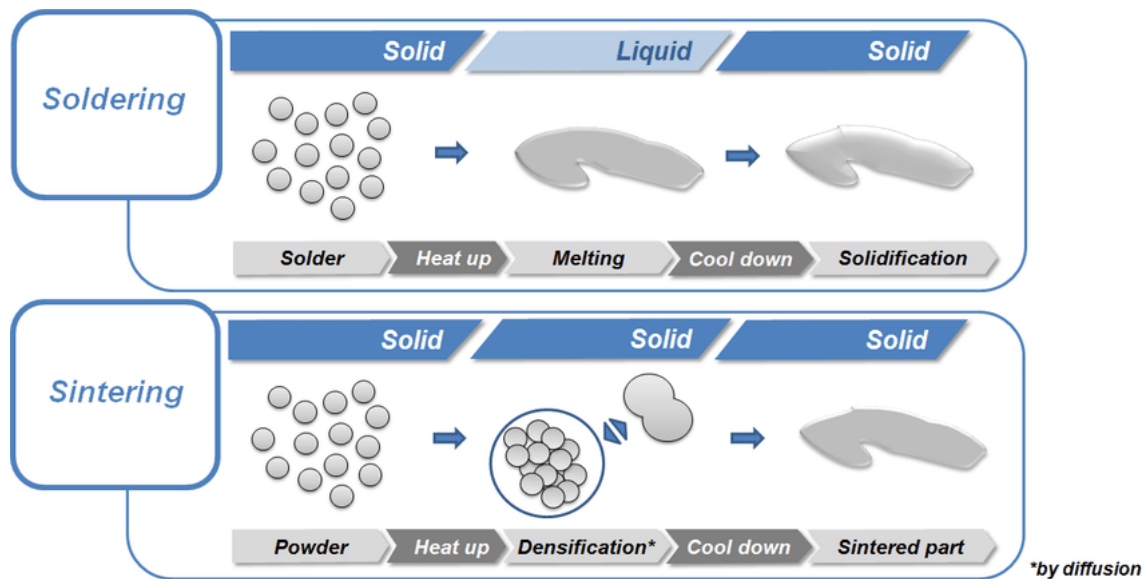


Fig. 1. 9 Comparison of soldering and metallic particles sintering [58]

For the metallic particle sintering joining technology, two typical choices are Ag-sintering and Cu-sintering. The history of the Ag sintering technique can date back to the late 1980s [57]. Ag particles pastes, which are mixed by organic solvent and Ag micro/nano particles, are the typical simple formulation for sinter joining. Ag pastes can be adjusted to have similar viscosity as solder pastes in order to apply conventional screen printing or dispensing followed by heating. Moreover, unlike the Ag stress-migration bonding requiring Ag metallization both on a substrate and a semiconductor chip, Ag sinter joining can be applied to various metalizations such as Ag, Al, Au, and etc., providing great applicability. Sintered Ag layer possess high electric and thermal conductivity, high melting point and high bonding strength [56, 61, 62].

Ag can be sintered at very low temperature even below 200 °C. Ag absorb oxygen along its grain boundary and forms Ag oxides resulting in Ag-O liquid. Under some stress, Ag-O liquid come out to surface and then decomposes to metallic Ag in sintering process, which was named as “Silver nano-volcanic eruption” [63]. This phenomenon can provide extra driving force and lower the sintering temperature. At present, Ag particles paste could be sintered at 180-250 °C in air without assisting pressure. This sintering condition

is very close to the conventional soldering process, which can benefit the application of Ag sinter joining in the commercial market.

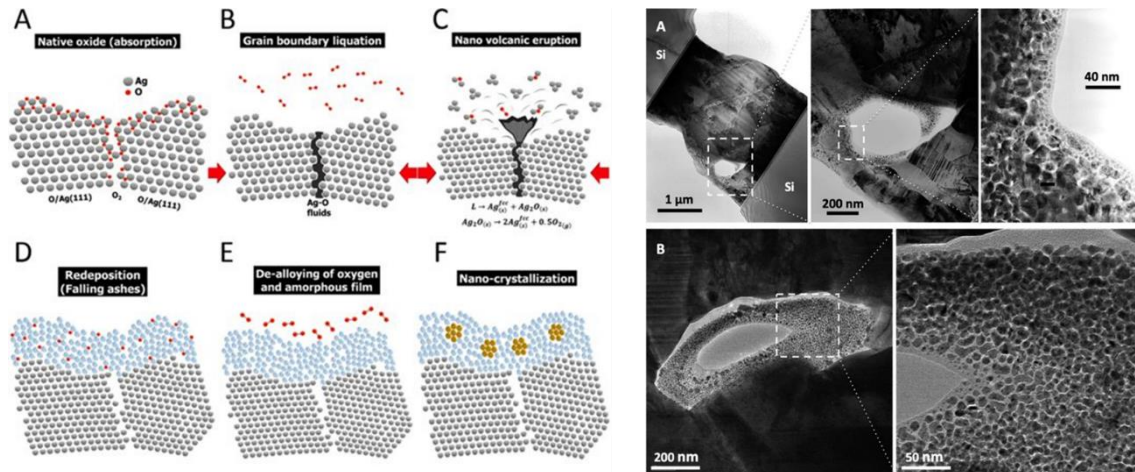


Fig. 1. 10 Schematic diagram of Ag nano-volcanic eruption (left) and the corresponding TEM micrographs (right) [63]

Ag sintered joining layer has a special micro-microporous microstructure, which is unavoidable due to low solid load in a printed paste layer. Even though a micro-porous structure has a lower bonding strength than fully sintered Ag. A micro-porous structure can relax thermal stress, providing good opportunity to maintain the die-attach structure without serious damage in severe thermal-fatigue. The ability bearing fatigue failure and relieving stress are proved useful for devices [56, 61, 64]. The excellent reliability of die-attach structure made by Ag sinter joining has been confirmed. However, using novel metal Ag for die-attach material still faces its relatively high cost, poor chemical migration properties and corrosion.

### 1.2.5 Cu particle sinter joining

Sinter joining with Cu particles is another alternative as a highly reliable die-attach technology. Cu has similar thermal and electric conductivity as Ag but its cost is far below that of Ag [65-67]. Moreover, high resistance toward chemical/gas corrosion also provides Cu sinter joining to wider application [68, 69].

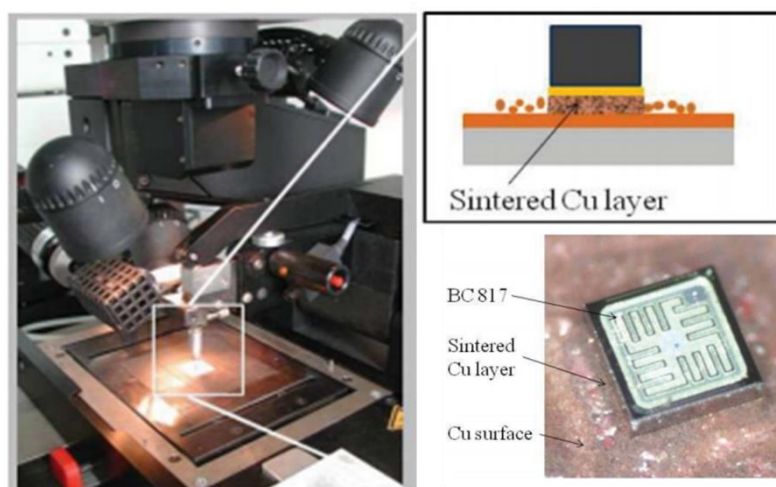


Fig. 1. 11 die-attach based on Cu particles sinter joining [70]

Cu-sinter joining has been widely studied in the past decades, which reported that sintered Cu joints possess similar properties as sintered Ag joints [71-75]. However, to achieve a reliable bonding, certain sintering-assist methods such as application of high pressure, of high temperature or of reductive protecting gas are necessary for Cu sintering. Difficulties of Cu sintering different from Ag sintering comes from two main aspects. Firstly, Cu possesses lower sinterability than Ag without the specific Ag-O reaction forming liquid phase. Secondly, Cu has a lower self-diffusion coefficient than that of Ag despite they have the same fcc crystal structure [76]. The second reason is the intrinsic oxidation tendency of Cu. The affinity of Cu to oxygen is much higher than that of Ag. An oxides layer on Cu surface prevent sintering at low temperature. Moreover, Cu oxides cannot decompose below 350 °C, while Ag oxides can naturally decompose to reform to metallic Ag when temperature is above 150 °C. Thus, most of Cu sintering trials were performed in the reductive atmosphere, which increases investment for bonding equipment and spoil the cost benefit of Cu. With these difficulties, the reports of reliability on Cu sinter joining has been still insufficient, which is necessary for industrial application.

Table 1.4 summarizes the advantages and disadvantages of current high-temperature

## Chapter 1 Introduction

die-attach materials. Among these materials, Cu particles sinter joining technology has many incomparable merits and is regarded as one of the best cost-performance die-attach methods for WBG power devices. However, the above mentioned issues must be solved in order to realize Cu sinter joining as the practical alternative as a high temperature interconnection method.

Table 1. 4 Summary of various die-attach materials

	Advantages	Disadvantages
Lead-free solder	<ul style="list-style-type: none"> <li>-similar bonding process as Pb-based solder</li> <li>-widely used in industry</li> <li>-acceptable price</li> <li>-acceptable bonding strength</li> </ul>	<ul style="list-style-type: none"> <li>-poor reliability</li> <li>-different properties according to alloy composition</li> <li>-should be carefully chose for various working condition</li> </ul>
TLP bonding	<ul style="list-style-type: none"> <li>-high bonding strength</li> <li>-high thermal reliability</li> <li>-acceptable price</li> </ul>	<ul style="list-style-type: none"> <li>-long bonding time</li> <li>-poor thermal/electrical conductivity</li> <li>- high brittleness</li> </ul>
Ag migration bonding	<ul style="list-style-type: none"> <li>-nearly perfect bonding layer</li> <li>-good thermal and fatigue reliability</li> <li>-superior electrical and thermal conductivity</li> </ul>	<ul style="list-style-type: none"> <li>-complicated manufacturing process</li> <li>-high price</li> <li>-pressure is needed</li> </ul>
Ag particles sinter joining	<ul style="list-style-type: none"> <li>-high electrical and thermal conductivity</li> <li>-high bonding strength</li> <li>-good thermal reliability</li> </ul>	<ul style="list-style-type: none"> <li>-high price</li> <li>-electromigration</li> </ul>
Cu particles sinter joining	<ul style="list-style-type: none"> <li>-high electrical and thermal conductivity</li> <li>-high bonding strength</li> <li>-acceptable price</li> </ul>	<ul style="list-style-type: none"> <li>-oxidation</li> <li>-high temperature, high pressure or reductive atmosphere is needed for bonding process</li> <li>-limited reliability reports</li> </ul>

### 1.3 Motivation of present research

As aforementioned, though Cu particles sinter joining has incomparable advantages, some serious issues still limit its practical application. In this part, the issues and challenge from the preparation of Cu particles and Cu paste to jointing technology will be discussed

in detail.

### **1.3.1 Preparation of Cu particles.**

The first issue is about the preparation of Cu particles, which include two aspects of preparation cost and size-controllability. Though Cu is much cheaper than Ag, high fabrication cost spoils price superiority. Thus, the establishment of a simple and commercially affordable method is one of the important topics for Cu sinter joining. In addition, the size-controlling method including size and size distribution of Cu particles largely influences its sintering performance.

There are various methods to synthesize Cu particles such as thermal decomposition [77, 78], laser irradiation [79], chemical reduction [80, 81], microwave-assisted [82], biological methods [83, 84], and conventional mechanical milling/melt blow methods. Some of them are limited by cost increase or low yield ratio. In contrast, the polyol process, wet-chemical process, is one of the attractive chemical synthetic method for metal, metal oxide, and alloy particles with various morphology and diameter. The polyol process is simple and provide controlling capability of size and size distribution by adjusting reaction time, temperature, additives such as capping agents, direction-growth controlling agents, and various metal sources [85-89]. Cu nanoparticles have been successfully synthesized by the polyol method and their size and morphologies could be easily modified by changing the chain length of polyol solvents and other parameters [88]. Although the polyol method is a very suitable one for Cu particles synthesis, the detail of synthesize condition and size-controlling capability should be further investigated for optimizing the performance as Cu sinter joining material.

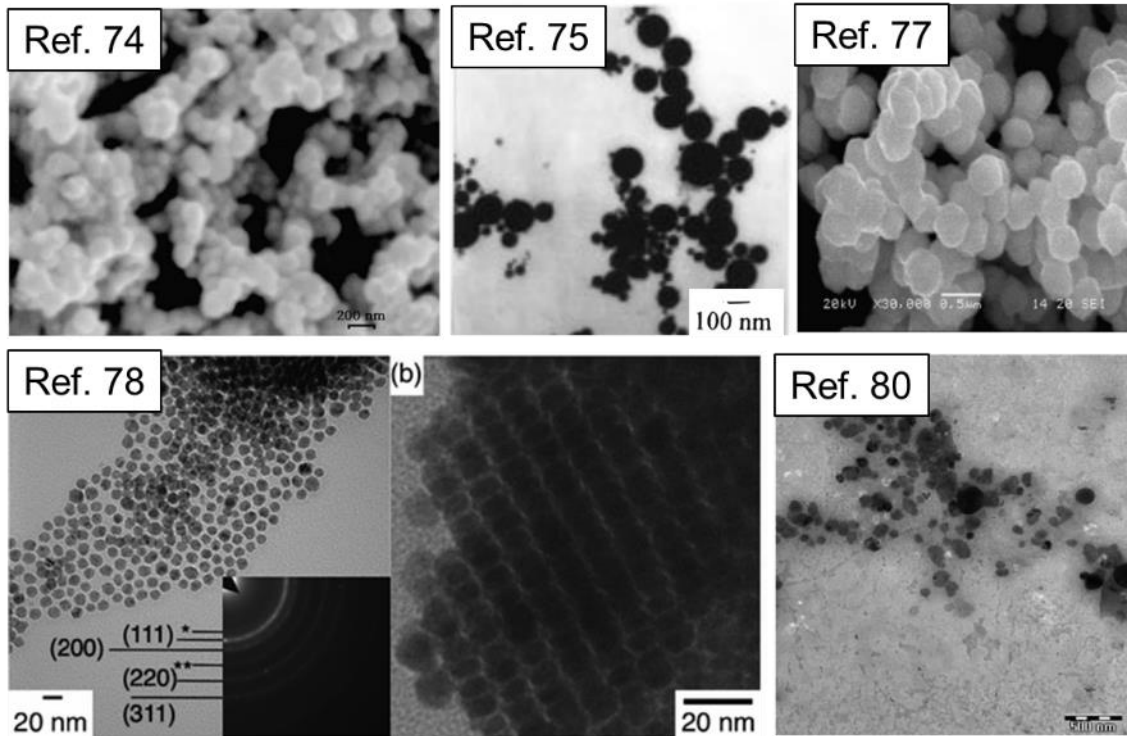


Fig. 1. 12 Synthesized Cu particles by various method.

### 1.3.2 Development and challenges of sinter Cu joining technology

Due to the intrinsic low diffusion rate and oxidation tendency, sintering of Cu particles is rather difficult than that of Ag. Table. 1.5 shows the relationship between strength and sintering parameters. High temperature, high pressure and protective or reductive atmosphere is necessary for sintering Cu particles. Considering industrial application of Cu particles, establishment of mild sintering methods is necessary, such as low temperature, low pressure, inert atmosphere ( $N_2$ , Ar or vacuum, etc). These conditions will depend on the formulation of a paste and properties of Cu particles itself.

Table 1. 5 Recent strength results of the sintered Cu joints and their sintering conditions

<b>Raw material</b>	<b>Temp (°C)</b>	<b>Pressure (MPa)</b>	<b>Atmosphere</b>	<b>Shear strength</b>	<b>Ref</b>
<b>Nano-Cu</b>	400	15	N <sub>2</sub>	~40MPa	[72]
<b>Nano-Cu</b>	400	1.2	H <sub>2</sub>	37.7 MPa	[90]
<b>Nano-Cu</b>	350	5	H <sub>2</sub>	>30 MPa	[91]
<b>CuO/micro- Cu</b>	350	40	H <sub>2</sub>	25.6 MPa	[70]
<b>Nano-Cu</b>	400	10	N <sub>2</sub> +H <sub>2</sub>	1.25 Kgf	[92]
<b>Nano-Cu</b>	400	15	Vacuum	>40 MPa	[93]
<b>Nano-Cu+ Ni<sub>3</sub>Sn<sub>2</sub></b>	400	Pressureless	H <sub>2</sub>	31.8 MPa	[94]
<b>Nano-Cu (Ni)</b>	300	Pressureless	H <sub>2</sub>	~20 MPa	[95]
<b>Nano-Cu</b>	400	1.2	H <sub>2</sub>	39.2 MPa	[96]
<b>Micro-CuO</b>	450	5	ambient	14 MPa	[71]
<b>Nano-Cu + NiO</b>	350	Pressureless	H <sub>2</sub>	~30 MPa	[97]
<b>Micro-Cu flake</b>	300	0.08	Formic acid	30.9 MPa	[74]
<b>Nano-Cu</b>	320	10	N <sub>2</sub> +H <sub>2</sub>	51.7 MPa	[98]
<b>Nano-Cu</b>	300	1.08	Ar+H <sub>2</sub>	31.88 MPa	[99]
<b>Nano-Cu</b>	300	10	ambient	40 MPa	[100]
<b>Nano-Cu</b>	250	10	Ar+H <sub>2</sub>	32.4 MPa	[101]

On the other hand, while there were many reports focusing on the bonding quality [74, 98, 102-104], a few of reports focus on the reliability of Cu joints, which is also a key point for the practical application in various devices [75]. Important information such as microstructure evolution, crack formation, or change in fracture modes has not been studied, which is very crucial for high temperature application of power devices [105]. Thermal shock resistance as well as high temperature storage resistance of joints with Cu

sinter joining.

#### **1.4 Purpose and scope of the present study**

Considering the superiority of Ag sinter joining of simple process of low sintering temperature and of low pressure in air atmosphere, Cu sinter joining must overcome current several drawbacks. The main purpose of the present study is to obtain a high-performance Cu sinter joining in conditions similar to Ag sinter joining, which will realize the affordability advantage of Cu sinter joining for opening the WBG power devices market. Hence, a simple preparation process of Cu particles, mild sintering capability such as low sintering temperature, low assisting pressure and no reductive atmosphere, and thermal stability evaluations for the joints with the developed Cu sinter pastes are three main objects of the present work. Firstly, a simple polyol method is used to synthesize bimodal Cu particles by changing additives, which easily tailor the size and size distribution of the Cu particles. Secondly, the Cu particles are fabricated into pastes for sinter joining. Lastly, the reliability of the obtained joints by using the developed Cu pastes was evaluated by aging test and thermal cycle test followed by clarification of their fracture mechanism.

In Chapter 1, the brief description of the background of power devices, the challenge and opportunity of WBG power device and its packaging technology including the important die-attach issue. Clarification of Cu sinter joining among various die-attach methods, the development and possibility of Cu sinter joining for WBG devices is also discussed. Base on the summarized background, the purpose of the present study is summarized.

In Chapter 2, a simple polyol method was proposed to synthesize bimodal Cu particles. The size of particles can be modified by adjusting additives, reaction time and temperature. The synthesis mechanism is also discussed. The relationship between bondability and particles diameter are clarified.

## Chapter 1 Introduction

In Chapter 3, efforts have been made to realize steady Cu sinter joining at a relative mild sintering condition ( $< 300\text{ }^{\circ}\text{C}$ , 30 min, 0.4 MPa and inert atmosphere), the effect of solvent in the developed Cu paste was studied. A reductive polyethylene glycol (PEG) solvent was used in paste, which avoided the complicated process with reductive atmosphere, achieved a simple sintering process under nitrogen or vacuum. The sintering behavior of Cu particles in different sintering atmosphere was investigated. Also, a Cu paste with self-reduction and self-protection solvent was designed to achieve improved performance. It is proved that the paste could reduce itself even at room temperature and could protect from being oxidized in sintering.

In Chapter 4, the joints by using the developed Cu paste were tested both by high temperature exposure and by thermal cycling, by humidity exposure. The evolution of microstructure and phase compositions were observed. A real device structure was fabricated by bonding a SiC die to a DBC substrate. Thermal cycle test was carried out. The changes of microstructure and of thermal performance were evaluated to understand the reliability of Cu joints.

In Chapter 5, the results were summarized and future prospect will be mentioned.

## References

- [1] J. Millán, A review of WBG power semiconductor devices, in: CAS 2012 (International Semiconductor Conference), IEEE, 2012, pp. 57-66.
- [2] B.J. Baliga, Fundamentals of power semiconductor devices, Springer Science & Business Media, 2010.
- [3] P.R. Morris, A history of the world semiconductor industry, IET, 1990.
- [4] K. Rajashekara, Z.J. Shen, Power Semiconductor Devices, in: Power Systems, CRC Press, 2016, pp. 370-378.
- [5] B.J. Baliga, Trends in power semiconductor devices, IEEE Transactions on electron Devices, 43 (1996) 1717-1731.
- [6] J.R. Brews, A charge-sheet model of the MOSFET, Solid-State Electronics, 21 (1978) 345-355.
- [7] A.R. Hefner Jr, D.L. Blackburn, An analytical model for the steady-state and transient characteristics of the power insulated-gate bipolar transistor, Solid-State Electronics, 31 (1988) 1513-1532.
- [8] B.B. Jayant, Silicon carbide power devices, World scientific, 2006.
- [9] B.K. Bose, Power electronics and motor drives: advances and trends, Elsevier, 2010.
- [10] J. Moll, M. Tanenbaum, J. Goldey, N. Holonyak, PNP transistor switches, Proceedings of the IRE, 44 (1956) 1174-1182.
- [11] H.S. Chin, K.Y. Cheong, A.B. Ismail, A review on die attach materials for SiC-based high-temperature power devices, Metallurgical and Materials Transactions B, 41 (2010) 824-832.
- [12] B. Ozpinci, L. Tolbert, S. Islam, M. Chinthavali, Comparison of wide bandgap semiconductors for power applications, in: Proceedings of the 10th Conference on Power Electronics and Applications, EPE, 2003.
- [13] L.A. Navarro, X. Perpina, P. Godignon, J. Montserrat, V. Banu, M. Vellvehi, X. Jorda, Thermomechanical assessment of die-attach materials for wide bandgap semiconductor devices and harsh environment applications, IEEE transactions on Power Electronics, 29 (2014) 2261-2271.
- [14] O. Deblecker, Z. De Grève, C. Versèle, Comparative Study of Optimally Designed DC-DC Converters with SiC and Si Power Devices, in: Advanced Silicon Carbide Devices and Processing, IntechOpen, 2015.
- [15] R. Singh, Reliability and performance limitations in SiC power devices, Microelectronics reliability, 46 (2006) 713-730.
- [16] H. Matsunami, Current SiC technology for power electronic devices beyond Si, Microelectronic Engineering, 83 (2006) 2-4.
- [17] U.K. Mishra, L. Shen, T.E. Kazior, Y.-F. Wu, GaN-based RF power devices and amplifiers, Proceedings of the IEEE, 96 (2008) 287-305.

- [18] C. Buttay, D. Planson, B. Allard, D. Bergogne, P. Bevilacqua, C. Joubert, M. Lazar, C. Martin, H. Morel, D. Tournier, State of the art of high temperature power electronics, *Materials Science and Engineering: B*, 176 (2011) 283-288.
- [19] J.N. Calata, J.G. Bai, X. Liu, S. Wen, G.-Q. Lu, Three-dimensional packaging for power semiconductor devices and modules, *IEEE Transactions on Advanced Packaging*, 28 (2005) 404-412.
- [20] J. Lutz, H. Schlangenotto, U. Scheuermann, R. De Doncker, Semiconductor power devices, *Physics, characteristics, reliability*, 2 (2011).
- [21] V.R. Manikam, K.Y. Cheong, Die attach materials for high temperature applications: A review, *IEEE Transactions on Components, Packaging and Manufacturing Technology*, 1 (2011) 457-478.
- [22] H. Ma, J.C. Suhling, A review of mechanical properties of lead-free solders for electronic packaging, *Journal of materials science*, 44 (2009) 1141-1158.
- [23] T. Siewert, *Properties of lead-free solders*, (2002).
- [24] L. Coppola, D. Huff, F. Wang, R. Burgos, D. Boroyevich, Survey on high-temperature packaging materials for SiC-based power electronics modules, in: *2007 IEEE Power Electronics Specialists Conference*, IEEE, 2007, pp. 2234-2240.
- [25] T. McNutt, B. Passmore, J. Fraley, B. McPherson, R. Shaw, K. Olejniczak, A. Lostetter, High-performance, wide-bandgap power electronics, *Journal of electronic materials*, 43 (2014) 4552-4559.
- [26] R. Thokala, J. Chaudhuri, Calculated elastic constants of wide band gap semiconductor thin films with a hexagonal crystal structure for stress problems, *Thin Solid Films*, 266 (1995) 189-191.
- [27] K. Kim, W.R. Lambrecht, B. Segall, Elastic constants and related properties of tetrahedrally bonded BN, AlN, GaN, and InN, *Physical Review B*, 53 (1996) 16310.
- [28] K. Zeng, R. Stierman, D. Abbott, M. Murtuza, Root cause of black pad failure of solder joints with electroless nickel/immersion gold plating, in: *Thermal and Thermomechanical Proceedings 10th Intersociety Conference on Phenomena in Electronics Systems*, 2006. IThERM 2006., IEEE, 2006, pp. 1111-1119.
- [29] C. Chen, S. Nagao, K. Suganuma, J. Jiu, H. Zhang, T. Sugahara, T. Iwashige, K. Sugiura, K. Tsuruta, Self-healing of cracks in Ag joining layer for die-attachment in power devices, *Applied Physics Letters*, 109 (2016) 093503.
- [30] K. Kim, S. Huh, K. Suganuma, Effects of intermetallic compounds on properties of Sn–Ag–Cu lead-free soldered joints, *Journal of Alloys and compounds*, 352 (2003) 226-236.
- [31] S. Menon, E. George, M. Osterman, M. Pecht, High lead solder (over 85%) solder in the electronics industry: RoHS exemptions and alternatives, *Journal of Materials Science: Materials in Electronics*, 26 (2015) 4021-4030.

- [32] D. Ivey, Microstructural characterization of Au/Sn solder for packaging in optoelectronic applications, *Micron*, 29 (1998) 281-287.
- [33] S. Anhock, H. Oppermann, C. Kallmayer, R. Aschenbrenner, L. Thomas, H. Reichl, Investigations of Au-Sn alloys on different end-metallizations for high temperature applications [solders], in: *Twenty Second IEEE/CPMT International Electronics Manufacturing Technology Symposium. IEMT-Europe 1998. Electronics Manufacturing and Development for Automotives (Cat. No. 98CH36204)*, IEEE, 1998, pp. 156-165.
- [34] V. Chidambaram, J. Hald, J. Hattel, Development of Au-Ge based candidate alloys as an alternative to high-lead content solders, *Journal of alloys and compounds*, 490 (2010) 170-179.
- [35] T. Shimizu, H. Ishikawa, I. Ohnuma, K. Ishida, Zn-Al-Mg-Ga alloys as Pb-free solder for die-attaching use, *Journal of electronic materials*, 28 (1999) 1172-1175.
- [36] N. Kang, H.S. Na, S.J. Kim, C.Y. Kang, Alloy design of Zn-Al-Cu solder for ultra high temperatures, *Journal of Alloys and compounds*, 467 (2009) 246-250.
- [37] S. Kim, K.-S. Kim, S.-S. Kim, K. Sukanuma, Interfacial reaction and die attach properties of Zn-Sn high-temperature solders, *Journal of Electronic Materials*, 38 (2009) 266-272.
- [38] J.-M. Song, H.-Y. Chuang, Z.-M. Wu, Interfacial reactions between Bi-Ag high-temperature solders and metallic substrates, *Journal of Electronic Materials*, 35 (2006) 1041-1049.
- [39] A. El-Daly, Y. Swilem, A. Hammad, Creep properties of Sn-Sb based lead-free solder alloys, *Journal of Alloys and Compounds*, 471 (2009) 98-104.
- [40] K. Sukanuma, S.-J. Kim, K.-S. Kim, High-temperature lead-free solders: Properties and possibilities, *JOM Journal of the Minerals, Metals and Materials Society*, 61 (2009) 64-71.
- [41] J.-W. Yoon, H.-S. Chun, S.-B. Jung, Liquid-state and solid-state interfacial reactions of fluxless-bonded Au-20Sn/ENIG solder joint, *Journal of Alloys and Compounds*, 469 (2009) 108-115.
- [42] V. Chidambaram, J. Hattel, J. Hald, High-temperature lead-free solder alternatives, *Microelectronic Engineering*, 88 (2011) 981-989.
- [43] K. Chu, Y. Sohn, C. Moon, A comparative study of Cu/Sn/Cu and Ni/Sn/Ni solder joints for low temperature stable transient liquid phase bonding, *Scripta Materialia*, 109 (2015) 113-117.
- [44] J.-B. Lee, H.-Y. Hwang, M.-W. Rhee, Reliability investigation of Cu/In TLP bonding, *Journal of Electronic Materials*, 44 (2015) 435-441.
- [45] W. MacDonald, T. Eagar, Transient liquid phase bonding, *Annual review of materials science*, 22 (1992) 23-46.

- [46] G.O. Cook, C.D. Sorensen, Overview of transient liquid phase and partial transient liquid phase bonding, *Journal of materials science*, 46 (2011) 5305-5323.
- [47] J. Li, P. Agyakwa, C. Johnson, Interfacial reaction in Cu/Sn/Cu system during the transient liquid phase soldering process, *Acta Materialia*, 59 (2011) 1198-1211.
- [48] A.A. Bajwa, Y. Qin, R. Reiner, R. Quay, J. Wilde, Assembly and packaging technologies for high-temperature and high-power GaN devices, *IEEE Transactions on Components, Packaging and Manufacturing Technology*, 5 (2015) 1402-1416.
- [49] B.J. Grummel, Z.J. Shen, H.A. Mustain, A.R. Hefner, Thermo-mechanical characterization of Au-In transient liquid phase bonding die-attach, *IEEE Transactions on Components, Packaging and Manufacturing Technology*, 3 (2013) 716-723.
- [50] H.A. Mustain, W.D. Brown, S.S. Ang, Transient liquid phase die attach for high-temperature silicon carbide power devices, *IEEE transactions on components and packaging technologies*, 33 (2010) 563-570.
- [51] S.W. Yoon, M.D. Glover, K. Shiozaki, Nickel–tin transient liquid phase bonding toward high-temperature operational power electronics in electrified vehicles, *IEEE Transactions on Power Electronics*, 28 (2013) 2448-2456.
- [52] X. Liu, S. He, H. Nishikawa, Thermally stable Cu<sub>3</sub>Sn/Cu composite joint for high-temperature power device, *Scripta Materialia*, 110 (2016) 101-104.
- [53] C. Oh, S. Nagao, T. Kunimune, K. Suganuma, Pressureless wafer bonding by turning hillocks into abnormal grain growths in Ag films, *Applied Physics Letters*, 104 (2014) 161603.
- [54] C. Oh, S. Nagao, T. Sugahara, K. Suganuma, Hillock growth dynamics for Ag stress migration bonding, *Materials Letters*, 137 (2014) 170-173.
- [55] C. Oh, S. Nagao, K. Suganuma, Silver stress migration bonding driven by thermomechanical stress with various substrates, *Journal of Materials Science: Materials in Electronics*, 26 (2015) 2525-2530.
- [56] K. Suganuma, S. Nagao, T. Sugahara, E. Yokoi, H. Zhang, J. Jiu, Silver sinter joining and stress migration bonding for WBG die-attach, in: 2016 International Symposium on 3D Power Electronics Integration and Manufacturing (3D-PEIM), IEEE, 2016, pp. 1-17.
- [57] H. Schwarzbauer, R. Kuhnert, Novel large area joining technique for improved power device performance, in: Conference Record of the IEEE Industry Applications Society Annual Meeting, IEEE, 1989, pp. 1348-1351.
- [58] C. Buttay, A. Masson, J. Li, M. Johnson, M. Lazar, C. Raynaud, H. Morel, Die Attach of Power Devices Using Silver Sintering – Bonding Process Optimisation and Characterization, 2011.

- [59] G.C. Kuczynski, Self-diffusion in sintering of metallic particles, in: *Sintering Key Papers*, Springer, 1990, pp. 509-527.
- [60] J. Pan, Solid-state diffusion under a large driving force and the sintering of nanosized particles, *Philosophical magazine letters*, 84 (2004) 303-310.
- [61] S. Soichi, K. Suganuma, Low-Temperature and Low-Pressure Die Bonding Using Thin Ag-Flake and Ag-Particle Pastes for Power Devices, *IEEE Transactions on Components, Packaging and Manufacturing Technology*, 3 (2013) 923-929.
- [62] J. Li, X. Li, L. Wang, Y.-H. Mei, G.-Q. Lu, A novel multiscale silver paste for die bonding on bare copper by low-temperature pressure-free sintering in air, *Materials & Design*, 140 (2018) 64-72.
- [63] S.-k. Lin, S. Nagao, E. Yokoi, C. Oh, H. Zhang, Y.-c. Liu, S.-g. Lin, K. Suganuma, Nano-volcanic eruption of silver, *Scientific reports*, 6 (2016) 34769.
- [64] S.A. Paknejad, S.H. Mannan, Review of silver nanoparticle based die attach materials for high power/temperature applications, *Microelectronics Reliability*, 70 (2017) 1-11.
- [65] K. Woo, D. Kim, J.S. Kim, S. Lim, J. Moon, Ink-Jet printing of Cu– Ag-based highly conductive tracks on a transparent substrate, *Langmuir*, 25 (2008) 429-433.
- [66] Y.-S. Goo, Y.-I. Lee, N. Kim, K.-J. Lee, B. Yoo, S.-J. Hong, J.-D. Kim, Y.-H. Choa, Ink-jet printing of Cu conductive ink on flexible substrate modified by oxygen plasma treatment, *Surface and Coatings Technology*, 205 (2010) S369-S372.
- [67] J. Niittynen, E. Sowade, H. Kang, R.R. Baumann, M. Mäntysalo, Comparison of laser and intense pulsed light sintering (IPL) for inkjet-printed copper nanoparticle layers, *Scientific Reports*, 5 (2015) 8832.
- [68] S.T. Pai, J.P. Marton, Electromigration in metals, *Canadian Journal of Physics*, 55 (1977) 103-115.
- [69] P.S. Ho, H. Huntington, Electromigration and void observation in silver, *Journal of Physics and Chemistry of Solids*, 27 (1966) 1319-1329.
- [70] J. Kahler, N. Heuck, A. Wagner, A. Stranz, E. Peiner, A. Waag, Sintering of copper particles for die attach, *Components, Packaging and Manufacturing Technology*, *IEEE Transactions on*, 2 (2012) 1587-1591.
- [71] T. Fujimoto, T. Ogura, T. Sano, M. Takahashi, A. Hirose, Joining of Pure Copper Using Cu Nanoparticles Derived from CuO Paste, *MATERIALS TRANSACTIONS*, (2015).
- [72] H. Nishikawa, T. Hirano, T. Takemoto, N. Terada, Effects of joining conditions on joint strength of Cu/Cu joint using Cu nanoparticle paste, *Open Surface Science Journal*, 3 (2011) 60-64.
- [73] S. Park, R. Uwataki, S. Nagao, T. Sugahara, Y. Katoh, H. Ishino, K. Sugiura, K. Tsuruta, K. Suganuma, Low-pressure sintering bonding with Cu and CuO flake

- paste for power devices, in: Electronic Components and Technology Conference (ECTC), 2014 IEEE 64th, IEEE, 2014, pp. 1179-1182.
- [74] X. Liu, H. Nishikawa, Low-pressure Cu-Cu bonding using in-situ surface-modified microscale Cu particles for power device packaging, *Scripta Materialia*, 120 (2016) 80-84.
- [75] S. Sun, Q. Guo, H. Chen, M. Li, C. Wang, Solderless bonding with nanoporous copper as interlayer for high-temperature applications, *Microelectronics Reliability*, 80 (2018) 198-204.
- [76] N.L. Peterson, Self-diffusion in pure metals, *Journal of Nuclear Materials*, 69-70 (1978) 3-37.
- [77] L. Liu, F. Li, L. Tan, L. Ming, Y. Yi, Effects of nanometer Ni, Cu, Al and NiCu powders on the thermal decomposition of ammonium perchlorate, *Propellants, Explosives, Pyrotechnics*, 29 (2004) 34-38.
- [78] M. Salavati-Niasari, F. Davar, N. Mir, Synthesis and characterization of metallic copper nanoparticles via thermal decomposition, *Polyhedron*, 27 (2008) 3514-3518.
- [79] M.-S. Yeh, Y.-S. Yang, Y.-P. Lee, H.-F. Lee, Y.-H. Yeh, C.-S. Yeh, Formation and characteristics of Cu colloids from CuO powder by laser irradiation in 2-propanol, *The Journal of Physical Chemistry B*, 103 (1999) 6851-6857.
- [80] M. Abdulla-Al-Mamun, Y. Kusumoto, M. Muruganandham, Simple new synthesis of copper nanoparticles in water/acetonitrile mixed solvent and their characterization, *Materials Letters*, 63 (2009) 2007-2009.
- [81] M. Biçer, İ. Şişman, Controlled synthesis of copper nano/microstructures using ascorbic acid in aqueous CTAB solution, *Powder Technology*, 198 (2010) 279-284.
- [82] T. Yamauchi, Y. Tsukahara, T. Sakata, H. Mori, T. Yanagida, T. Kawai, Y. Wada, Magnetic Cu-Ni (core-shell) nanoparticles in a one-pot reaction under microwave irradiation, *Nanoscale*, 2 (2010) 515-523.
- [83] H.-J. Lee, G. Lee, N.R. Jang, J.H. Yun, J.Y. Song, B.S. Kim, Biological synthesis of copper nanoparticles using plant extract, *Nanotechnology*, 1 (2011) 371-374.
- [84] H.J. Lee, J.Y. Song, B.S. Kim, Biological synthesis of copper nanoparticles using *Magnolia kobus* leaf extract and their antibacterial activity, *Journal of Chemical Technology & Biotechnology*, 88 (2013) 1971-1977.
- [85] W. Chen, L. Li, Q. Peng, Y. Li, Polyol synthesis and chemical conversion of Cu<sub>2</sub>O nanospheres, *Nano Research*, 5 (2012) 320-326.
- [86] A.R. Tao, S. Habas, P. Yang, Shape control of colloidal metal nanocrystals, *small*, 4 (2008) 310-325.
- [87] J. Jiu, H. Zhang, S. Koga, S. Nagao, Y. Izumi, K. Suganuma, Simultaneous synthesis of nano and micro-Ag particles and their application as a die-attachment material, *Journal of Materials Science: Materials in Electronics*, 26 (2015) 7183-7191.

- [88] K.J. Carroll, J.U. Reveles, M.D. Shultz, S.N. Khanna, E.E. Carpenter, Preparation of elemental Cu and Ni nanoparticles by the polyol method: an experimental and theoretical approach, *The Journal of Physical Chemistry C*, 115 (2011) 2656-2664.
- [89] D.M. Clifford, C.E. Castano, A.J. Lu, E.E. Carpenter, Synthesis of FeCo alloy magnetically aligned linear chains by the polyol process: structural and magnetic characterization, *Journal of Materials Chemistry C*, 3 (2015) 11029-11035.
- [90] Y. Kobayashi, T. Shirochi, Y. Yasuda, T. Morita, Metal–metal bonding process using metallic copper nanoparticles prepared in aqueous solution, *International Journal of Adhesion and Adhesives*, 33 (2012) 50-55.
- [91] T. Ishizaki, R. Watanabe, A new one-pot method for the synthesis of Cu nanoparticles for low temperature bonding, *Journal of Materials Chemistry*, 22 (2012) 25198-25206.
- [92] S. Krishnan, A. Haseeb, M.R. Johan, Preparation and low-temperature sintering of Cu nanoparticles for high-power devices, *Components, Packaging and Manufacturing Technology, IEEE Transactions on*, 2 (2012) 587-592.
- [93] T. Yamakawa, T. Takemoto, M. Shimoda, H. Nishikawa, K. Shiokawa, N. Terada, Influence of joining conditions on bonding strength of joints: efficacy of low-temperature bonding using Cu nanoparticle paste, *Journal of electronic materials*, 42 (2013) 1260-1267.
- [94] R. Watanabe, T. Ishizaki, High -Strength Pressure -Free Bonding Using Cu and Ni - Sn Nanoparticles, *Particle & Particle Systems Characterization*, (2014).
- [95] T. Ishizaki, K. Akedo, T. Satoh, R. Watanabe, Pressure-Free Bonding of Metallic Plates with Ni Affinity Layers Using Cu Nanoparticles, *Journal of Electronic Materials*, 43 (2014) 774-779.
- [96] Y. Kobayashi, Y. Abe, T. Maeda, Y. Yasuda, T. Morita, A metal–metal bonding process using metallic copper nanoparticles produced by reduction of copper oxide nanoparticles, *Journal of materials research and technology*, 3 (2014) 114-121.
- [97] T. Satoh, T. Ishizaki, Enhanced pressure-free bonding using mixture of Cu and NiO nanoparticles, *Journal of Alloys and Compounds*, 629 (2015) 118-123.
- [98] J. Liu, H. Chen, H. Ji, M. Li, Highly Conductive Cu–Cu Joint Formation by Low-Temperature Sintering of Formic Acid-Treated Cu Nanoparticles, *ACS Applied Materials & Interfaces*, 8 (2016) 33289-33298.
- [99] J. Li, X. Yu, T. Shi, C. Cheng, J. Fan, S. Cheng, G. Liao, Z. Tang, Low-Temperature and Low-Pressure Cu–Cu Bonding by Highly Sinterable Cu Nanoparticle Paste, *Nanoscale research letters*, 12 (2017) 255.
- [100] J.-W. Yoon, J.-H. Back, Effect of Sintering Conditions on the Mechanical Strength of Cu-Sintered Joints for High-Power Applications, *Materials*, 11 (2018) 2105.
- [101] Y. Mou, Y. Peng, Y. Zhang, H. Cheng, M. Chen, Cu-Cu bonding enhancement at low temperature by using carboxylic acid surface-modified Cu nanoparticles,

- Materials Letters, 227 (2018) 179-183.
- [102] Y. Jianfeng, Z. Guisheng, H. Anming, Y.N. Zhou, Preparation of PVP coated Cu NPs and the application for low-temperature bonding, *Journal of Materials Chemistry*, 21 (2011) 15981-15986.
- [103] T. Fujimoto, T. Ogura, T. Sano, M. Takahashi, A. Hirose, Joining of Pure Copper Using Cu Nanoparticles Derived from CuO Paste, *MATERIALS TRANSACTIONS*, 56 (2015) 992-996.
- [104] Y.Y. Dai, M.Z. Ng, P. Anantha, Y.D. Lin, Z.G. Li, C.L. Gan, C.S. Tan, Enhanced copper micro/nano-particle mixed paste sintered at low temperature for 3D interconnects, *Applied Physics Letters*, 108 (2016) 263103.
- [105] H. Niu, A review of power cycle driven fatigue, aging, and failure modes for semiconductor power modules, in: 2017 IEEE International Electric Machines and Drives Conference (IEMDC), IEEE, 2017, pp. 1-8.

## **Chapter 2**

### **One-step synthesis of bimodal Cu particles**



## 2.1 Introduction

Bimodal metallic particles, which contain two types of particles with different sizes, have been proven to be a better kind material for fabrication of sinter wiring and joining because of their dense packing effect [1-4]. Tam et al. fabricated bimodal Cu paste by mixing micron Cu flakes and Cu nanoparticles, which contributed to excellent Cu wirings with much lower resistivity due to the size matching effect. The performance of the Cu wirings were superior to all other Cu wirings composed by sole nano or micro-Cu particle pastes [2]. Dai et al. also found that the Cu joints sintered with bimodal Cu paste showed a much higher shear strength than that of sole nano or micro-Cu particles pastes [3]. While these results proved that bimodal Cu particle pastes can deliver superior sintering performance, the fabrication of desired bimodal Cu particles is still challenging.

Generally, bimodal Cu particles are fabricated by multistep process consisting of synthesizing two different sizes of Cu particles separately and following mechanical mixing process. The process always increases the exposure of Cu particle to air atmosphere leading to serious surface oxidization of Cu particles [5]. Especially, the smaller the particle, the greater the chance of oxidation for Cu particles even at room temperature. This oxide layer on the surface of the Cu particles hinders its sintering of Cu particles or has to be removed through a reduction process with high temperature. Therefore, suitable synthesis method of bimodal Cu particles should be carefully considered to simplify the fabrication process and minimize the oxidation probability of the Cu particles.

Among the various synthesis methods, polyol method is a possible method to synthesize bimodal Cu particles by one step. The polyol method is a popular and effective way to synthesize metallic, metal oxide, and alloy particles with various morphology and diameter. The process is simple and easily controllable by adjusting reaction time, temperature, reagents such as capping agents, direction-growth controlling agents, and metal sources [6-10]. For example, Kyler et. al. fabricated Cu nanoparticles with various

morphologies and diameters by changing the chain length of polyol solvents [9]. Park. et. al reported synthesis monodisperse Cu particles by polyol method, and they also pointed out the possibility of synthesizing polydisperse Cu particle with wide size distribution by adjusting synthesis condition. However, the nucleation mechanism, the growth process of Cu particles, the relationship between Cu particles size and size distribution and solvent, additive and reaction time are still unclear.

Herein, the effect of reaction parameters, such Cu sources and additives, on the size, size distribution and morphology of Cu particles was carefully investigated. Soluble  $\text{Cu}(\text{NO}_3)_2$  and insoluble  $\text{Cu}(\text{OH})_2$  were used as Cu source. Sodium sulfide ( $\text{Na}_2\text{S}$ ), which was widely used as size controlling agent [11, 12], was applied in the synthesis. The result showed insoluble Cu source is suitable for the formation of bimodal Cu particles as they provide a slow and steady supply of fresh Cu nuclei which modify the nucleation and growth of Cu particles. Moreover,  $\text{Na}_2\text{S}$  additive has accelerated the growth of Cu particles due to its reduction capability. After the synthesis process, the obtained bimodal Cu particles were mixed with a solvent to make Cu pastes for the fabrication of sintered Cu joint for high power devices. The effect of Cu particle size distribution on the shear strength of Cu joints was investigated. In addition, the effect of Cu particle oxidization on the performance of joints was also discussed.

## **2.2 Experiments**

### **2.2.1 Cu particles preparation**

Soluble or insoluble Cu sources and various amount of  $\text{Na}_2\text{S}$  additive was added into the reaction system to control the size and size distribution of Cu particles. In detail, polyvinyl pyrrolidone (PVP) was firstly dispersed into a solution of 1,3-propanediol (PDO) in a flask. After PVP was completely dissolved and the PDO solution became transparent again, Copper nitrate ( $\text{Cu}(\text{NO}_3)_2$ , soluble) or Copper hydroxide ( $\text{Cu}(\text{OH})_2$ , insoluble) was introduced into the mixture solution for uniform dissolution/dispersion. After that, various amounts of  $\text{Na}_2\text{S}$  additive was added to the solution. The solution was

then immediately placed in a thermostat heating mantle preheated to 190 °C and kept in air for at least 60 min. The solution color slowly changed to red, implying the formation of Cu particles. Lastly, the reaction products were centrifuged at speed of 6000 rpm and washed with ethanol for four or five times in air to remove residuals, excess solvent, and PVP. The final red precipitation was kept in ethanol at room temperature for further use. Table.2.1 shows the detailed recipes of various synthesized Cu samples.

Table 2. 1 Reagent of synthesis groups

s	PDO(ml)	Cu(NO <sub>3</sub> ) <sub>2</sub> (mM)	Cu(OH) <sub>2</sub> (mM)	PVP (μM)	Na <sub>2</sub> S (μM)
<b>Sample I</b>	100	150	-	24	-
<b>Sample II</b>	100	-	150	24	-
<b>Sample III</b>	100	150	-	24	75
<b>Sample IV</b>	100	150	-	24	150
<b>Sample V</b>	100	-	150	24	75
<b>Sample VI</b>	100	-	150	24	150

### 2.2.2 Characterization of Cu particles

X-ray diffraction (XRD, RINT2500 Rigaku, Japan) was used to identify the phases of the product with a CuK $\alpha$  ( $\lambda = 0.154$  nm) radiation source, operating at a voltage of 40 kV and a current of 30 mA, respectively. The morphologies of Cu particles were examined by field emission scanning electron microscope (FE-SEM, SU8020, Hitachi). The size and distribution of Cu particles were evaluated by laser diffraction systems (MT3000II, Microtrac) and dynamic light scattering (DLS) with an ELS-Z (V670, JASCO Corp.) particle analyzer. Ultraviolet-visible (UV-Vis) absorption spectra of the samples dispersed in ethanol were measured using a UV-visible-near infrared spectrophotometer (V670, JASCO Corp.) in order to examine the formation of Cu particles by the surface plasmon resonance.

### 2.2.3 Fabrication and evaluation of Cu joints

Two Cu plates were bonded to evaluate the sintered joints with the synthesized Cu particles. The Cu plates for bonding experiments were square plates: 8 mm×8 mm×1 mm for a substrate and 4 mm×4 mm×0.8 mm for a dummy chip. These plates were polished with 4000 abrasive paper to remove the surface contamination. Cu pastes were prepared by mixing the synthesized Cu particles and ethylene glycol (EG) solvent at a weight ratio of 85 : 15. The Cu pastes were first printed onto a Cu substrate by using a 4 mm×4 mm×0.1 mm stainless steel mask. A Cu dummy chip was then placed on the printed Cu paste. The Cu joints were sintered in nitrogen (N<sub>2</sub>) or formic acid atmosphere from 250 °C to 350 °C for 30 min with a slight assisting pressure of 0.4 MPa after drying in the air for several minutes. The vacuum condition was retained to 1 mbar. The mechanical property of the metallic Cu joint was evaluated by the shear test (DAGE, series 4000) with a shear strain rate of 1 mm/min.

## 2.3 Results and discussion

### 2.3.1 The effect of soluble/insoluble Cu salt on Cu particles

Fig. 2.1a and 2.1b show the FE-SEM micrographs of Cu particles synthesized with soluble Cu(NO<sub>3</sub>)<sub>2</sub> (Sample I) and insoluble Cu(OH)<sub>2</sub> (Sample II) under the same conditions. Synthesized Cu particles in both of the cases had a wide size range from tens to hundreds of nanometers. But the obvious difference was that the small particles in sample II were very much smaller than those in Sample I. Fig. 2.1c and 2.1d show the size distribution of Cu particles obtained by the laser diffraction systems. Big size distribution peak (main peak) was observed in the two cases, which were 0.53 μm and 0.49 μm for Sample I and Sample II respectively. Moreover, Sample I had a clear small size distribution peak (side-peak) of 0.19 μm in the low-diameter range. This result indicated that the Cu particles synthesized with soluble Cu(NO<sub>3</sub>)<sub>2</sub> (Sample I) also had bimodal characteristics. On the other hand, the relative size distribution of Cu particles obtained by the laser diffraction systems did not respond to the actual situation in Sample II because the measurement range of the laser diffraction system is 0.1-10 μm. From FE-SEM observation, the small particles in Sample II were almost all below 100 nm, which

was undetectable for the laser diffraction systems. Thus, the DLS method was used to measure the size distribution of small particles because the DLS method was strong enough for the measurement of small particles, especially for nanometer scale. The as-synthesized particles were dispersed into ethanol and kept in room temperature to 12 h for natural subsidence of big particles. After that, the supernatant containing small particles was examined by DLS. The results are showed in the insert images of Fig 2.1c and 2.1d. The results show the mean particles size of small particles obtained in sample I, II were  $183.2 \pm 17.1$  and  $74.8 \pm 8.2$  nm, respectively. The mean size of small particles in Sample I also corresponded to the side-peak detected by laser diffraction systems showed in Fig. 2.1c ( $0.19 \mu\text{m}$ ). The corresponding FE-SEM images were showed in Fig. S2.2 These small particles have a diameter less than 300 nm in the case of Sample I while most of particles in Sample II have a diameter below 200 nm. The results consistent with the DLS results and supported the bimodal morphology of particles. Fig. 2.1e shows the XRD pattern of these synthesized Cu particles. In both samples, three main characteristic peaks located at  $2\theta = 43.3^\circ$ ,  $50.4^\circ$ , and  $74.08^\circ$  were detected, which corresponded to diffraction of planes (111), (200), and (220) of the face-centered cubic (fcc) Cu crystal, respectively. No impurity phases such as CuO, Cu<sub>2</sub>O, or Cu(OH)<sub>2</sub> were observed. The XRD results indicated pure Cu particles could be successfully synthesized in air by the one-step polyol process.

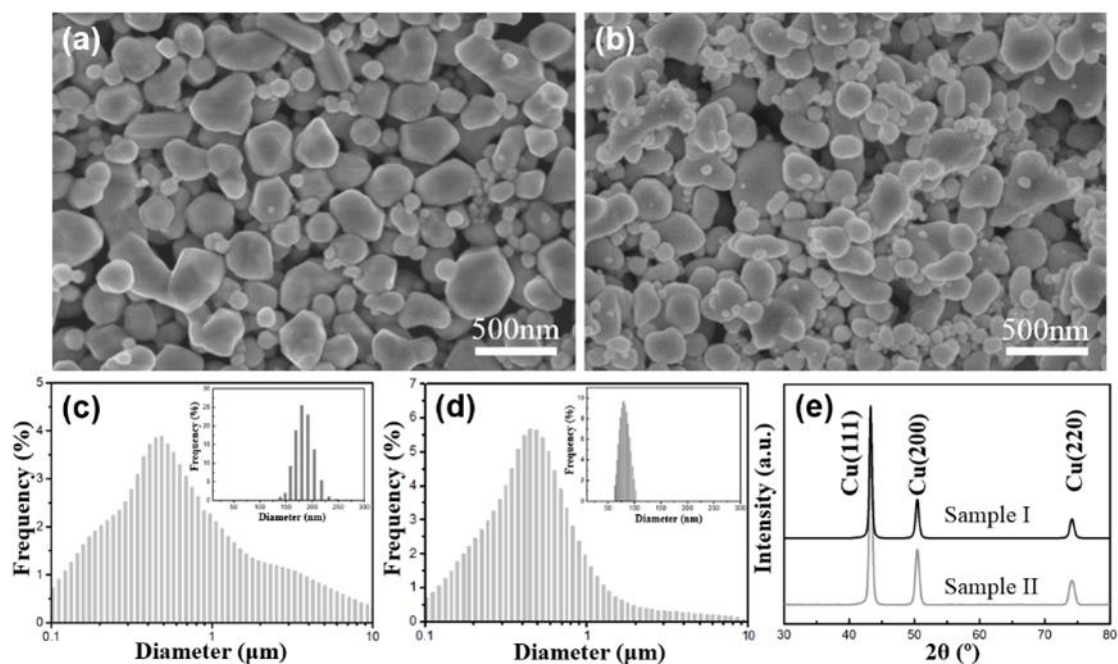


Fig. 2. 1 FE-SEM micrographs, size distribution and corresponding XRD patterns (e) of Sample I (a, c, e) and Sample II (b, d, e), the insert images in 1c and id indicate the size distribution measured by DLS of the supernatant of Sample I and Sample II.

The synthesis process was recorded by the photos of the reacting solution and UV-Vis absorption spectra to understand the reaction. Fig. 2.2 shows the synthesis process of Sample I with soluble  $\text{Cu}(\text{NO}_3)_2$ . At the initial stage, the blue and limpid solution of Sample I attributed to the dissolution of  $\text{Cu}(\text{NO}_3)_2$ . After about 15 min, the solution turned green and cloudy, then turning a dark red color (after about 30 min) which represented the generation of Cu particles. UV-Vis absorption spectra showed a clear absorption peak at around 580 nm appeared at 30 min during synthesis, which was consistent with the color change showed in Fig. 2.2a. This peak is related to the surface plasmon resonance due to the formation of Cu particles [13-15]. The XRD pattern (Fig. 2.2c) also confirmed the formation of Cu particles after the synthesis time of 30 min. Within 30 min, no identifiable characteristics were observed. These results indicated the formation of Cu particles directly related to the reduction process from soluble  $\text{Cu}^{2+}$ .

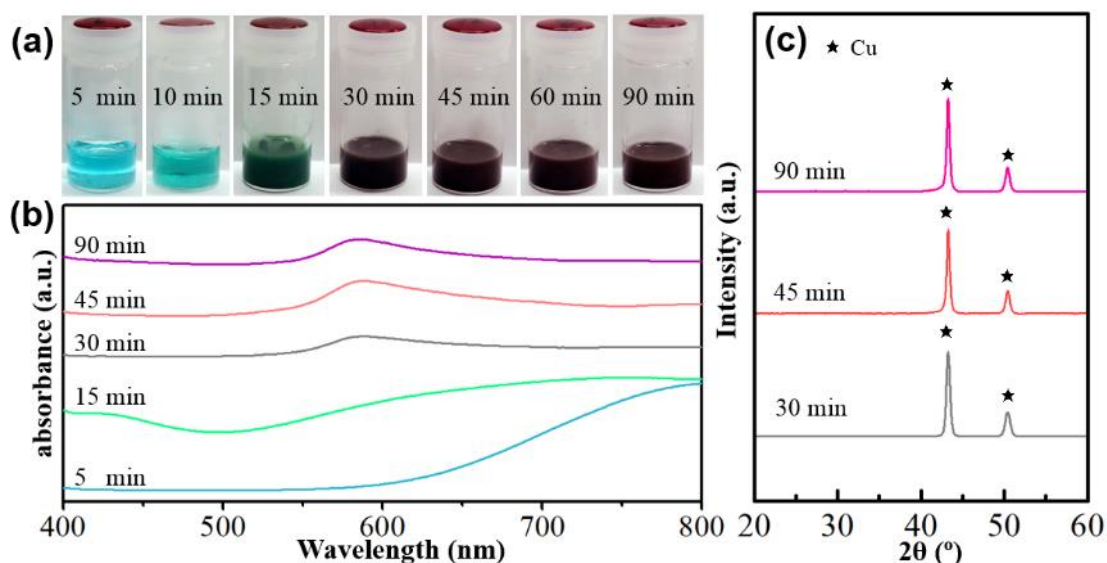


Fig. 2. 2 Color change of reaction solution (a), UV-Vis absorption spectra (b) and XRD patterns (c) during synthesis process of Sample I.

In contrast, the synthesis process is very different when insoluble  $\text{Cu}(\text{OH})_2$  was used. Fig. 2.3 shows the synthesis process of Sample II. The blue suspension solution turned dark green at 10 min then changed to black in 15-30 min which was not observed in the case of soluble  $\text{Cu}(\text{NO}_3)_2$ . The solution became dark red when the time extended to 45 min, and the dark red color did not change until the reaction was completed. UV-Vis absorption spectra showed that the characteristic absorption peak of Cu appeared when the time reached 45 min. The XRD records also confirmed the formation process of Cu particles (Fig. 2.3c). In the beginning of the process, the sample mainly included  $\text{Cu}(\text{OH})_2$  from the Cu source. At the reaction time of 30 mins, the characteristic peaks belonged to CuO was clearly observed. At 45 mins, only characteristic peak belonged to Cu phase were obtained without other impurities peak. The results implied that  $\text{Cu}(\text{OH})_2$  was first changed into CuO, which was further reduced into Cu particles in the polyol synthesis. And the black color of CuO was consistent with the color evolution of solution during the reaction of 15-30 min. In addition, it was noteworthy that  $\text{Cu}(\text{OH})_2$  existed until 30 min, which suggested that  $\text{Cu}(\text{OH})_2$  was slowly transferred into CuO and metallic Cu. After 45 min, both  $\text{Cu}(\text{OH})_2$  and CuO peaks had completely disappeared, only metal Cu peaks

were detected, which corresponded to the red precipitation with a typical Cu absorption peak at around 580 nm in UV-Vis spectra. These results indicated the formation of metal Cu particles from insoluble  $\text{Cu}(\text{OH})_2$  include a continuous reduction of  $\text{Cu}(\text{OH})_2/\text{CuO}$  to Cu, which required a longer reaction time than that from soluble  $\text{Cu}(\text{NO}_3)_2$ .

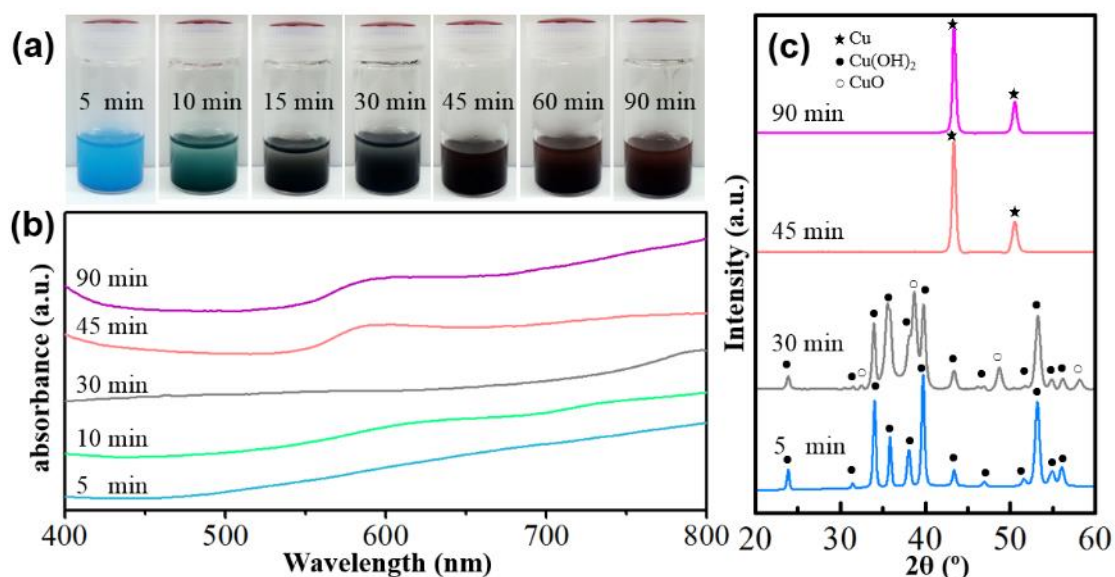


Fig. 2. 3 Color change of reaction solution (a), UV-Vis absorption spectra (b) and XRD patterns (c) during synthesis process of Sample II.

Generally, the formation of metallic particles was described by LaMer's model [16], in which the synthesis of particles is divided into two events: initial nucleation and subsequent growth. The happening of nucleation and growth is determined by the concentration of metallic atoms. Given critical concentration, spontaneous nucleation could take place to form nano-particles (nuclei) when metallic atoms reach the critical concentration, and continuous growth of those nuclei could take place when metallic atoms below the critical concentration. According to this theory, high atom concentration in the initial step contributes to the acceleration of nucleation while decreasing the growth and then achieving monodisperse particles. In the present process, soluble  $\text{Cu}(\text{NO}_3)_2$  provided a relative high atom concentration due to the complete dissolution character of Cu salt, which accelerated the formation of Cu nucleus without insignificant growth.

Therefore most of the synthesized Cu particles maintained uniform size.

In contrast, Cu particles prepared from  $\text{Cu}(\text{OH})_2$  exhibited relative non-uniformity because the insoluble Cu source always underwent a slow dissolution-reduction process. [13, 17]. In present work, the insoluble  $\text{Cu}(\text{OH})_2$  first transferred into  $\text{CuO}$ , then reduced and changed into Cu atoms which provided a steady stream of Cu atoms. Cu nuclei were formed owing to the concentration of Cu atoms and slowly rose and eventually exceeded critical concentration. Because of the steady stream of Cu atoms provided by slow reduction from insoluble Cu source, the concentration of Cu atoms stayed at a high level and fluctuated around the critical concentration of nucleation. This led not only to the growth of old Cu nuclei but also to the multi-step formation of fresh Cu nuclei. Thus, the final Cu particles exhibited a wide size distribution with bimodal type.

### **2.3.2 The effect of $\text{Na}_2\text{S}$ agent**

The  $\text{Na}_2\text{S}$  additive was used to control the size of Cu particles synthesized by soluble  $\text{Cu}(\text{NO}_3)_2$  (sample III and IV). Fig. 2.4 shows SEM images of Samples III and IV with  $\text{Na}_2\text{S}$  concentration of 75  $\mu\text{M}$  and 150  $\mu\text{M}$  (Fig. 2.4a and 2.4b). From SEM observation, both samples included Cu particles with increasing diameter. The significant size increase of Cu particles might correspond to the reducibility and reactivity of  $\text{Na}_2\text{S}$  [11, 12, 18]. Unfortunately, the impurity peak corresponding to  $\text{CuS}$  was clearly detected with XRD patterns (Fig 2.4c).  $\text{CuS}$  particles, several micrometers in diameter, were also observed in FE-SEM (Fig. S2.2). Although the size of Cu particles was controlled by adding  $\text{Na}_2\text{S}$ , the  $\text{CuS}$  impurity was not desirable and harmful to the subsequent sintering process.

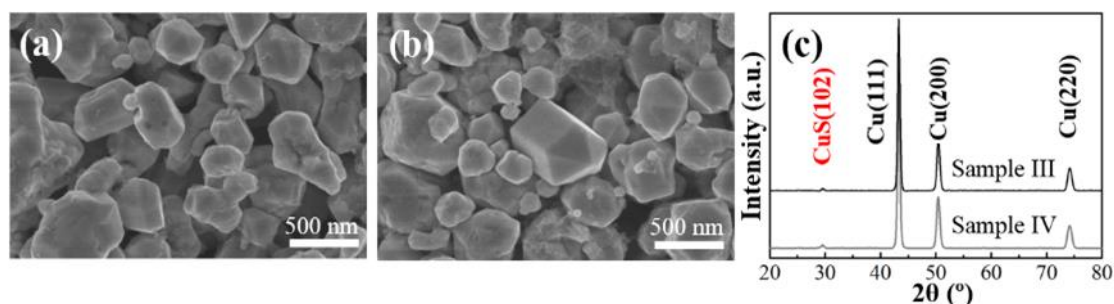


Fig. 2. 4 FE-SEM micrographs of Sample III (a) and Sample IV (b) and corresponding XRD pattern (c).

The  $\text{Na}_2\text{S}$  additive was also added in the synthesis process with insoluble  $\text{Cu}(\text{OH})_2$  source. Fig. 2.5a and 2.5b show the SEM images of Samples V and VI with  $\text{Na}_2\text{S}$  concentration of  $75 \mu\text{M}$  and  $150 \mu\text{M}$ , respectively. From SEM images, the similar morphology Cu particles in Sample II were observed. However, the size of Cu particles was clearly increased with the addition of  $\text{Na}_2\text{S}$ . As  $75 \mu\text{M}$   $\text{Na}_2\text{S}$  was added, the main peak of Cu size distribution was shifted to  $0.69 \mu\text{m}$  with and side-peak shift to  $0.17 \mu\text{m}$  (Fig. 2.5c, sample V). These particles were significantly larger than the synthesized particles formed without the  $\text{Na}_2\text{S}$  additives (Sample I,  $0.49$  and  $0.07 \mu\text{m}$ ). Further increasing the concentration of  $\text{Na}_2\text{S}$  to  $150 \mu\text{M}$  (Sample VI), the main peak shifted to around  $1 \mu\text{m}$  and the side-peak shifted to  $0.24 \mu\text{m}$  (Fig. 2.5d). The XRD patterns of these prepared Cu particles proved that the products from both groups were pure Cu (Fig. 2.5e). The DLS measurement of supernatant was also performed to confirm the size of small particles (Fig. S2.3). The mean diameter of the small particles was  $174.6 \pm 17.1 \text{ nm}$  and  $224.3 \pm 15 \text{ nm}$ , respectively, which was consistent with the FE-SEM observation. This also corresponded to the side-peak detected by laser diffraction systems shown in Fig. 2.5c ( $0.17 \mu\text{m}$ ) and 2.5d ( $0.24 \mu\text{m}$ ).

To conclude, the addition of  $\text{Na}_2\text{S}$  was able to control the size of Cu particles without changing the bimodal morphology and phase of Cu particles which synthesized by polyol method with the existence of insoluble  $\text{Cu}(\text{OH})_2$ . However, the  $\text{Na}_2\text{S}$  additive introduced impure CuS when soluble  $\text{Cu}(\text{NO}_3)_2$  was used as the Cu source.

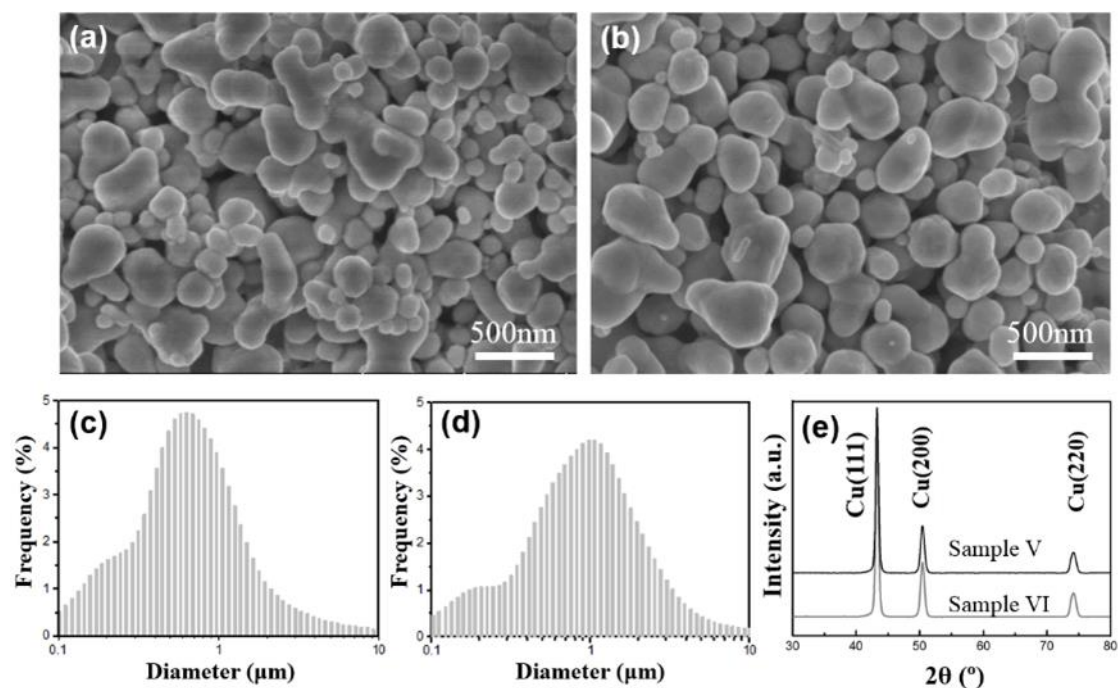


Fig. 2. 5 FE-SEM micrographs, size distribution and corresponding XRD patterns (e) of Sample V (a, c, e) and Sample VI (b, d, e).

To investigate the effects of  $\text{Na}_2\text{S}$  additive on the reaction evolution, the photos of reacted solution, UV-Vis absorption spectra and XRD pattern with different reaction times of Sample IV synthesized with 150  $\mu\text{M}$   $\text{Na}_2\text{S}$  adding were recorded and showed in Fig. 2.6. In the beginning, the synthesis process was similar to that of Sample II where only bright blue  $\text{Cu}(\text{OH})_2$  suspension was observed. However, the solution turned to black at 10-15 min which was earlier than that of Sample II which around 30 min. As reaction time was extended to 30 min, the color of the solution changed to bright red (Fig. 2.6a). The red color indicated the formation of Cu particles, which was also verified by surface UV-vis spectra (Fig. 2.6b) and XRD (Fig. 2.6c). Similarly, CuO peaks were observed before the formation of metallic Cu particles, which confirmed that the CuO was an intermediate from  $\text{Cu}(\text{OH})_2$  to metal Cu. The results showed the existence of  $\text{Na}_2\text{S}$  additive significantly accelerated the formation of metallic Cu particles. In addition, the final solution of Sample VI showed a bright red, which was different from that in (Fig. 2.1b and Fig. 2.3c). This difference in color could attribute to the size effect, as small particles possess a darker color.

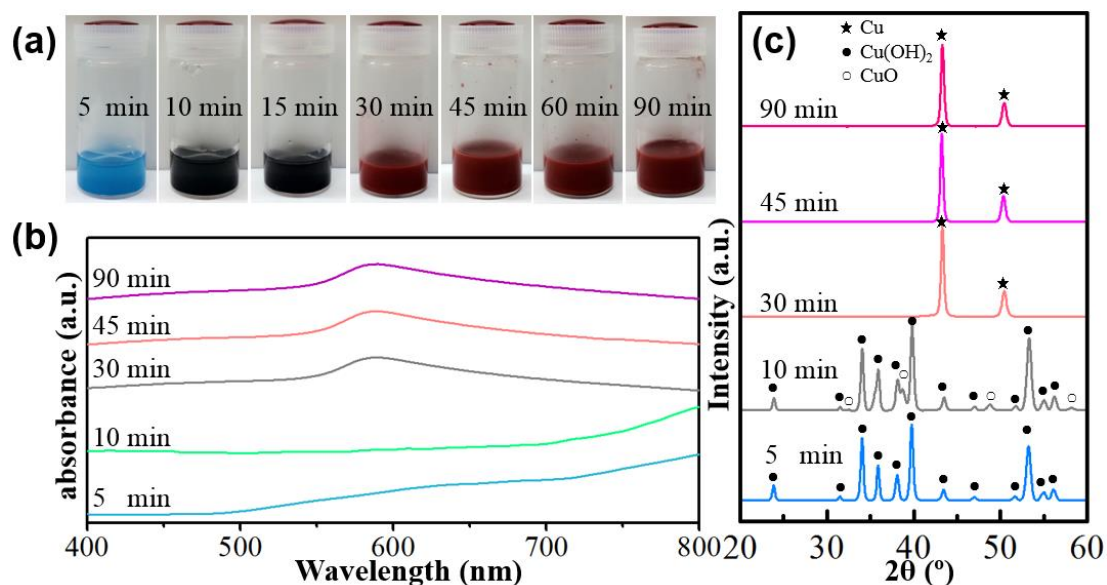


Fig. 2. 6 Color change of reaction solution (a), UV-Vis absorption spectra (b) and XRD patterns (c) during synthesis process of Sample VI.

$\text{Na}_2\text{S}$  additive increased the size of Cu particles in present polyol processes is related to its reactivity and reducibility [11, 12, 18]. Sulfide species are known to interact quite strongly with metal to form sulfides. These metal sulfides particles have been shown to catalyze the reduction of metal ions in a mechanism analogous to the autocatalytic reduction of metal clusters by drastically reducing the reduction potential [37-39]. With the enhanced ratio of sulfides particles, the evolution of Cu particles was dominated by the fast kinetic growth leading to large size. However,  $\text{S}^{2-}$  would easily reacts with free  $\text{Cu}^{2+}$  and formed CuS precipitation. When soluble  $\text{Cu}(\text{NO}_3)_2$  was introduced, high concentration  $\text{Cu}^{2+}$  ions firstly induced the formation of CuS. Although the CuS nuclei could accelerate the formation of Cu particles, excessive CuS nuclei were left to form impurities. In contrast, insoluble  $\text{Cu}(\text{OH})_2$  had no capability to provide excessive  $\text{Cu}^{2+}$  ions due to its slow dissolution. It contributed a perfect concentration of CuS nuclei as foreign nuclei which accelerated the growth of Cu particles. However, when the concentration of  $\text{Na}_2\text{S}$  additive exceeded 300  $\mu\text{M}$ , the same CuS precipitation was

observed in the final product. These results indicated that Na<sub>2</sub>S additive with proper concentration was able to tailor the size and size distribution of Cu particles. In the present work, the insoluble Cu salt combined with the Na<sub>2</sub>S additive represented a perfect synthesis system to control the size and size distribution of bimodal Cu particles.

### 2.3.3 Bonding property of bimodal Cu particles pastes

Four kinds of bimodal metal Cu particles were successfully synthesized by the simple polyol process (Samples I, II, V and VI). Their bonding abilities were evaluated by Cu-Cu bonding test. Fig. 2.7 shows the shear strength of sintered Cu joints with different sintering temperature in both N<sub>2</sub> and formic acid atmosphere. The higher shear strength was obtained at higher sintering temperature. In N<sub>2</sub>, The highest results were achieved in Sample V. However, the strength was only 20.6 MPa even at high sintering temperature of 350 °C. As comparison, the shear strength of Sample I, II and VI at the same condition were 9.1 MPa, 14.3 MPa and 16.6 MPa respectively. When temperature decreased to 300 °C or below, the shear strength of all the joints could hardly reach to 15 MPa. In contrast, sintered Cu joints obtained from formic acid exhibited better bonding strength. At 250 °C, the highest shear strength was 16.6 MPa. At 300°C, it raised to 20.3 MPa. And when sintering temperature raise to 350 °C, the shear strength reached to 25.0 MPa, which was higher than Pn-5Sn solder (23 MPa). However, it was interesting that the best results came from the Sample II instead of the Sample V which is the champion when sintering was performed in N<sub>2</sub> atmosphere. Besides, Sample I, which had a monodisperse size distribution, exhibited an inferior bonding strength when compared with others from bimodal samples. These joints fabricated by the bimodal Cu paste also achieved higher strength at milder sintering conditions comparing with those monodispersed nano-Cu or micro-Cu pastes [19, 20]. These results proved that bimodal Cu pastes achieved perfect bonding strength which was regarded as an illuminating candidate as die bonding materials.

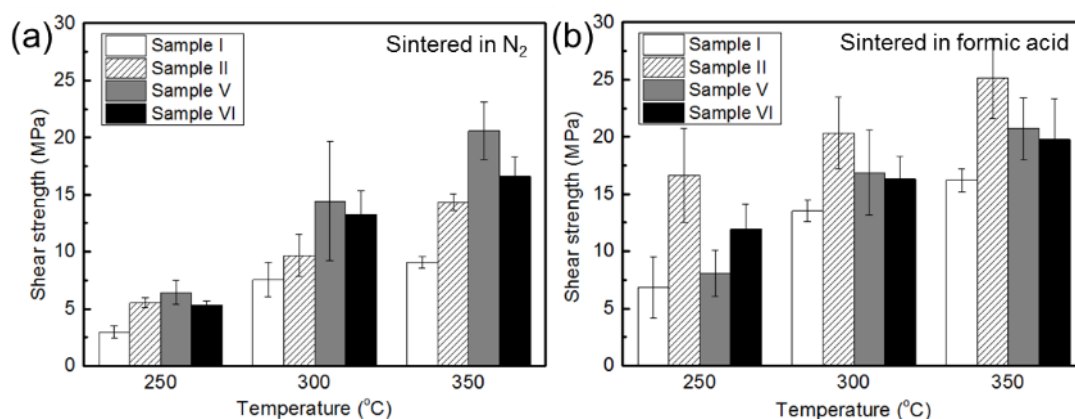


Fig. 2. 7 The shear strength of the Cu joints sintered in N<sub>2</sub> (a) and in formic acid (b).

Fig. 2.8 shows SEM images of the fracture surface of Cu joints obtained at 350°C both in N<sub>2</sub> and formic acid. Beginning with the joints obtained in N<sub>2</sub>. In the case of Sample I, the connection between particles was partly formed (Fig. 2.8a) when sintered in N<sub>2</sub>. However, the neck-growth was weak and observed in small area range without clear large grains, which corresponded to low shear strength. Moreover, it was clear that there were numerous isolated Cu particles which lost the opportunity to connect with neighboring particles and thus formed defects leading to weak mechanical strength. In contrast, clear neck-growth between Cu particles was observed in Sample II, V and VI without significant distinction between different particles. Also, huge grains were formed to contribute to the high shear strength (Fig. 2.7). However, some small Cu particles were still left, especially in Sample II (Fig. 2.8b), which led to its weaker strength in comparison to the Sample V and Sample VI. These small particles were significantly decreased and almost entirely absent in Sample V and VI (Fig. 2.8c and 2.8d), indicating particles with bigger diameter were more easily sintered in N<sub>2</sub>.

The SEM observation of sintered Cu joints obtained from formic acid sintering condition had a much denser structure. Though coarsen necking growths were observed in all samples, there was still some difference. The microstructure in Sample V and VI was similar to those obtained in N<sub>2</sub>, steady necking growths were obtained, but big pores still existed. In contrast, the microstructure of Sample II became much denser than that obtained in N<sub>2</sub>. Moreover, the residual small particles, impressively, all disappeared. The final microstructure was even denser than those obtained by Sample V and Sample VI.

Generally, smaller particles were easily sintered. Those small particles residue in N<sub>2</sub> suggested the small particles might have already been oxidized and could not be sintered which hindered the sintering progress. On the other hand, the oxidation small particles were reduced in formic acid condition, and filled the gap between necking growth then melt and formed steady bonding, which propelled sintering progress. Thus, the superior sintering degree was achieved in Sample II. Besides, poor sintering progress was still observed in Sample I, the necking growth is weak and a lot of pores were found, indicating the weak bonding strength.

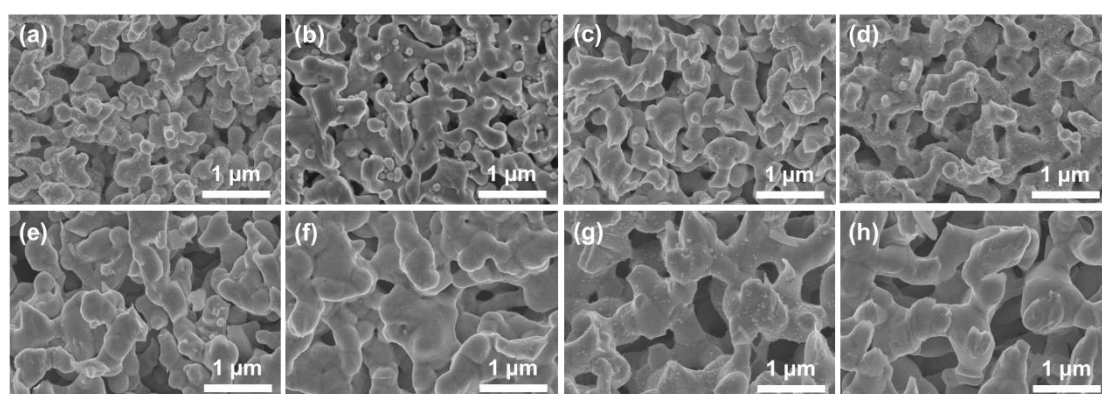


Fig. 2. 8 FE-SEM micrographs of Cu joints fracture surface obtained by Sample I (a) II (b), V (c) and VI (d).

Based on the result above, it is clear that the shear strength of sintered Cu joints prepared from bimodal Cu particles is directly related to the size and size distribution. In the N<sub>2</sub> condition, Sample V shows the highest bondability, but in formic acid condition, Sample II showed the best performance. But the Sample I showed the worst bondability in both conditions. This result may largely attribute to the diameter matching effect of Cu particles. Table 2.2 concluded the diameter of Sample I, II, V and VI. It is known that when two types of spheres are packed together the smaller spheres can fit in the interstitial space formed by the larger spheres. This structure largely improves the contact with all spheres and increases the overall density. A structure of such interstitial filling is strongly dependent on the radius ratio between small particles and big particles [21]. When the ratio is less than 0.29099, small spheres can fit excellently into interstitial space to form

a dense structure providing the largest contact between particles [22]. Except for Sample I, the other three samples have a radius ratio of about 0.15, 0.25 and 0.24 for Sample II, V and VI, respectively. It indicated the dense package was formed in the three samples. Thus, the surface diffusion, volume diffusion, grain boundary diffusion, and other mass transport between the Cu particles could happen readily and form the large grains (Fig. 2.8), which correspond to higher shear strength. On the other hand, the radius ratio in Sample I is 0.36, which is larger than the value of 0.29099. It implies that the contact probability between particles is decreased and resulting in bad sintering evolution. This is confirmed with the fracture SEM images shown in Fig. 2.8a and Fig. 2.8e. Therefore, the design of size and the size distribution of Cu particles is critical to achieving high performance joints.

Table 2. 2 Summary of particles size and the radius ratio between small and big particles

	Small particles ( $\mu\text{m}$ )	Big particles ( $\mu\text{m}$ )	Radius ratio
Sample I	0.19	0.53	0.36
Sample II	0.07	0.49	0.15
Sample V	0.17	0.69	0.25
Sample VI	0.24	1.00	0.24

On the other hand, according to the dense packaging theory, Sample II should reflect the largest density with the highest strength due to the easy fitting effect of its very small particles. However, it only worked when the joints were sintered in formic acid atmosphere. A possible reason for this was the intrinsic oxidization of Cu particles. Cu particles was are easily oxidized in air, especially small particles below 100 nm [23]. When oxidized Cu particles were sintered, the oxidized layer on the surface of particles must be removed to expose a clean surface for the mass transport. In the present work, Sample II included too many small Cu particles, which might have been oxidized during the process and resulted in inferior sintering. This also explained the existence of small particles due to possible oxidation (Fig. 2.8b). An actual experiment was designed to evaluate the oxide-resistivity of the bimodal Cu particles. Cu particles in Sample II and

Sample VI were stored in ethanol for 8 weeks in air. The XRD pattern of Sample II shows a new peak at  $36.4^\circ$  after 4 weeks, which was identified as Cu oxides (Fig. 2.9). This indicated that Sample II was vulnerable to oxidation even at room temperature. In contrast, no oxide peak was found for Sample VI and only very weak peaks of oxide were observed after 8 weeks, indicating that Sample VI was oxide-resistive. In the present work, although  $N_2$  atmosphere was used to sinter the bimodal Cu particles, the inevitable trace oxygen enhanced the oxidization of small Cu particles and decreased the sintering behavior. These results strongly suggested that the size of Cu particles should be carefully considered and designed to contribute to the sintering process, especially under non-reduced atmosphere sintering conditions.

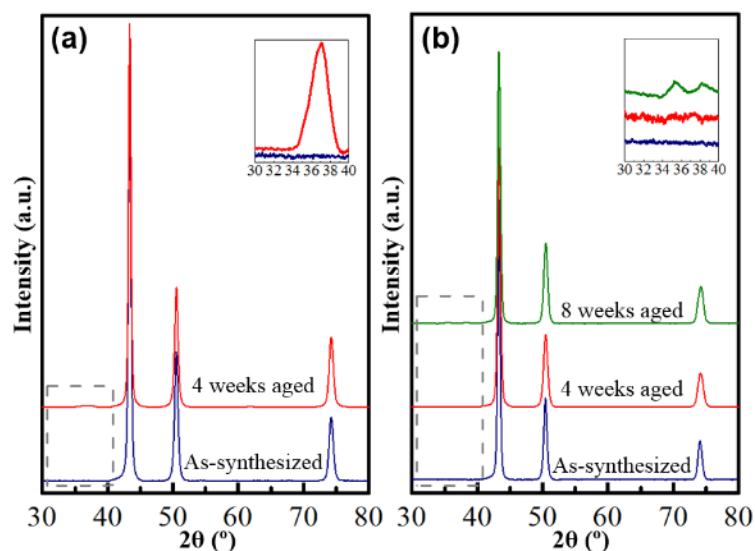


Fig. 2. 9 XRD patterns of sample II (a) and VI (b) aged in air. (Inset: enlarge part of 30-40° range)

## 2.4 Conclusion

In summary, bimodal Cu particles of the desired size distribution were successfully synthesized by a simple and large-scale polyol process. In comparison to soluble Cu sources, insoluble Cu sources achieved a wider distribution of Cu particles due to their slow and stable dissolution process.  $Na_2S$  additive can largely accelerate the reduction reaction and control the size of Cu particles in both cases. However, impure CuS as found in soluble Cu sources system due to the fast reaction between  $Cu^{2+}$  ions and  $S^{2-}$  ion. High bonding strength above 25 MPa was easily obtained at  $350^\circ C$  with a slight assisting

## Chapter 2

### One-step synthesis of bimodal Cu particles

pressure in formic acid protection. This strength is superior to many joints utilizing uniform nano-Cu paste. The bonding strength was highly dependent on both the size and the size distribution of Cu particles, this a result of the size matching effect of Cu particles. Due to their intrinsic oxidation, small Cu particles could hinder the sintering process. This work strongly suggests that bimodal Cu particles of a suitable size distribution are promising materials for power devices, particularly when compared to expensive nano-Ag and nano-Cu particles pastes. Cu particles with bimodal, tri-modal or multi-modal particles should be afforded greater attention as die bonding materials and frequently candidates for next-generation power device packaging. However, the intrinsic oxidation property of Cu particles was still problem and need to be take into consideration.

## Reference

- [1] K. Suganuma, J. Jiu, Advanced Bonding Technology Based on Nano-and Micro-metal Pastes, in: *Materials for Advanced Packaging*, Springer, 2017, pp. 589-626.
- [2] S.K. Tam, K.Y. Fung, K.M. Ng, Copper pastes using bimodal particles for flexible printed electronics, *Journal of Materials Science*, 51 (2016) 1914-1922.
- [3] Y.Y. Dai, M.Z. Ng, P. Anantha, Y.D. Lin, Z.G. Li, C.L. Gan, C.S. Tan, Enhanced copper micro/nano-particle mixed paste sintered at low temperature for 3D interconnects, *Applied Physics Letters*, 108 (2016) 263103.
- [4] M. Kuramoto, S. Ogawa, M. Niwa, K.-S. Kim, K. Suganuma, Die bonding for a nitride light-emitting diode by low-temperature sintering of micrometer size silver particles, *IEEE Transactions on components and Packaging Technologies*, 33 (2010) 801-808.
- [5] S. Park, R. Uwataki, S. Nagao, T. Sugahara, Y. Katoh, H. Ishino, K. Sugiura, K. Tsuruta, K. Suganuma, Low-pressure sintering bonding with Cu and CuO flake paste for power devices, in: *Electronic Components and Technology Conference (ECTC), 2014 IEEE 64th*, IEEE, 2014, pp. 1179-1182.
- [6] W. Chen, L. Li, Q. Peng, Y. Li, Polyol synthesis and chemical conversion of Cu<sub>2</sub>O nanospheres, *Nano Research*, 5 (2012) 320-326.
- [7] A.R. Tao, S. Habas, P. Yang, Shape control of colloidal metal nanocrystals, *small*, 4 (2008) 310-325.
- [8] J. Jiu, H. Zhang, S. Koga, S. Nagao, Y. Izumi, K. Suganuma, Simultaneous synthesis of nano and micro-Ag particles and their application as a die-attachment material, *Journal of Materials Science: Materials in Electronics*, 26 (2015) 7183-7191.
- [9] K.J. Carroll, J.U. Reveles, M.D. Shultz, S.N. Khanna, E.E. Carpenter, Preparation of elemental Cu and Ni nanoparticles by the polyol method: an experimental and theoretical approach, *The Journal of Physical Chemistry C*, 115 (2011) 2656-2664.
- [10] D.M. Clifford, C.E. Castano, A.J. Lu, E.E. Carpenter, Synthesis of FeCo alloy magnetically aligned linear chains by the polyol process: structural and magnetic characterization, *Journal of Materials Chemistry C*, 3 (2015) 11029-11035.
- [11] T. Zhao, J.-B. Fan, J. Cui, J.-H. Liu, X.-B. Xu, M.-Q. Zhu, Microwave-controlled

- ultrafast synthesis of uniform silver nanocubes and nanowires, *Chemical Physics Letters*, 501 (2011) 414-418.
- [12] A.R. Siekkinen, J.M. McLellan, J. Chen, Y. Xia, Rapid synthesis of small silver nanocubes by mediating polyol reduction with a trace amount of sodium sulfide or sodium hydrosulfide, *Chemical physics letters*, 432 (2006) 491-496.
- [13] T. Ishizaki, R. Watanabe, A new one-pot method for the synthesis of Cu nanoparticles for low temperature bonding, *Journal of Materials Chemistry*, 22 (2012) 25198-25206.
- [14] M. Abdulla-Al-Mamun, Y. Kusumoto, M. Muruganandham, Simple new synthesis of copper nanoparticles in water/acetonitrile mixed solvent and their characterization, *Materials Letters*, 63 (2009) 2007-2009.
- [15] M. Biçer, İ. Şişman, Controlled synthesis of copper nano/microstructures using ascorbic acid in aqueous CTAB solution, *Powder Technology*, 198 (2010) 279-284.
- [16] P. Lignier, R. Bellabarba, R.P. Tooze, Scalable strategies for the synthesis of well-defined copper metal and oxide nanocrystals, *Chemical Society Reviews*, 41 (2012) 1708-1720.
- [17] B.K. Park, S. Jeong, D. Kim, J. Moon, S. Lim, J.S. Kim, Synthesis and size control of monodisperse copper nanoparticles by polyol method, *Journal of colloid and interface science*, 311 (2007) 417-424.
- [18] Z. Li, A. Gu, M. Guan, Q. Zhou, T. Shang, Large-scale synthesis of silver nanowires and platinum nanotubes, *Colloid and Polymer Science*, 288 (2010) 1185-1191.
- [19] H. Nishikawa, T. Hirano, T. Takemoto, N. Terada, Effects of joining conditions on joint strength of Cu/Cu joint using Cu nanoparticle paste, *Open Surface Science Journal*, 3 (2011) 60-64.
- [20] J. Kahler, N. Heuck, A. Wagner, A. Stranz, E. Peiner, A. Waag, Sintering of copper particles for die attach, *Components, Packaging and Manufacturing Technology*, *IEEE Transactions on*, 2 (2012) 1587-1591.
- [21] D.R. Hudson, Density and packing in an aggregate of mixed spheres, *Journal of Applied Physics*, 20 (1949) 154-162.
- [22] C. Zong, From deep holes to free planes, *Bulletin of the American Mathematical*

Chapter 2  
One-step synthesis of bimodal Cu particles

Society, 39 (2002) 533-555.

- [23] S. Jeong, K. Woo, D. Kim, S. Lim, J.S. Kim, H. Shin, Y. Xia, J. Moon, Controlling the thickness of the surface oxide layer on Cu nanoparticles for the fabrication of conductive structures by ink -jet printing, *Advanced Functional Materials*, 18 (2008) 679-686.

Supplementary Materials

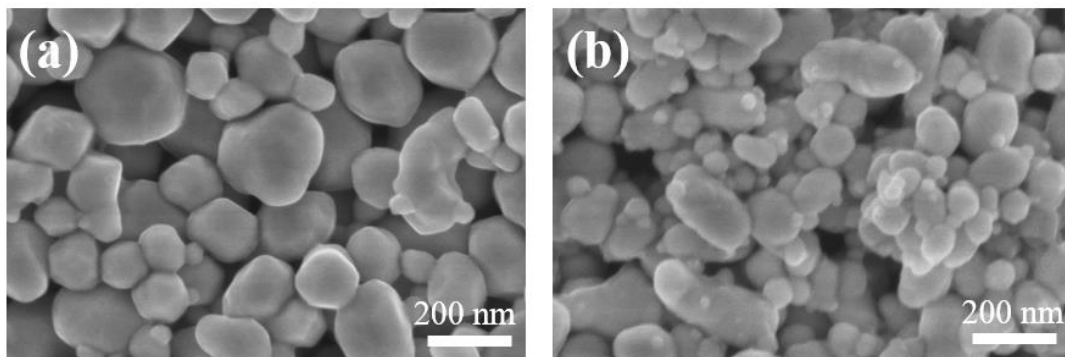


Fig. S2. 1 FE-SEM micrographs for supernatant of sample I (a) and sample II (b).

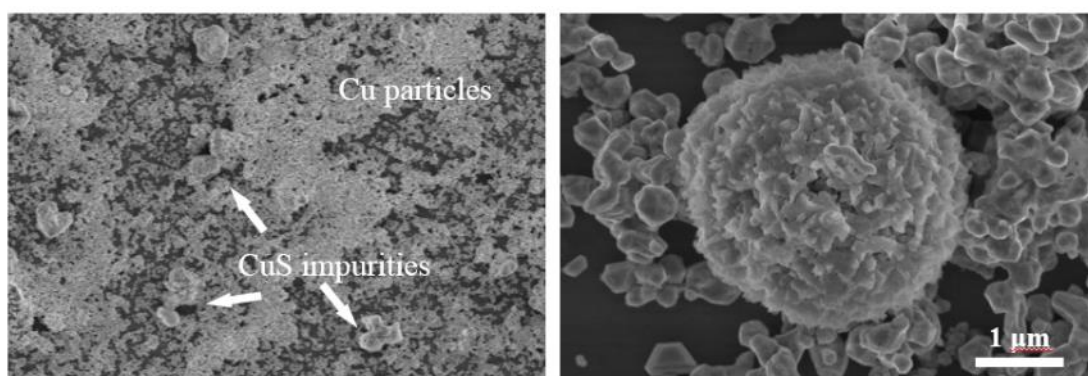


Fig. S2. 2 FE-SEM observation of CuS impurities in sample VI.

Chapter 2  
One-step synthesis of bimodal Cu particles

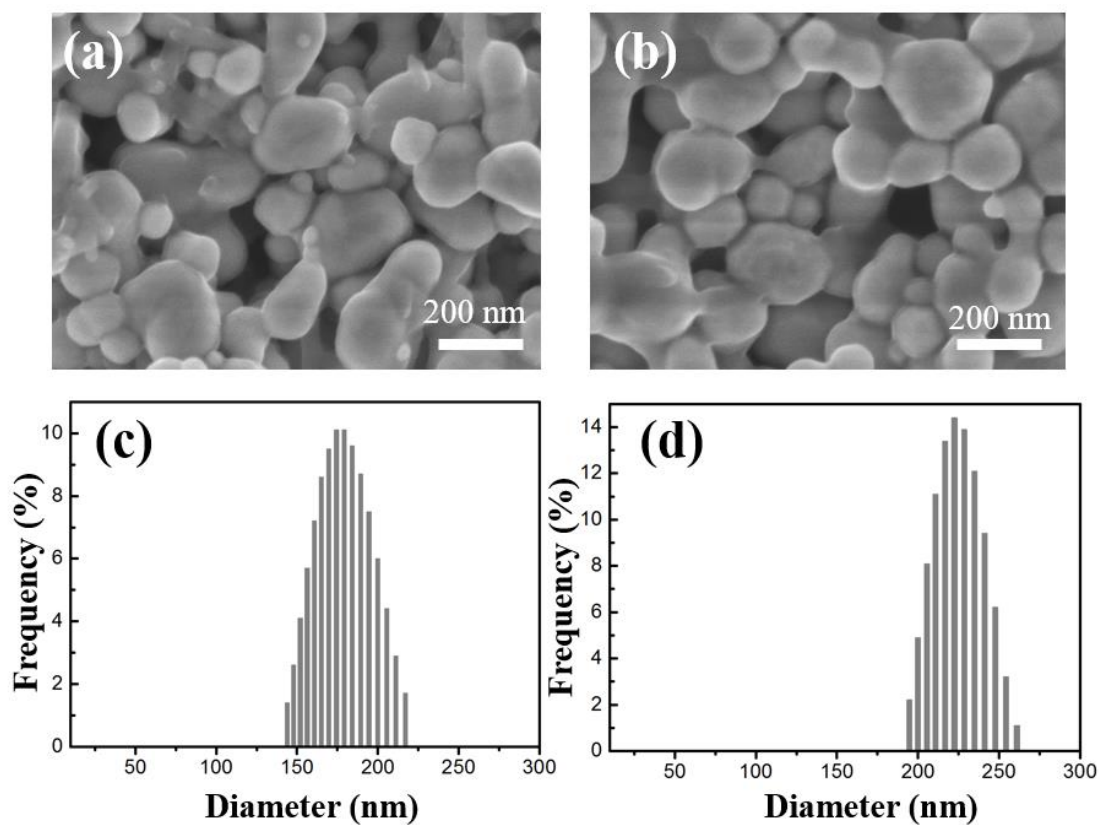


Fig. S2. 3 FE-SEM micrographs and size distribution measured by DLS for supernatant of Sample V (a, c) and Sample VI (b, d).



## **Chapter 3**

### **Realization of high-strength Cu sinter joining by ascorbic acid-treated Cu particle paste**



### 3.1 Introduction

In the last chapter, the influence of particles size and size distribution on sintered Cu joints were investigated. The bonding strength over 25 MPa was achieved. However, the result was only obtained at high temperature of 350 °C and under reductive formic acid protection, which was far from the objective sintering condition (<300 °C, inert atmosphere, with low assisting pressure). The intrinsic oxidation property of Cu was proved to significantly hinder the bondability of paste if the sintering was performed in the non-reductive atmosphere. In this chapter, the efforts had been made to achieve satisfied sintered Cu joints below the sintering temperature of 300 °C without reductive atmosphere protection.

The fact that oxidation is the main reason for the inferior bondability of Cu paste has been proved in the last chapter. To deal with the oxidation problem, many efforts have been made in recent years. Protective coating on Cu particles has been proved to be a feasible approach. For example, a thick polymer layer coated on the surface of Cu particles has been shown as an effective way to prevent oxidation. However, to completely remove the thick polymer layer requires high temperatures in excess of 350 °C or even 400 °C [1]. Coating a metallic shell such as Pt [2, 3], Ni [4, 5] and Ag [6-9] on the surface of Cu particles is another choice and could lower the sintering temperature below 300 °C. However, the complicated fabrication processes of the core-shell structures drastically increase the price of Cu particle paste. Worse yet, the formation of the intermetallic compound or alloy between the Cu core and the metallic protective shell presents a significant problem for the thermal and electrical conductivity.

On the other hand, it has been widely studied that Cu particles can be reduced by some solvent or reductant. Adding reductive solvent in Cu particle pastes is one of the most attractive approaches to provide for a highly efficient sintering ability. The successful result proved that reductive solvent in Cu/CuO paste significantly reduces CuO into Cu during the sintering process and helps to achieve strong sintered joints with a shear strength of 20 MPa [10]; Cu particles treated with liquid formic acid have improved the strength and electrical conductivity of sintered Cu joints [11]. However, the liquid

Chapter 3  
Realization of high-strength Cu sinter joining by  
Ascorbic acid-treated Cu particle paste

formic acid is highly corrosive and toxic to human skin and eyes, and its extremely active reactivity may cause serious damage to semiconductor devices. Therefore, in order to design a safe and effective Cu paste for achieving sintered Cu joints with high quality bonding under suitable sintering conditions, various reductants were added into Cu paste to acquire good bondability. In present work, glucose, citric acid, ascorbic acid, formic acid,  $\text{Cu}(\text{COOH})_2$  were selected as the reductant candidates. Glucose, citric acid and ascorbic acid are the common reductant and stabilizer of the synthesis of metallic materials, which are supposed to eliminate the Cu oxides because of their reduction [12-16]. Liquid formic acid, which can eliminate Cu oxides on Cu particles, surely improves the bondability of Cu paste [11].  $\text{Cu}(\text{COOH})_2$  is able to decompose to Cu during heating process and the new formed Cu may contribute to the necking growth and improve the interconnections. Those properties are supposed to accelerate the sintering process of Cu paste and can realize reliable sintered Cu joints.

## 3.2 Experimental

### 3.2.1 Improve Cu paste with reductant additive

Firstly, glucose, citric acid (CA), Ascorbic acid (AA), formic acid (FA),  $\text{Cu}(\text{COOH})_2$  (Cuf) were mixed with ethylene glycol (EG) as the mass ratio of 1 : 0.1, Then, the prepared solvents with reductant were mixed with Cu particles as mass ratio of 85 : 15, the final content of reductants in Cu paste was 1.3 wt.%. Also, pure EG was mixed with Cu particles to fabricate paste as the comparison.

### 3.2.2 Fabrication of sintered Cu joints

The fabricated Cu pastes were printed onto Cu-substrates by a 4 mm×4 mm×0.1 mm stainless steel mask. Cu chips were set on the surface of the paste to make sandwich structures then sintered in  $\text{N}_2$  (>99.99%) at various temperature with an assisting pressure of 0.4 MPa to form Cu-Cu joints. The sintering time was 30 min and the heating rate was 25 °C/min.

### 3.2.3 Characterization and evaluation

The bonding strength of sintered Cu joints was evaluated by a shear test stage (DAGE, series 4000). The shear height was set to 100 μm and shear strain rate was 1 mm/min. Cross-section samples were fabricated via an ion-milling polishing process (IM4000, Hitachi). The sintering behaviors of Cu pastes were investigated by thermogravimetric/differential thermal analysis (TG-DTA, STA449F3, NETZSCH) in  $\text{N}_2$  and the heating rate was 25 °C/min, simulating the sintering process. The phase composition was recorded by X-ray diffraction (XRD, RINT 2500, Rigaku). The morphology was investigated by scanning electron microscope (FE-SEM, SU8020, Hitachi) and by transmission electron microscope (TEM, JEM-ARM200F, JEOL). Cross-section samples were fabricated via an ion-milling polishing process (IM4000, Hitachi). The surface chemical composition was detected by X-ray photoelectron spectroscopy (XPS, JPS-9010MC, JEOL). The data analysis (peaks fitting) was carried out by

specialized software for the XPS equipment. (SpecSurf, JEOL, ver.1.9.2). liner background and fitted by the auto-mode by the default parameter. The peaks were assumed to obey the Gaussian distribution.

### **3.3 Results and discussion**

#### **3.3.1 Shear strength result of sintered Cu joints**

Fig. 3.1 shows the shear strength of sintered Cu joints obtained by Cu paste improved by various reductant additives. Among those additives, ascorbic acid and formic acid exhibited good performance on improving the bondability of Cu paste. Glucose and citric acid exhibited good reducing property during the synthesis of metallic materials. However, it seemed they had no significant effect on improving the bondability of Cu paste. The strength of EG-glucose and EG-CA Cu paste were 10.9 MPa and 11.8 MPa, respectively. As the comparison, the shear strength of EG-Cu paste was 9.8 MPa. Though EG-Cuf Cu paste exhibited a slight improved shear strength of 12.5 MPa, the strength is still too weak for application. In contrast, the shear strength of EG-AA Cu paste and EG-FA Cu paste were 24.8 MPa and 25.9 MPa. Considering the tiny content of reductant additive (1.3 wt%). The improving effect of AA and FA additives was impressive. The good performance of FA had been largely reported, but its corrosive property determined that FA was not suitable as the additive in Cu paste. Thus, only AA was regarded as the promising additive for Cu paste. The impressive performance of AA may largely rely on the strong reducibility, which will be explained in the following paragraphs.

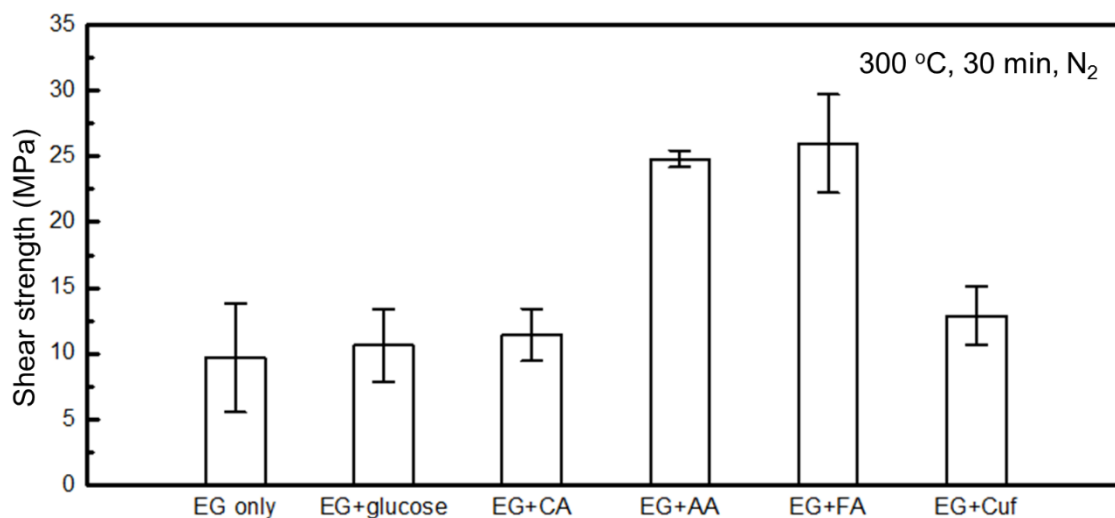


Fig. 3. 1 Shear strength of sintered Cu joints obtained by Cu paste using various additives

### 3.3.2 The effect of AA additive

To evaluate the detail effect introduced by AA addition, the as-synthesized Cu particles were immersed in an ethanol-5wt.%AA solvent for 10 min at room temperature. Fig. 3.2 shows the XRD (a,b) and XPS patterns (c,d) of as-synthesized particles (Fig. 3.2 and 3.2c) and particles after AA treatment (Fig. 3.2b and 3.2d). Three main characteristic peaks located at  $2\theta = 43.3^\circ$ ,  $50.4^\circ$ , and  $74.08^\circ$  were detected in both situations. These peaks corresponded to diffraction of planes (111), (200), and (220) of the face-centered cubic (fcc) Cu, respectively. Besides, small peaks around  $37.0^\circ$  and  $38.2^\circ$  representing  $\text{Cu}_2\text{O}$  and  $\text{CuO}$  were also detected in the as-synthesized Cu particles (Fig. 3.2a). In contrast, after AA treatment, the  $\text{Cu}_2\text{O}$  peak totally disappeared and the intensity of  $\text{CuO}$  decreased (Fig. 3.2b), indicating that AA can effectively remove Cu oxides even at room temperature. There are two reasons to explain the existence of  $\text{CuO}$ . One is the stability of  $\text{CuO}$  compared to  $\text{Cu}_2\text{O}$ . Another is the weak reducing ability due to a limited amount of AA in the paste. Further investigation toward the complete removal of oxide in Cu paste should be a priority in future research.

The XPS was utilized to identify the surface chemical composition and to evaluate the

reduction effect of AA on Cu particles. The Cu 2p<sub>3/2</sub> spectra of untreated Cu particles showed two clear and asymmetric peaks which could be fitted to several peaks. The peak at 932.6 eV was assigned to the bonding energy of pure Cu or Cu<sub>2</sub>O because their binding energies almost overlapped and the peaks at 935.0 eV along with two satellite peaks at 942.3 eV, and 944.2 eV represented the bond of CuO (Fig. 3.2c) [11, 15, 17]. After AA treatment the two peaks at around 942.3 and 944.2 eV disappeared and the main peak at 935.0 eV became noticeably sharper. (Fig. 3.2d). These results suggest that the oxides were largely removed by the AA treatment. Moreover, the residual of CuO may also be related to regeneration because its oxide layer grows rapidly on very pure Cu particles even in ambient condition [12]. In the present work, these Cu particles were treated with AA and then put in air for measurement, thus accelerating oxidation on the Cu particles. However, AA was able to remove a significant amount of Cu oxides which proved beneficial in the following sintering process. Additionally, and to avoid re-oxidation of the Cu particles, keeping AA reductant in the Cu paste will prove beneficial, however, the AA reductant will be removed in any subsequent sintering process.

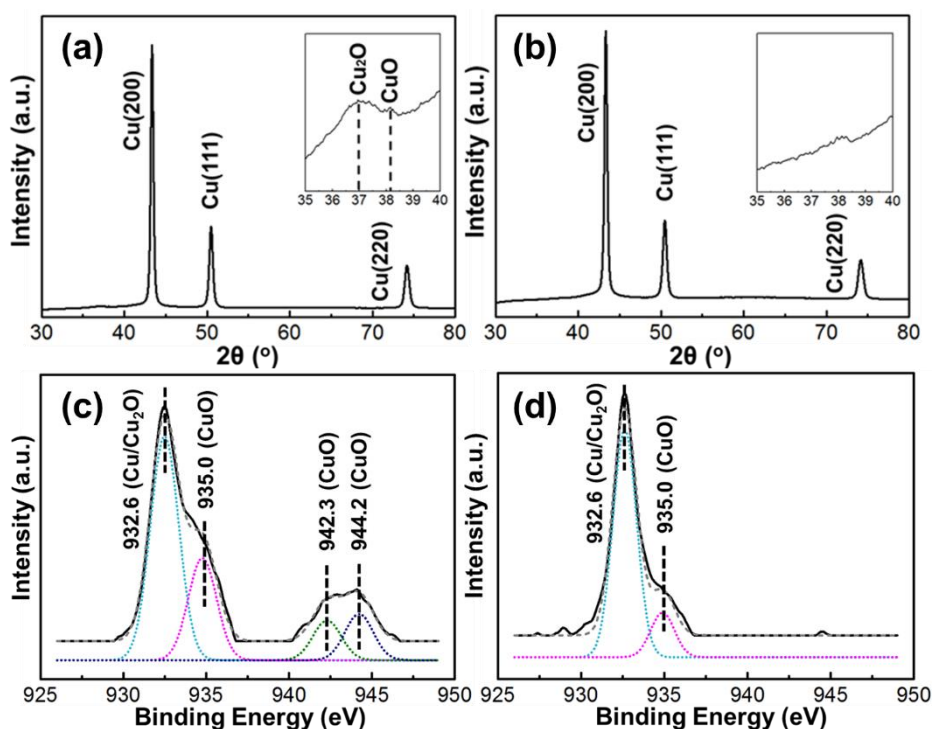


Fig. 3. 2 XRD and XPS patterns of as-synthesized Cu particles before (a,c) and after AA treatment (b,d). Insert images in a and b are enlarged part at range of 35°-40°.

Fig. 3.3 shows the TEM micrographs of Cu particles before and after AA treatment. The particles were angular shape with a wide size distribution from tens to hundreds of nanometers (Fig. 3.3a, 3.3b), which was consistent with the SEM observation. The high magnification image clearly showed that there was an amorphous layer coated on the surface of Cu particles before AA treatment. This layer was regarded as the existence of impurities which included Cu oxides, PVP residue etc. The thickness of the layer was approximately 1-2 nm (Fig. 3.3c). In contrast, the amorphous impurity layer was almost completely eliminated, and a clear and sharp surface was observed after AA treatment (Fig. 3.3d). Combining with the result of XPS, TEM micrographs confirmed the reduction and the cleaning ability of AA on the Cu oxide and other impurity layer. This property was defined as the self-reduction characteristic of the AA-treated Cu paste.

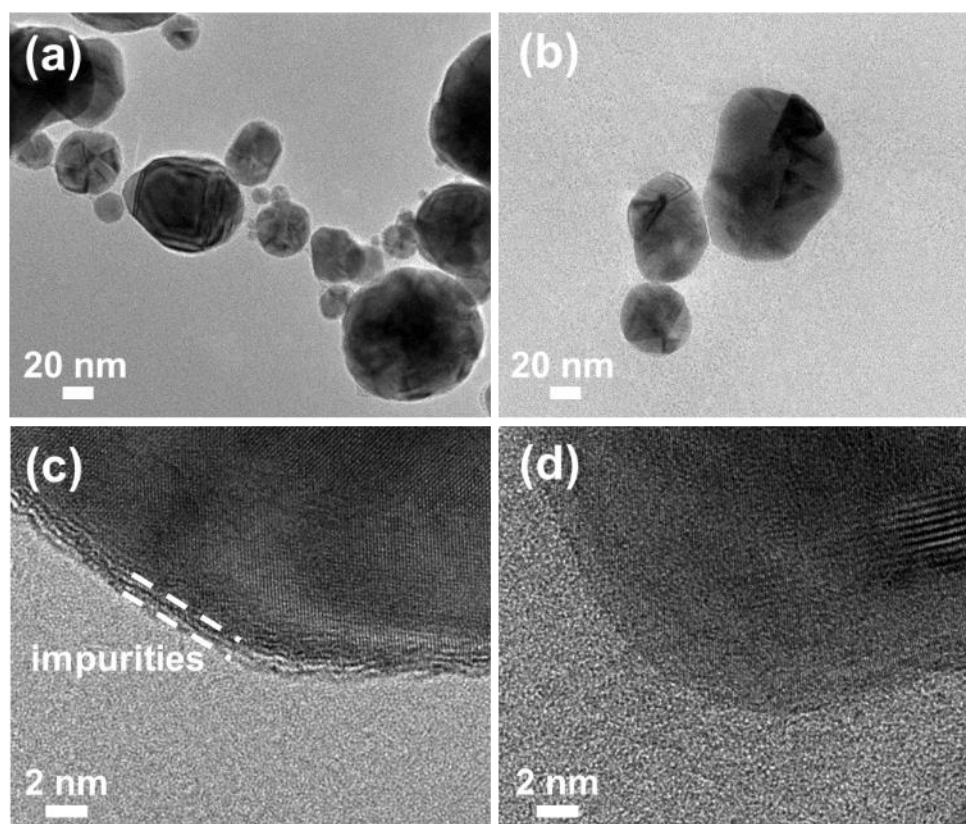


Fig. 3. 3 TEM micrographs of Cu particles before (a,c) and after AA treated (b,d) in both low (a,b) and high (c,d) magnification.

During the sintering process of Cu particle paste, all the organics including AA should be removed to a great extent for improving the diffusion of Cu atoms between adjacent Cu particles. TG-DTA analysis of pure AA, EG-0wt.%AA Cu paste and EG-10wt.%AA Cu paste in N<sub>2</sub> were carried out to evaluate the removal of AA in Cu paste during the sintering process (Fig. 3.4). In the TG-DTA curve of pure AA, there was an endothermic valley located at around 195 °C without weight loss (Fig. 3.4a). It was related to the melting of AA (192 °C, the melting point of AA). With further increase of the temperature to around 210 °C, a rapid weight loss was observed, which was regarded as the decomposition of AA [18, 19]. On the other hand, in the TG-DTA curve of EG-0wt.%AA Cu paste, an endothermic valley accompanying an obvious weight loss was detected at about 160 °C (Fig. 3.4b), relating to the evaporation of EG solvent (197 °C, the boiling point of EG). The weight loss ended at about 180 °C and the residual mass was around 85 wt.% which corresponded to the Cu load in the Cu paste and indicated the complete removal of EG solvent. However, it should be noted that with the further increase of temperature to 400 °C, the weight of the residual mass began to increase. This was likely because the Cu particles had been oxidized even in a N<sub>2</sub> atmosphere. In the TG-DTA curve of 10 wt.% AA paste (Fig. 3.4c), a endothermic valley with a rapid weight loss appeared at about 160 °C, which is related to the evaporation of EG. After that, the weight loss stopped at around 180°C for a short time with the residue weight of 87 wt.%. When the temperature rose to 210 °C, the weight loss, which corresponded to the decomposition of AA, started again and then ended at 300 °C. Almost no weight loss was found as the temperature rose to over 300 °C. The final residual mass was around 85 wt.% which corresponded to the Cu load in the EG-10wt.%AA Cu paste, indicating the almost complete removal of EG solvent and AA in the sintered paste.

Chapter 3  
Realization of high-strength Cu sinter joining by  
Ascorbic acid-treated Cu particle paste

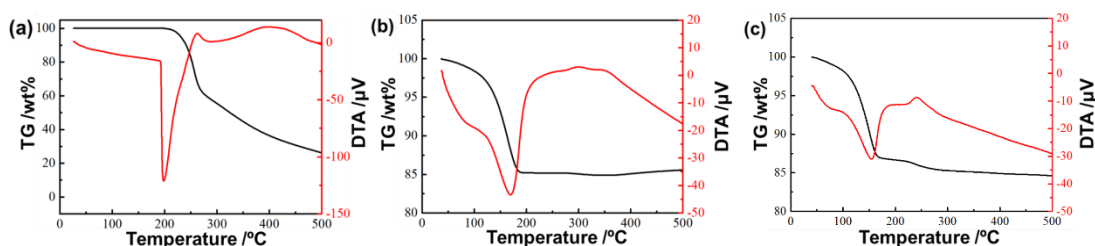


Fig. 3. 4 TG-DTA plots of pure AA (a), EG-0wt.% AA paste (b) and EG-10wt.% AA paste (c).

The composition of Cu pastes during the sintering process at different temperatures was evaluated by XRD (Fig. 3.5). Though the EG-Cu paste was almost composed by pure Cu, a  $\text{Cu}_2\text{O}$  peak around  $37.0^\circ$  as well as a CuO peak around  $38.2^\circ$  were observed at initial stage. With increase of the temperature above  $200^\circ\text{C}$ , the oxide peaks in EG-Cu paste became clear and sharp. As the temperature raised to  $300^\circ\text{C}$ ,  $\text{Cu}_2\text{O}$  peak disappeared and only CuO peak was observed. The disappearance of  $\text{Cu}_2\text{O}$  was likely attributed to the instability of  $\text{Cu}_2\text{O}$  over  $300^\circ\text{C}$ , and unstable  $\text{Cu}_2\text{O}$  was easily oxidized to CuO [20-22]. In contrast, in EG-AA Cu paste the  $\text{Cu}_2\text{O}$  peak significantly decreased, and the intensity of CuO peak was also harder to be detected than that in EG-Cu paste. This result confirmed the self-reduction ability in EG-AA Cu paste mentioned above. Moreover, it should be noted that the  $\text{Cu}_2\text{O}$  peak never appeared during the sintering of EG-AA Cu paste even at high temperature while the  $\text{Cu}_2\text{O}$  peak became sharp and clear during the sintering of EG-Cu paste. In the previous works, Vernin et. al. investigated the decomposition products of AA in  $\text{N}_2$  at  $300^\circ\text{C}$  and found several reductive organics such as aldehydes and alcohols [18]. Shi et. al. also reported that the decomposed gas from AA included CO,  $\text{CH}_4$  and formic acid [19]. These products could reduce metallic oxides during sintering process [23, 24]. Therefore, the decomposition of AA in the developed Cu particle paste was expected to protect Cu particles from oxidation and ensure the effective sintering of Cu particles. This property was defined as a self-protection characteristic of the AA-treated Cu paste.

Generally, Cu oxidation during the sintering process follows two steps [21, 22]:



Cu<sub>2</sub>O was firstly formed, then was further oxidized to CuO due to its instability at high temperature. The formation of Cu oxides in paste resulted from two factors. One was innate oxides during synthesis mentioned above. The other one was because of the O<sub>2</sub> impurity in N<sub>2</sub> gas, which reacted with Cu to form oxides. During the sintering process of EG-Cu paste, both Cu<sub>2</sub>O and CuO were detected and increased with temperature, which suggested that the formation of oxides was inevitable even under N<sub>2</sub> atmosphere. The similar results were also reported by the previous works [13, 14, 25-27]. On the other hand, no Cu<sub>2</sub>O phase was found in EG-AA-Cu paste during the whole sintering process. These results confirmed that the AA addition endowed Cu particle paste with self-reduction and self-protection characteristics which have significantly diminished oxide formation during the sintering process and thereby greatly improving the sintering of Cu particles.

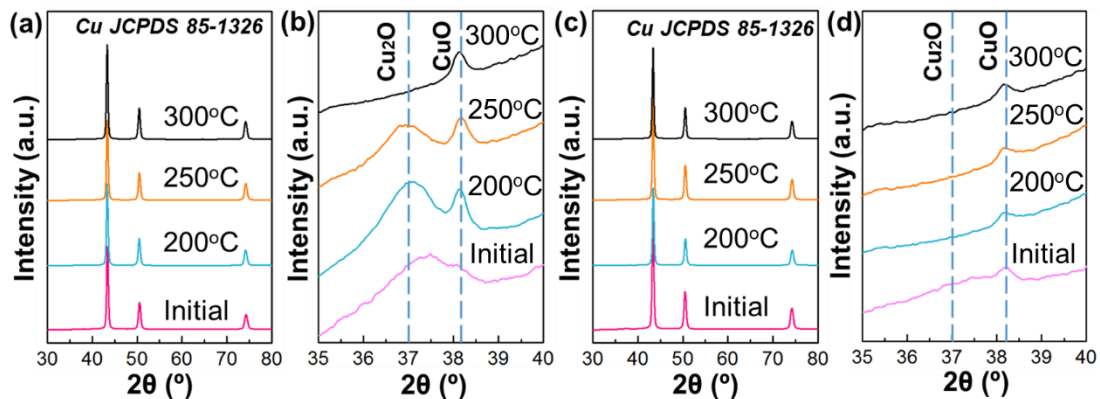


Fig. 3. 5 XRD patterns of EG-Cu paste (a, b) and EG-AA-Cu paste (c, d). Note that (b) and (d) were enlarged parts in 35°- 40° of (a) and (c), respectively.

Fig. 3.6 shows the shear strength of sintered Cu joints fabricated from Cu particle

Chapter 3  
Realization of high-strength Cu sinter joining by  
Ascorbic acid-treated Cu particle paste

pastes with different AA contents. Firstly, AA dissolving various amounts of AA (5 wt.%, 10 wt.%, and 15 wt.%, respectively) in EG at 60 °C. The dried Cu particles were then mixed with the AA treated solvents with a mass ratio of 85:15 to form EG-AA-Cu pastes with various AA contents. For ease of description, the four kinds of Cu paste were named as EG-0wt.%AA paste (EG-Cu paste, above), EG-5wt.%AA paste, EG-10wt.%AA paste (EG-Cu-AA paste in above), and EG-15wt.%AA paste. The total contents of AA in these four kinds of Cu pastes were 0 wt.%, 0.65 wt.%, 1.3 wt.% and 1.96 wt.%, respectively. The shear strengths of the joints fabricated from AA-treated pastes were much higher than those obtained from the paste without AA treatment. The shear strengths of the sintered Cu joints obtained by EG-0 wt% AA paste was relatively low. The bonding strength was only 14.4 MPa even sintered at 350°C. When 5 wt.% AA was added into the EG solvent, the shear strengths of the sintered Cu joints improved significantly. Then increase of AA content in solvent to 10 wt.%, the shear strengths of sintered joints increased as well. Relatively high shear strength of 24.8 MPa at 300°C was obtained, which was also reported in Fig 3.1. These results of EG-10wt.%AA Cu paste represented about a 112-379 % increase in the shear strength compared with those joints fabricated from EG-Cu paste. With further increase of AA in EG to 15 wt.%, the improvement of shear strength of sintered Cu joints was not obvious. Based on these results, it is believed that the addition of AA improves the sintering of Cu particle paste and the 10 wt.% AA in solvent is sufficient to significantly enhance the bonding strength of sintered Cu joints.

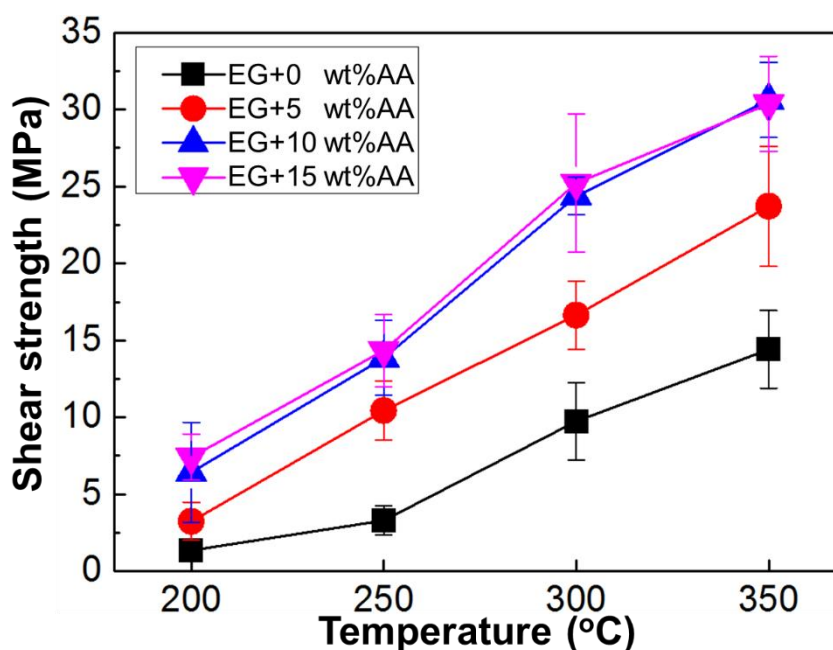


Fig. 3. 6 Variation in shear strength of sintered Cu-Cu joints by Cu paste with different AA contents at different sintering temperatures.

Fig. 3.7 shows the fracture surfaces of the sintered Cu joints fabricated at 300°C by using the EG-0wt.% AA paste, the EG-5wt.% AA paste, the EG-10wt.% AA paste, and the EG-15wt.% AA paste, respectively. Even though necks between adjacent Cu particles were observed in all joints, the sintering degree was highly dependent on the composition of the Cu pastes. In the joints fabricated from EG-0wt.% AA paste, most Cu particles kept their original shapes and only weak necks could be found between adjacent particles (Fig. 3.7a); thus the average shear strength is as low as 9.7 MPa. With the addition of 5 wt.% AA, even though the isolated particles were still observed, the necks between adjacent Cu particle became thicker (Fig. 3.7b), which contributed to the enhancement of bonding strength. When the AA content in solvent raised to 10 wt.%, most particles had been sintered and the microstructure with coarse necks was obtained (Fig. 3.7c). In addition, obvious tensile deformation could be observed (arrows in Fig. 3.7b-3.7d), which indicated the sintered Cu joints experienced an elongation-to-failure process because of the enhanced mechanical strength of the sintered Cu joints. These results confirmed that the addition of AA endowed Cu particle paste with high bondability due to the

introduction of self-reduction and self-protection characteristics, which significantly promoted the diffusion of Cu atoms between adjacent Cu particles and therefore largely improved the sintering of these Cu particles. Further raising the AA content in solvent to 15 wt.%, the improvements of neck growth between adjacent Cu particles (Fig. 3.7d) as well as the bonding strength of sintered Cu joints (Fig. 3.6) were not obvious, which indicated the addition of 10 wt.% AA is sufficient for the improvement of sintering of Cu particle paste.

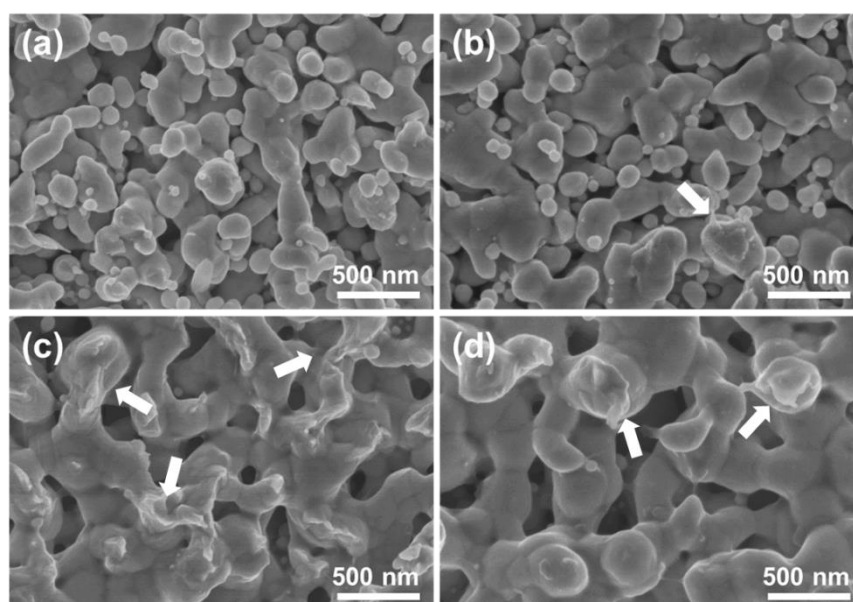


Fig. 3. 7 Fracture surfaces of sintered Cu-Cu joints at 300°C by using EG-0wt.%AA paste (a), EG-5wt.% AA paste (b), EG-10wt.% AA paste (c), and EG-15wt.% AA paste (d). The arrows indicate the tensile deformation.

Fig. 3.8 shows the cross-section images of the sintered Cu joints obtained at various temperatures by using the EG-0wt.% AA paste and the EG-10wt.% AA paste. The sintered Cu joints fabricated by using EG-10wt.% AA paste exhibited a more rapid sintering evolution than those joints fabricated by using the EG-0wt.% AA paste. When the sintering temperature was 200 °C, the joints fabricated by using the EG-0wt.% AA paste was nearly un-sintered (Fig. 3.8a) and a visible gap between paste and Cu substrate was observed. As sintering temperature rose to 250 °C, neck growths were observed in some

local areas (Fig. 3.8b). When sintering temperature further rose to 300 °C, obvious neck growths appeared between neighboring particles (Fig. 3.8c), leading to an increase in shear strength (Fig. 3.6). Further raising the sintering temperature to 350 °C, neck growths became thick and venation-shape microstructure was formed. However, the gap between sintered Cu paste and substrate was still clearly observed (Fig. 3.8d). The formation of the gap might be attributed to two factors. One factor is the initial oxides on the surface of the Cu substrate, and the second factor is the formed Cu oxides during the sintering process because of O<sub>2</sub> impurity in N<sub>2</sub> mentioned above. Thus, the diffusion channels between Cu particles and Cu substrate were blocked, leading to inferior sintering and poor bonding strength of the sintered Cu joints.

On the other hand, a relatively rapid sintering process was realized in the EG-10wt.% AA paste. For the EG-10wt.% AA paste sintered at 200 °C, the boundaries between particles became indistinct and some Cu particles seem interconnected to the substrate (Fig. 3.8e). When the sintering temperature rose to 250 °C (Fig. 3.8f), local dense areas were formed due to obvious neck growths. As sintering temperature rose to 300 °C (Fig. 3.8g), the microstructures of joints were further coarsened and continuous venation penetrated the whole joint. Moreover, the venations fused with the Cu substrate. The interface between the sintered paste and the Cu substrate was difficult to be distinguished, corresponding to the high bonding strength. When the temperature was further increased to 350 °C, the width of venations became much larger than those appearing on joints sintered by EG-0wt.% AA paste. The rapid sintering of Cu particles and compact interface indicated that the self-reduction and self-protection characteristics introduced by AA addition largely accelerated the diffusion of Cu particles in the paste and further enhanced the bonding ability of Cu paste.

Chapter 3  
Realization of high-strength Cu sinter joining by  
Ascorbic acid-treated Cu particle paste

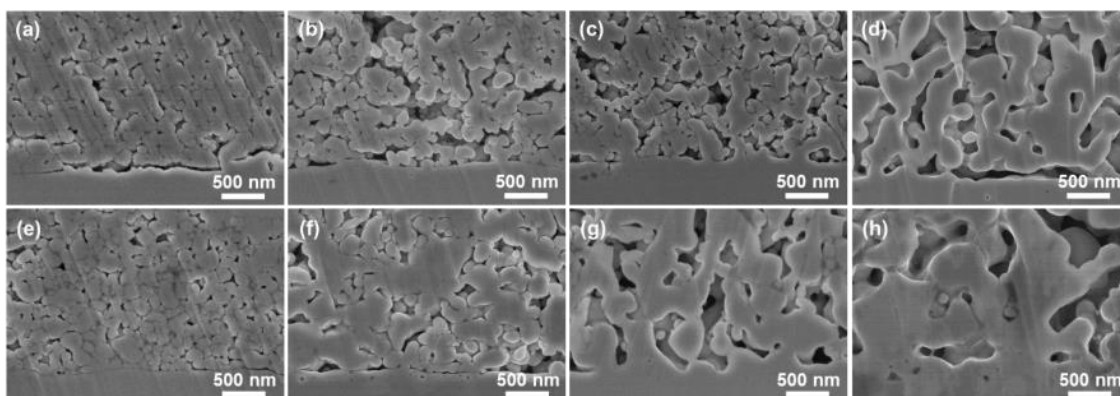


Fig. 3. 8 Cross-section images of sintered Cu-Cu joints by using the EG-0wt.%AA paste (a-d) and the EG-10wt.%AA paste (e-h) at sintering temperature of 200 °C (a,e), 250 °C (b,f), 300 °C (c,g) and 350 °C (d,h).

Fig. 3.9 gives a simple sintering mechanism of the sintered Cu joints prepared with our developed Cu paste. The as-synthesized Cu particles were coated with a thin oxide layer in the initial stage. The oxide layer would continually grow due to the O<sub>2</sub> impurity in N<sub>2</sub> during the sintering of EG-0wt.%AA paste (upper line). The layer was hardly removed even under high temperatures, finally resulting in the poor local sintering of Cu particles. The similar phenomenon occurred between the Cu paste and the Cu substrate and a clear gap was formed between them (Fig. 3.8a-d). In contrast, the Cu oxide layer was almost totally removed in EG-10wt.%AA Cu paste due to the self-reduction reaction between AA and Cu oxides (down line). Without the interruption of the oxide layer, the efficient diffusion of Cu atoms happened between the adjacent particles and contributed to the highly effective sintering of Cu particles. Similarly, the addition of AA also provided a self-protection ability to Cu paste which prevented the Cu particles and the Cu substrates from oxidization during the sintering process and contributed to tight interconnection. These results strongly suggest that a suitable reductant, which can provide self-reduction and self-protection characteristics for Cu paste, is essential and necessary for economical yet easily oxidized Cu particle pastes for use as die-attach material.

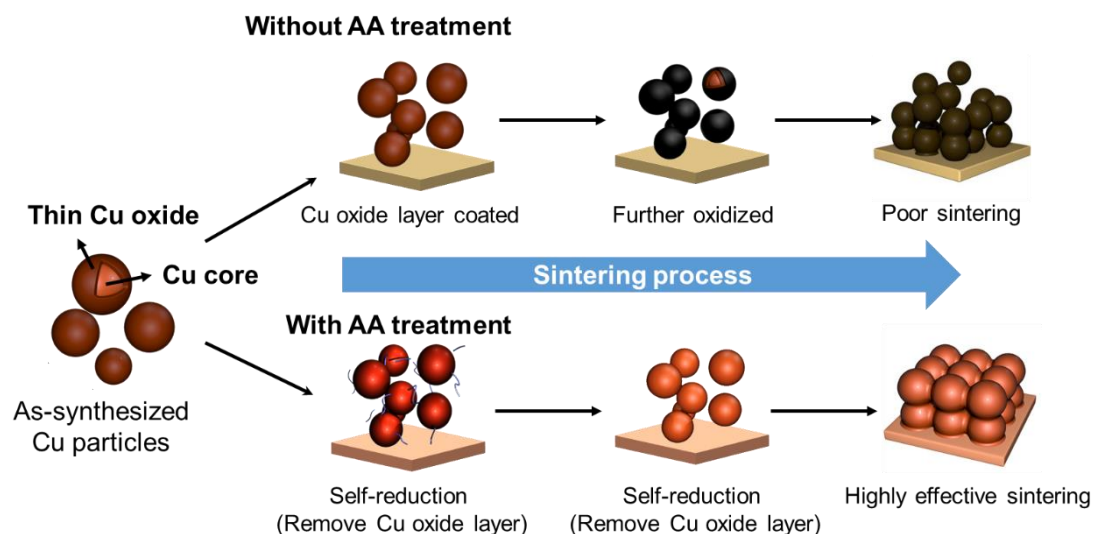


Fig. 3. 9 The promotion mechanism of AA in Cu pastes.

### 3.3.3 Development on Cu paste with AA-treated solvent

Considering the AA mainly improved Cu paste by its intrinsic self-reduction and self-protection characteristics, the AA additive may have the effect on other solvent. To identify its potential application in other solvents, various solvents were mixed with Cu particles to fabricate Cu paste. The candidates including the diethylene glycol (DG), triethylene glycol (TEG), and polyethylene glycol (PEG) which have reducibility during sintering process and are proved to be beneficial for the bondability of Cu paste [10, 28]. 2-amino-2-methyl-1-propanol (AMP) and 1-amino-2-propanol (IPA), which with the amino-group and can accelerate the decomposition of Cu oxides, are also selected as solvents [29-31]. Moreover, the pure water is also tested as a reference. When the DG, TEG, PEG and water were used as solvent. 10 wt% AA were added into DG and TEG to make reductive solvents. In contrast, only 5 wt% AA was added into PEG AMP and IPA because of the limitation of solubility. Then, those solvents were mixed with Cu particles as the mass ratio of 85: 15 to form Cu paste. The shear test was applied to the sintered Cu joints obtained from those paste which were sintered in the same condition (300 °C, 30 min, 0.4MPa, N<sub>2</sub>)

The shear strength of the sintered Cu joints obtained by those Cu paste were showed in Fig. 3.10. It was interesting that all the paste, even the pure water as solvent, could be

Chapter 3  
Realization of high-strength Cu sinter joining by  
Ascorbic acid-treated Cu particle paste

improved by AA additive, suggesting that AA has the excellent potential of applying in various solvent. The highest strength, which was obtained by TEG-AA paste, was 27.8 MPa. The sintered Cu joints obtained by DG-AA paste showed the shear strength of 26.1 MPa respectively, which are much higher to paste used pure DG solvent. PEG-AA paste showed the shear strength of 25.9 MPa, which was slightly higher than the PEG-Cu paste. The intrinsic reducibility of PEG and less AA content might be the reason. On the other hand, AA exhibited excellent effect on IPA and AMP. The joints obtained by AMP-AA Cu paste and IPA-AA Cu paste exhibited high shear strength of 19.6 MPa and 18.6 MPa respectively. However, those strength were still incomparable to that of TEG-AA paste.

In conclusion, AA shows excellent effect on improving the bondability of Cu paste in various solvent. Sintered Cu joints with high bonding strength could be obtained under the sintering condition of the low temperature of 300 °C, low pressure of 0.4 MPa, and an N<sub>2</sub> atmosphere with TEG-10wt% AA Cu paste. Moreover, TEG is toxic less. AA, known as vitamin C, is a mild antioxidant existing in nature without biohazards, even was used as a food additive to prevent spoilage [32, 33]. Thus, the presented TEG-AA Cu paste is totally safe and suitable for industrial application.

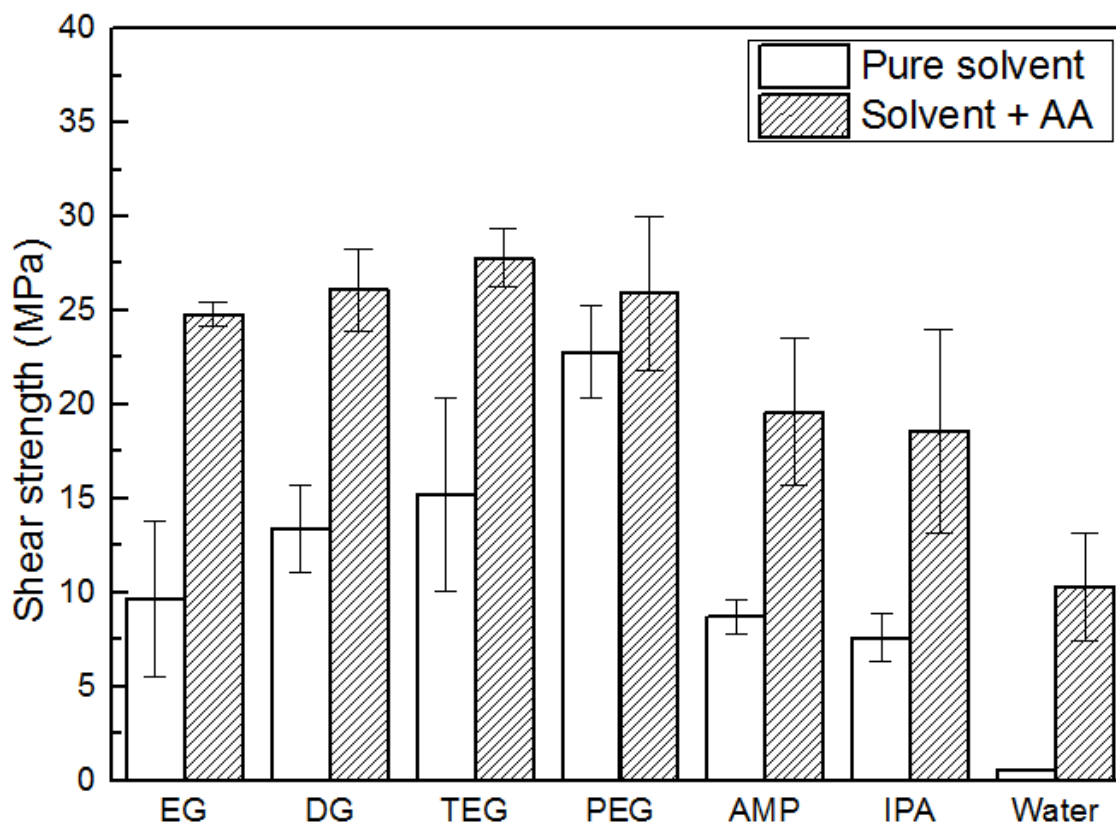


Fig. 3. 10 Shear strength of sintered Cu joints obtained by Cu paste using various solvent and AA additive

### 3.4 Conclusions

Sintered Cu joints with a high bonding strength were successfully achieved by using the improved Cu particle paste with novel reductant additive (AA). The AA additive endowed Cu paste self-reduction and self-protection characteristics. The oxide layer on the surface of Cu particles was reduced even at room temperature because of the efficient self-reduction characteristic. The self-protection characteristic further suppressed Cu particles and substrate from oxidation during the sintering process. These advantages promoted the diffusion of Cu atoms and accelerated the low-temperature and low-pressure sintering of Cu particle paste. Also, AA exhibited excellent applicability on various solvent, ensuring its industrial potential. Sintered Cu joints with high strength of

Chapter 3  
Realization of high-strength Cu sinter joining by  
Ascorbic acid-treated Cu particle paste

27.8 MPa were easily obtained from the Cu paste with TEG solvent including 1.3 wt.% AA under a suitable sintering condition (low temperature of 300 °C, low pressure of 0.4 MPa, and an N<sub>2</sub> atmosphere), which is comparable to the sintered Ag joints and Pb-Sn solder joints. This work illuminates a die-attach material which can be bonded in mild conditions and deliver a highly reliable bonding structure. This work further demonstrates that Cu paste with self-reduction and self-protection characteristics is an effective strategy to extend the applications of economical Cu pastes in high power semiconductor devices.

## References

- [1] Y. Jianfeng, Z. Guisheng, H. Anming, Y.N. Zhou, Preparation of PVP coated Cu NPs and the application for low-temperature bonding, *Journal of Materials Chemistry*, 21 (2011) 15981-15986.
- [2] A. Sarkar, A. Manthiram, Synthesis of Pt@ Cu core– shell nanoparticles by galvanic displacement of Cu by Pt<sup>4+</sup> ions and their application as electrocatalysts for oxygen reduction reaction in fuel cells, *The Journal of Physical Chemistry C*, 114 (2010) 4725-4732.
- [3] S. Zhou, B. Varughese, B. Eichhorn, G. Jackson, K. McIlwrath, Pt–Cu core–shell and alloy nanoparticles for heterogeneous NO<sub>x</sub> reduction: anomalous stability and reactivity of a core–shell nanostructure, *Angewandte Chemie*, 117 (2005) 4615-4619.
- [4] T. Yamauchi, Y. Tsukahara, T. Sakata, H. Mori, T. Yanagida, T. Kawai, Y. Wada, Magnetic Cu–Ni (core–shell) nanoparticles in a one-pot reaction under microwave irradiation, *Nanoscale*, 2 (2010) 515-523.
- [5] G. Ferik, J. Stergar, M. Drogenik, D. Makovec, A. Hamler, Z. Jagličić, I. Ban, The synthesis and characterization of nickel–copper alloy nanoparticles with a narrow size distribution using sol–gel synthesis, *Materials Letters*, 124 (2014) 39-42.
- [6] S. Magdassi, M. Grouchko, A. Kamyshny, Copper nanoparticles for printed electronics: routes towards achieving oxidation stability, *Materials*, 3 (2010) 4626-4638.
- [7] M. Grouchko, A. Kamyshny, S. Magdassi, Formation of air-stable copper–silver core–shell nanoparticles for inkjet printing, *Journal of Materials Chemistry*, 19 (2009) 3057-3062.
- [8] K. Woo, D. Kim, J.S. Kim, S. Lim, J. Moon, Ink-Jet printing of Cu– Ag-based highly conductive tracks on a transparent substrate, *Langmuir*, 25 (2008) 429-433.
- [9] W. Li, D. Hu, L. Li, C.-F. Li, J. Jiu, C. Chen, T. Ishina, T. Sugahara, K. Suganuma, Printable and Flexible Copper–Silver Alloy Electrodes with High Conductivity and Ultrahigh Oxidation Resistance, *ACS applied materials & interfaces*, 9 (2017) 24711-24721.

- [10] T. Fujimoto, T. Ogura, T. Sano, M. Takahashi, A. Hirose, Joining of Pure Copper Using Cu Nanoparticles Derived from CuO Paste, *MATERIALS TRANSACTIONS*, (2015).
- [11] J. Liu, H. Chen, H. Ji, M. Li, Highly Conductive Cu–Cu Joint Formation by Low-Temperature Sintering of Formic Acid-Treated Cu Nanoparticles, *ACS Applied Materials & Interfaces*, 8 (2016) 33289-33298.
- [12] S. Ding, J. Jiu, Y. Tian, T. Sugahara, S. Nagao, K. Suganuma, Fast fabrication of copper nanowire transparent electrodes by a high intensity pulsed light sintering technique in air, *Physical Chemistry Chemical Physics*, 17 (2015) 31110-31116.
- [13] S. Ding, J. Jiu, Y. Gao, Y. Tian, T. Araki, T. Sugahara, S. Nagao, M. Nogi, H. Koga, K. Suganuma, One-step fabrication of stretchable copper nanowire conductors by a fast photonic sintering technique and its application in wearable devices, *ACS applied materials & interfaces*, 8 (2016) 6190-6199.
- [14] Z. Liu, Y. Yang, J. Liang, Z. Hu, S. Li, S. Peng, Y. Qian, Synthesis of copper nanowires via a complex-surfactant-assisted hydrothermal reduction process, *The Journal of Physical Chemistry B*, 107 (2003) 12658-12661.
- [15] C.-J. Wu, Y.-J. Sheng, H.-K. Tsao, Copper conductive lines on flexible substrates fabricated at room temperature, *Journal of Materials Chemistry C*, 4 (2016) 3274-3280.
- [16] N.M. Zain, A. Stapley, G. Shama, Green synthesis of silver and copper nanoparticles using Ascorbic acid and Chitosan for antimicrobial applications, *Carbohydrate polymers*, 112 (2014) 195-202.
- [17] T. Ghodselahi, M. Vesaghi, A. Shafiekhani, A. Baghizadeh, M. Lameii, XPS study of the Cu@ Cu<sub>2</sub>O core-shell nanoparticles, *Applied Surface Science*, 255 (2008) 2730-2734.
- [18] G. Vernin, S. Chakib, S.M. Rogacheva, T.D. Obretenov, C. Párkányi, Thermal decomposition of ascorbic acid, *Carbohydrate Research*, 305 (1997) 1-15.
- [19] S. Jingyan, L. Yuwen, W. Zhiyong, W. Cunxin, Investigation of thermal decomposition of ascorbic acid by TG-FTIR and thermal kinetics analysis, *Journal of pharmaceutical and biomedical analysis*, 77 (2013) 116-119.

- [20] A. Kosenko, G. Emel'chenko, Equilibrium phase relationships in the system Cu-O under high oxygen pressure, *Journal of phase equilibria*, 22 (2001) 12-19.
- [21] M. Lenglet, K. Kartouni, J. Machefer, J.M. Claude, P. Steinmetz, E. Beauprez, J. Heinrich, N. Celati, Low temperature oxidation of copper: The formation of CuO, *Materials Research Bulletin*, 30 (1995) 393-403.
- [22] Y. Zhu, K. Mimura, M. Isshiki, Oxidation Mechanism of Copper at 623-1073 K, *MATERIALS TRANSACTIONS*, 43 (2002) 2173-2176.
- [23] K. Suganuma, J. Jiu, Advanced Bonding Technology Based on Nano-and Micro-metal Pastes, in: *Materials for Advanced Packaging*, Springer, 2017, pp. 589-626.
- [24] X. Liu, H. Nishikawa, Low-pressure Cu-Cu bonding using in-situ surface-modified microscale Cu particles for power device packaging, *Scripta Materialia*, 120 (2016) 80-84.
- [25] S. Jeong, K. Woo, D. Kim, S. Lim, J.S. Kim, H. Shin, Y. Xia, J. Moon, Controlling the thickness of the surface oxide layer on Cu nanoparticles for the fabrication of conductive structures by ink -jet printing, *Advanced Functional Materials*, 18 (2008) 679-686.
- [26] E. Ye, S.Y. Zhang, S. Liu, M.Y. Han, Disproportionation for growing copper nanowires and their controlled self -assembly facilitated by ligand exchange, *Chemistry-A European Journal*, 17 (2011) 3074-3077.
- [27] W. Li, C.-F. Li, F. Lang, J. Jiu, M. Ueshima, H. Wang, Z.-Q. Liu, K. Suganuma, Self-catalyzed copper-silver complex inks for low-cost fabrication of highly oxidation-resistant and conductive copper-silver hybrid tracks at a low temperature below 100° C, *Nanoscale*, 10 (2018) 5254-5263.
- [28] S. Park, R. Uwataki, S. Nagao, T. Sugahara, Y. Katoh, H. Ishino, K. Sugiura, K. Tsuruta, K. Suganuma, Low-pressure sintering bonding with Cu and CuO flake paste for power devices, in: *Electronic Components and Technology Conference (ECTC)*, 2014 IEEE 64th, IEEE, 2014, pp. 1179-1182.
- [29] W. Li, L. Li, Y. Gao, D. Hu, C.-F. Li, H. Zhang, J. Jiu, S. Nagao, K. Suganuma, Highly conductive copper films based on submicron copper particles/copper complex inks for printed electronics: Microstructure, resistivity, oxidation resistance,

Chapter 3  
Realization of high-strength Cu sinter joining by  
Ascorbic acid-treated Cu particle paste

- and long-term stability, *Journal of Alloys and Compounds*, 732 (2018) 240-247.
- [30] W. Li, H. Zhang, Y. Gao, J. Jiu, C.-F. Li, C. Chen, D. Hu, Y. Goya, Y. Wang, H. Koga, Highly reliable and highly conductive submicron Cu particle patterns fabricated by low temperature heat-welding and subsequent flash light sinter-reinforcement, *Journal of Materials Chemistry C*, 5 (2017) 1155-1164.
- [31] T. Yonezawa, H. Tsukamoto, Y. Yong, M.T. Nguyen, M. Matsubara, Low temperature sintering process of copper fine particles under nitrogen gas flow with Cu 2+-alkanolamine metallacycle compounds for electrically conductive layer formation, *RSC advances*, 6 (2016) 12048-12052.
- [32] M.Y. Lachapelle, G. Drouin, Inactivation dates of the human and guinea pig vitamin C genes, *Genetica*, 139 (2011) 199-207.
- [33] R. Caspi, *MetaCyc Compound: monodehydroascorbate radical*, (2009).



## **Chapter 4**

### **Reliability analysis of Cu sinter joining**

Chapter 4  
Reliability analysis of Cu sinter joining

#### 4.1 Introduction

Much work has already reported about the successful realization of sintered Cu joints with good bonding strength [1-5]. However, the reliability of sintered Cu joints during service has not been widely studied due to its complicated evolution. Sun et al. mentioned that sintered Cu joints exhibited a good stability under high temperature storage condition by focusing on the microstructure and mechanical properties changes [6]. However, there is no information about the composition evolution. In fact, metallic sintered joints with microporous microstructure was largely influenced by environmental factor such as oxygen, temperature and humidity, especially for Cu microporous microstructure. Cu oxides are easily formed in high temperature and high humidity air, which significantly influence the mechanical, electrical and thermal property of sintered Cu joints [7]. Unfortunately, no clear and detail reports in references can be found on the composition evolution during the reliability test. These information is very crucial for the application of the cheap and robust Cu joint in various devices.

In the last chapter, developed bimodal Cu particles paste with TEG-AA as solvent was proposed, which realized excellent bondability with good shear strength of 27.8 MPa when sintered in a relative mild condition (300 °C, 30 min, 0.4 MPa, and N<sub>2</sub>). In order to apply the Cu sinter joining in the devices, the reliability of the Cu joints was evaluated in this chapter.

Firstly, the environment stability of Cu joints is enforced. These Cu joints were put in high temperature (200 °C, in air or in vacuum) and in high humidity chamber (85 °C /85 RH) to observe the evolution in microstructure. Secondly, the thermal shock stability of the Cu joints was performed. In these tests, SiC dummy chips were firstly used to obtain the information of microstructure evolution. And then real SiC MOSFETs were directly bonded to DBC substrates by the Cu paste to make a simple devices for power cycle test. The bonding strength of Cu joints was also evaluated. Field emission scanning electron microscope (FE-SEM), energy-dispersive X-ray spectroscopy (EDX) and X-ray diffractometer (XRD) were used as well to monitor the evolution of microstructure,

element composition, and phase composition.

## **4.2 Experimental**

### **4.2.1 Fabrication of bonded sample**

The TEG-AA Cu paste was used to fabricate three kinds of test structures: i) Cu dummy chips (3 mm x 3 mm x 1 mm) bonded to Cu substrate; ii) SiC dummy chips (3 mm x 3 mm x 0.525 mm) sputtered with Ti (0.2  $\mu\text{m}$ ) and Cu (2  $\mu\text{m}$ ) bonded to DBC substrate. iii) SiC dummy chips bonded to Cu substrate. DBC substrate was a commercial one with  $\text{Si}_3\text{N}_4$  isolation interlayer. For the sake of clearness, the three kinds of samples have been called i) Cu-Cu, ii) SiC-Cu, and iii) SiC-DBC, respectively, in the following sections. The bonding process was performed at sintering temperature of 300 °C and in  $\text{N}_2$  (>99.9%) protective atmosphere.

### **4.2.2 Thermal/humidity storage test**

The Cu-Cu bonding samples was kept at thermal environment of 200 °C (in both  $\text{N}_2$  and vacuum) and high humidity environment of 85 °C/85 RH (relative humidity), for 50h, 100h, 200h, 500h and 1000h, respectively.

### **4.2.3 Thermal shock test and power cycle test**

The thermal shock test was performed on SiC-DBC bond samples from -40 °C to 250 °C for 1000 cycles both in the ambient atmosphere and the vacuum. The samples were hold for 30 min at each temperature step and the whole shock cycle last to 60 min, and. The power cycling test was performed on SiC MOSFETs (3 x 4.4 x 0.525 mm, Rohm. Co. Ltd.) which were bonded to DBC ( $\text{Si}_3\text{N}_4$ ) patterned substrates. The on-time was set to 3s and the temperature measurement at the initial step showed that the highest temperature during the test was reached 200 °C. Then during the 30s cooling process, the temperature decreased to 25 °C for the next cycle.

### **4.2.4 Characterization and evaluation**

The shear strength obtained from the shear test was used as the evaluation of bonding

strength. The shear height was 0.1 mm and the shear speed was 1 mm/min. FE-SEM was applied on the cross-section observation of joints to investigate their microstructure. In this study, the observation was performed both on the center and the edge part of chip because the defects caused by thermal shock usually occurred at the edge part of the chips. EDX was also used during FE-SEM observation to trace the element distribution. The XRD were applied on the broken fracture of the joints after the shear test to record the phase composition. Thermal transient tester (T3ester) was applied on SiC MOSFETs with DBC substrate before and after the power cycle test to monitor the evolution in thermal conductivity of joining layer.

### **4.3 Results and discussion**

#### **4.3.1 Bondability of sintered Cu joints on different structures**

Fig. 4.1 summarizes the shear strength performance of the sintered Cu joints in different structure. The highest shear strength was 27.8 MPa, achieved in Cu-Cu specimens. The strengths in SiC-DBC and SiC-Cu specimens were 25.5 MPa and 21.4 MPa, respectively. As a reference, the shear strength of traditional Pb-Sn solder is 23 MPa. The difference in strength might be attributed to the mismatch in coefficients of thermal expansion (CTEs) between chips and substrates. The SiC has a CTE of 4.9 ppm/°C, which is much lower than Cu (13.8 ppm/°C). After sintering process, which involves high temperature, a great internal stress could have been generated during cooling process, causing the inferior shear strength performance. In contrast, the DBC substrate, which embeds a low-CTE Si<sub>3</sub>N<sub>4</sub> ceramic layer, has a limited CTE and dramatically reduces the generation of internal stress during cooling. The aforementioned conclusion is in agreement with the well-known result, that using DBC substrate largely increases the reliability of semiconductor devices [8]. However, the thermal/humidity storage test had no concern of internal stress. Therefore, the Cu-Cu joints were used for thermal/humidity storage test while the SiC-DBC specimens were selected for the shock and power cycling tests.

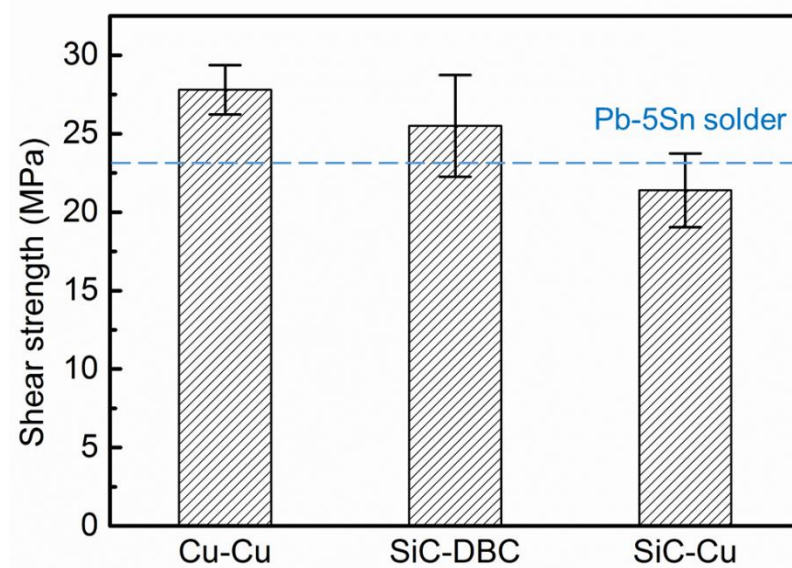


Fig. 4. 1 Shear strength of sintered Cu joints between different chips and substrate

#### 4.3.2 Thermal storage test and humidity storage test

Fig. 4.2 showed the shear strength evolution during thermal storage and humidity storage tests when aging time acted as variable. It was observed that the shear strengths of all aged Cu-Cu joints were higher than initial state. The shear strengths of Cu-Cu joints aged in the air shows an increase trend before 100 h storage, after 100 h storage in air, a small decrease was observed in shear strength. The shear strengths were 35.0 MPa, 38.8 MPa, 36.7 MPa, 34.4 MPa and 35.6 MPa when storage times were 50 h, 100 h, 200 h, 500 h and 1000 h, respectively. Interestingly, the corresponding strength value in vacuum were 29.9 MPa, 30.1 MPa, 32.5 MPa, 32.6 MPa and 33.4 MPa, respectively, which is inferior to the strength obtained in the air storage. On the other hand, only increase in shear strength was observed when joints were aged high humidity environment. The shear strengths of Cu-Cu joints were 28.6 MPa, 33.2 MPa 38.9 MPa, 38.2MPa and 40.1 MPa when storage times were 50 h, 100 h, 200 h, 500 h and 1000 h, respectively. The shear strength result is impressive because other high temperature die attach materials, such as sintered Ag joints and Pb-Sn solder joints, always exhibited deterioration in bonding strength during storage test [9-11]. In contrast, no deterioration in bonding strength even after 1000 h storage. This mechanical enforce property is attractive as a die-attach material.

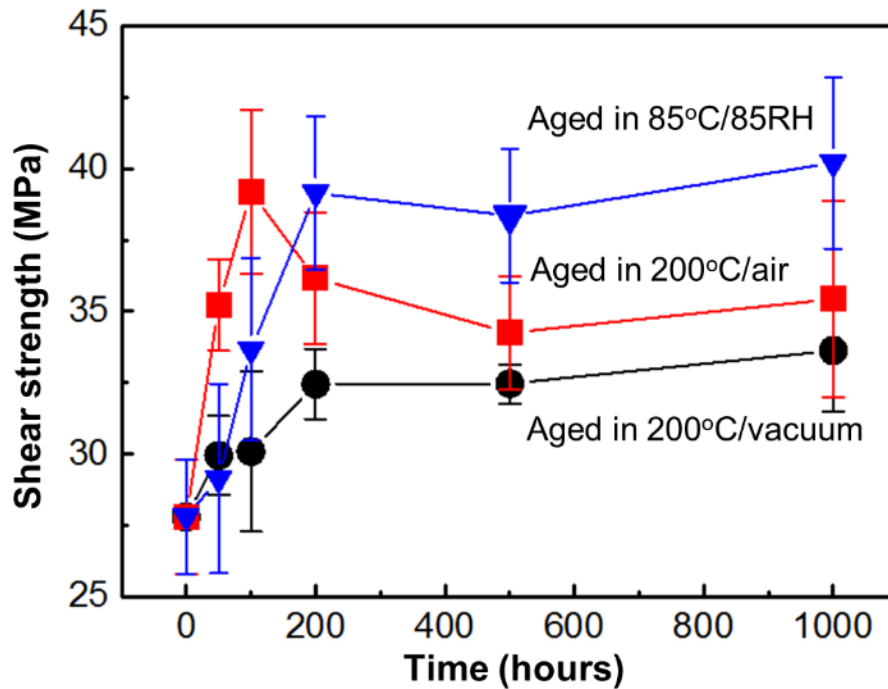


Fig. 4. 2 Shear strength of sintered Cu joints during various storage test

Fig. 4.3 shows the fracture and cross-section SEM observation of joints at the initial state and stored at 200 °C in air, at 200 °C in vacuum and at 85 °C/85 RH for 1000 h. It is observed that the microstructure of stored sintered Cu joints is denser than initial state. However, the structures in different storage condition exhibited different morphology. Nearly bulk-like microstructure was formed when the sintered Cu joints was aged in 200 °C, air. Pores were seldom observed, indicating a high bonding strength (Fig. 4.3b). From the cross-section micrograph (Fig. 4.3e), except for the denser structure of aged Cu joints was observed, the interconnection between sintered Cu and substrate was hardly distinguished. Also, the materials filled the pores in joints had a darker color than the Cu substrate and sintered Cu matrix in Fig. 4.3b. Considering the storage condition of 200 °C in the air, it was largely possible that the Cu joints were oxidized. On the other hand, the joints stored at 200 °C in vacuum did not exhibit much change in the morphology (Fig. 4.3c, 4.3 g). However, the more fracture traces than those of the initial state was observed (Fig. 4.3c), suggesting the thermal storage process improved the formation of necking growth and the interconnection between sintered paste and substrate. The microstructure of joints stored in 85 °C/85 RH did not exhibit the bulk-like structure but largely remained

the initial morphology. However, a shell-like coating was found to coat on the sintered Cu matrix (Fig. 4.3d). The coating was also observed in cross-section micrograph and likely enhanced the necking growths in sintered Cu joint (Fig. 4.3h).

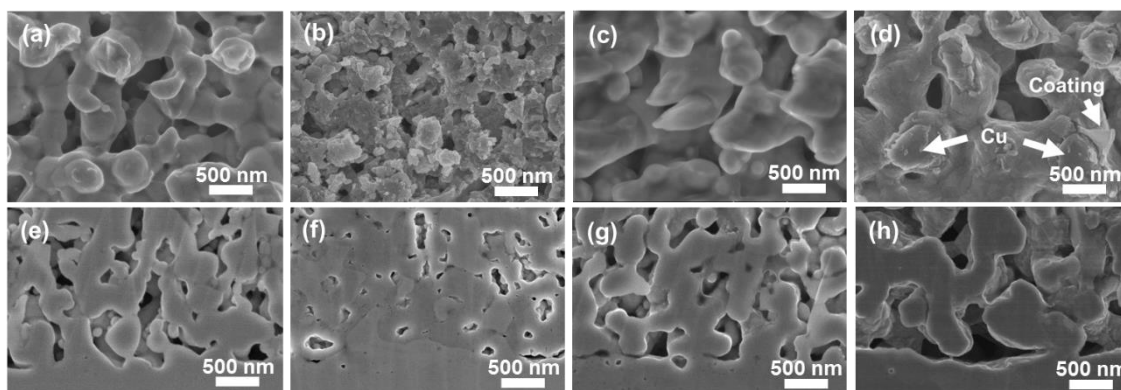
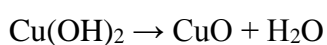
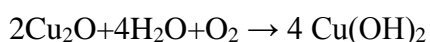


Fig. 4. 3 the fracture (a-d) and cross-section SEM observation of joints at the initial state (a,e) and stored at 200 °C in air (b,d), at 200 °C in vacuum (c,g) and 85 °C/85 RH (d,h) for 1000h

Fig. 4.4 showed the XRD patterns of sintered Cu joints in initial state and stored in 200 °C/air, 200 °C /vacuum and 85 °C/85 RH for 1000 h. The peaks assigned to Cu oxides appeared in joints aged in 200 °C/air and 85 °C/85 RH, indicating Cu joints could be easily oxidized. However, it is noticed that the Cu oxides formed in high temperature and high humidity aging test were different. Only Cu<sub>2</sub>O was detected in joints aged at high temperature in air, but both Cu<sub>2</sub>O and CuO were detected in joints aged in high humidity test. On the other hand, no Cu oxide was detected after aged in vacuum. The result indicated Cu<sub>2</sub>O was the main side-production during the thermal storage test. And the humidity accelerated the Cu<sub>2</sub>O to CuO by the following reaction:



The different Cu oxides formed in the air and humidity condition might contribute

to the different morphology,  $\text{Cu}_2\text{O}$  tended to fill the pores, and  $\text{CuO}$  was shell-like and coated to the Cu matrix. Considering the denser microstructure and stronger bonding strength. The formation of Cu oxides was regarded as beneficial to the mechanical properties of sintered Cu joints.

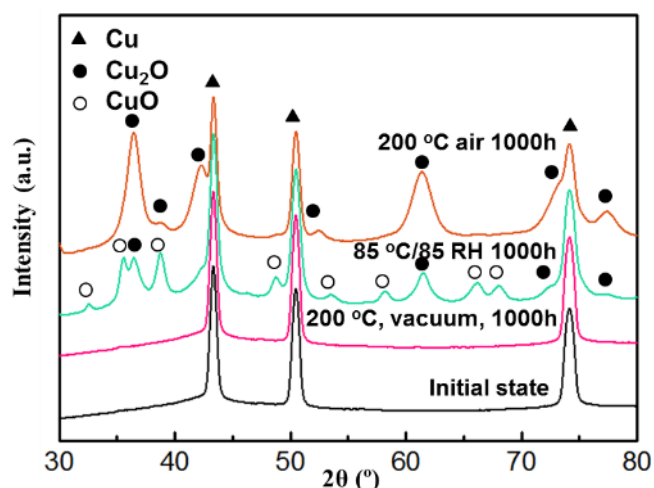


Fig. 4. 4 XRD pattern of intered Cu joints at as-bonded state, after 1000 h in thermal storage test and humidity storage test

The O content in aged Cu joints was measure by EDX during the observation of fracture surface of Cu joints. The result was depicted in Fig. 4.5. The O content in Cu joints increased when aging time extended. The initial joints contained O element around 0.7wt.%, which might be introduced by sintering and oxides residual in Cu paste due to the high oxidation tendency of Cu particles. The O content increased rapidly at the early step of aging. However, the O content increasing rate in 85 °C/85 RH test is slower than that in 200 °C aging test, indicating Cu oxides formed faster in high temperature rather than high humidity. After 1000 h aging, about 7.5wt.% O content was detected in high temperature aged Cu joint and around 4.3 wt.% O content was detected in high humidity aged Cu joint. The highest shear strength during storage in air was obtained at the time of 100 h, when the highest strength in high humidity was obtained at the time of 1000 h. the O content in both conditions were around 4 wt%, indicating the proper oxides content

could improve the bonding strength of sintered Cu joints.

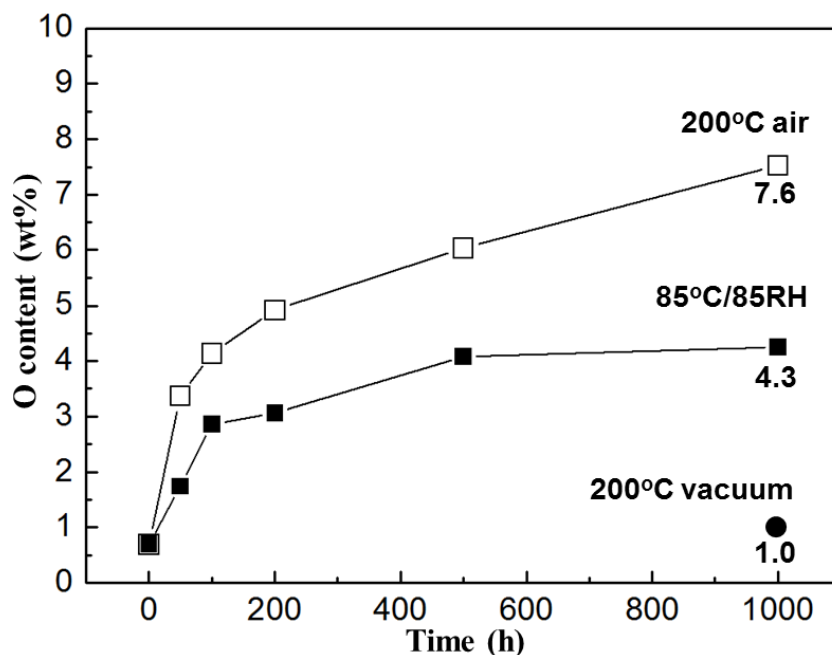


Fig. 4. 5 O element content in sintered Cu joints during thermal storage test and humidity storage test

In conclusion, the thermal storage test proved that sintered Cu joints could remain high level bonding strength in high temperature and high humidity. However, the formation of Cu oxides was hardly avoidable. Generally, the oxidation always happens during the storage of joints. Most oxidation is regarded as the reason for the defects [12, 13]. Seldom die-attach materials acted like sintered Cu joints which the oxides could improve the bonding strength. Considering the basic need of die-attach layer should possess both good bondability, the sintered Cu joint which can maintain considerable bonding strength in various environment has no doubt to be the promising die-attach material. However, the oxidation phenomenon of sintered Cu joints should be further investigated and the balance between bonding strength and electrical resistance should be fully evaluated before the commercial application of sintered Cu joints.

### 4.3.3 Thermal shock test

The storage test proved that sintered Cu joints maintained a good bondability under various storage condition. However, reliability can only be assessed through thermal cycle testing. Before the thermal shock test, a cross-section analysis was performed on the as-bonded specimens, as showed in Fig. 4.6. The SiC chips and DBC substrates were steadily connected by the sintered Cu joints. The typically porous structure was observed both at center and edge part of the chip (Fig. 4.6a and 4.6b). The high-resolution images indicated that a reliable interconnection was formed and no significant difference in the center and edge part was observed (Fig. 4.6c and 4.6d).

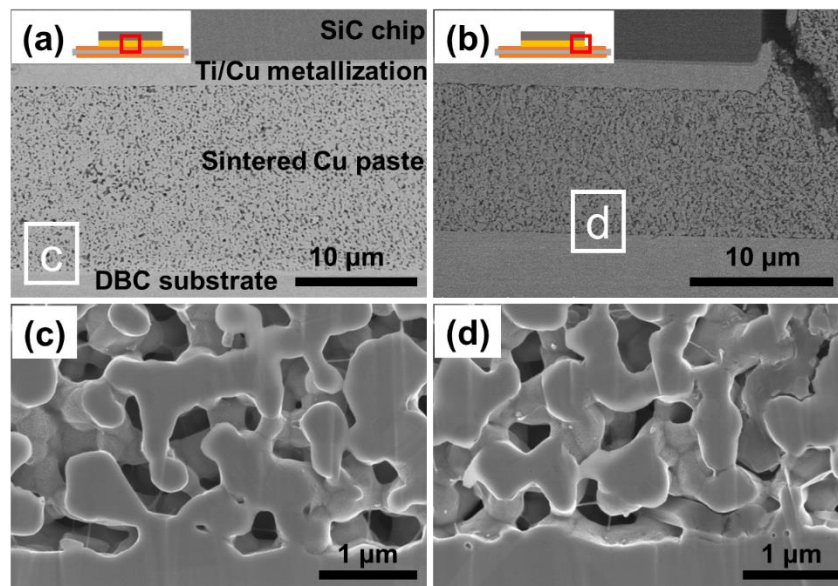


Fig. 4. 6 Cross-section observation on center (a) and edge (b) part of the as-bonded specimens, (c) and (d) are the high-resolution images of the corresponding parts in (a) and (b).

Fig. 4.7 shows the variation in shear strength of SiC-DBC specimens during thermal shock test both in ambient and vacuum. It was observed that the specimens aged in ambient atmosphere exhibited much higher strength the ones that aged in vacuum. More in detail, a significant increase in strength was observed after 100 cycles thermal shock test. The final strength after 1000 cycles was 45.1 MPa. The bonding strength was even higher than that obtained during storage test (Fig. 4.2). In contrast, the shear strength of

the specimens stressed in vacuum exhibited a continuous decrease. After 1000 cycles, only 9.6 MPa in strength could be achieved. The result in vacuum is similar to the sintered Ag joints [10]. To investigate the difference in bonding performance, the microstructure observation on specimens aged both in ambient atmosphere and vacuum were performed.

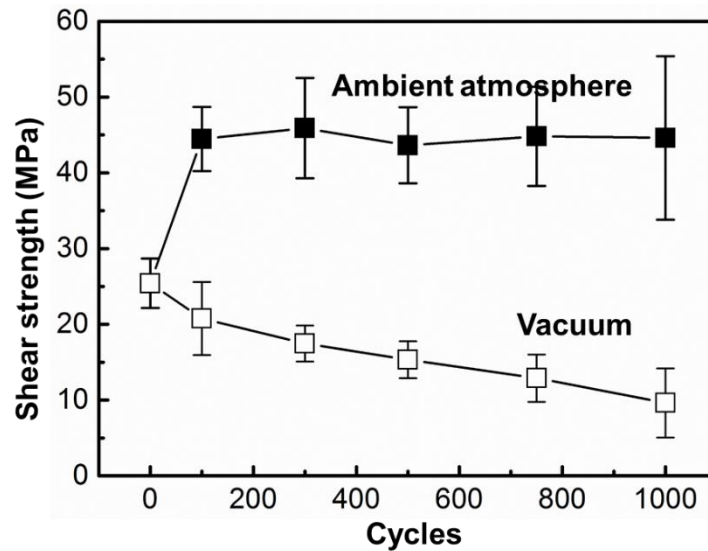


Fig. 4. 7 The shear strength evolution of SiC-DBC specimens were tested in ambient and vacuum

Fig. 4.8 shows the cross-section of the center part in the chip after specimens were tested in ambient atmosphere. The pores were filled up almost completely at the end of the stress test. Moreover, nearly no difference was discovered as the cycles increased from 100 cycles to 500 cycles and even 1000 cycles (Fig. 4.8a, 4.8b and 4.8c), indicating the joints were quite stable during the thermal shock test. The high resolution images confirmed the phenomenon that the pores were largely filled. The microstructure is similar to that obtained in thermal storage test, which indicate the formation of Cu oxides. Moreover, those Cu oxides filled Cu joints had a high resistance toward thermal shock. No defect was detected in the center observation.

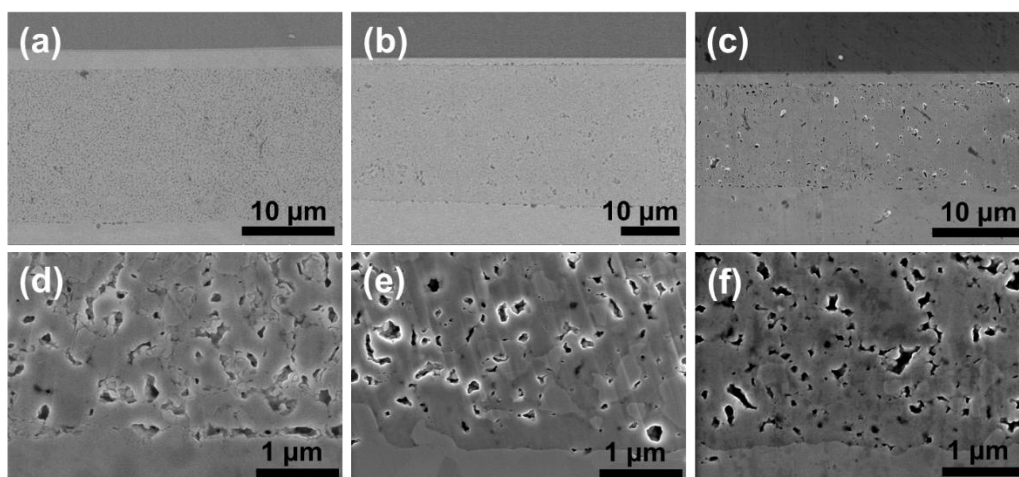


Fig. 4. 8 Cross-section observation on center part of specimens accomplished with thermal shock test of 100 cycles (a), 500 (b) and 1000 (c) in ambient, d, e and f were the high-resolution images of a, b and c, respectively.

Fig. 4.9 shows the cross-section of the edge part in the chips. The similar morphology of that in the center observation was obtained. No obvious defects such as crack and lift-off which was often caused by internal stress were observed until 1000 cycles (Fig. 4.10a 5b and 5c). Some defects could be observed when cycles reached to 1000 cycles. Those defects included fracture in metallization (Fig. 4.10d), cracks (Fig. 4.10e) and lift-off at the substrate. However, those defects seemed to have limited influence on bonding performance because the joints with high strength could still be achieved. This result is quite interesting because the sintered Cu joints

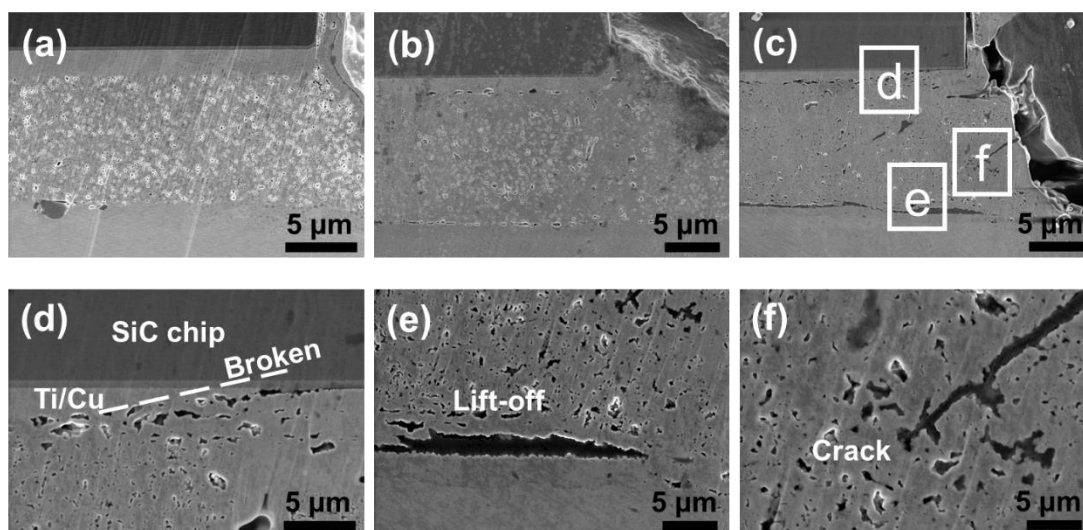


Fig. 4. 9 Cross-section observation on edge of specimens after thermal shock test of 100

cycles, 500 cycles and 1000 cycles in ambient, d, e and f, which show the defects, are the high-resolution images of the corresponding parts in c.

The situation was quite different when specimens were tested in the vacuum. Fig. 4.10 shows the cross-section of the center part in the chip after specimens were tested in the vacuum. The specimens in vacuum preserved its porous structure, which is significantly different from what happened in ambient atmosphere. Moreover, the low magnification image (Fig. 4.10a) showed that an obvious deformation occurred on the substrate, indicating the internal stress significantly influence the bonding performance. The deformation caused variation in distance between chip and substrate and formed hills and valleys on the substrate. At the hills (Fig. 4.10b), the distance between chips and substrate decreased. The porous structure seemed to be compressed and a denser structure was observed (Fig. 4.10b). In contrast, at the valleys (Fig. 4.10c), the distance between chips and substrate increased, and some cracks due to the enlarged distance were observed. Although the Cu joints still stay unbroken, the uneven structure can be certainly regarded as the inferior in bonding strength. On the other hand, the deformation in substrate can hardly observed when sintered Cu joints were tested in ambient atmosphere, indicating the denser structure has a high resistance toward deformation in substrate and prevented the formation of uneven bonding layer.

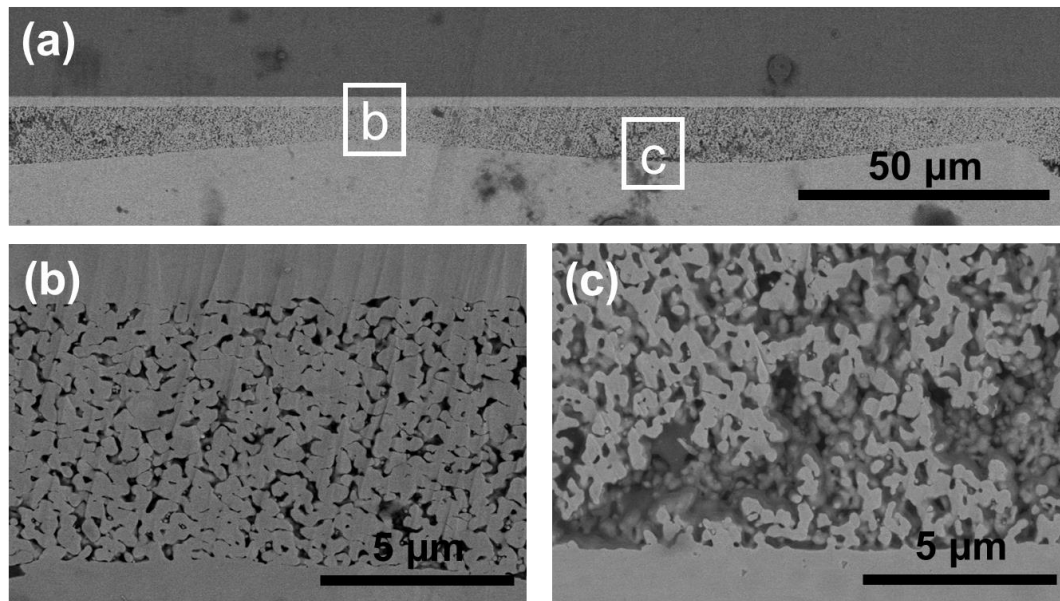


Fig. 4. 10 Cross-section observation on the center of specimens after thermal shock test of 1000 cycles in vacuum, b and c are the high-resolution images of the corresponding parts in a.

Fig. 4.11 shows the cross-section of the edge part in the chips after the specimens were tested in vacuum. The edge part of the chip was nearly broken in this case (Fig. 4.11a). The sintered Cu at edge had a similar porous structure (Fig. 4.11b). Hills and valley in substrate were also observed (Fig. 4.11c and 4.11d). Unlike the center part, in the edge part the chip was nearly taken apart from the substrate because of the cracks and compressions. It can be expected that the observed defects would propagate inwards with testing, with a significant deterioration in shear strength.

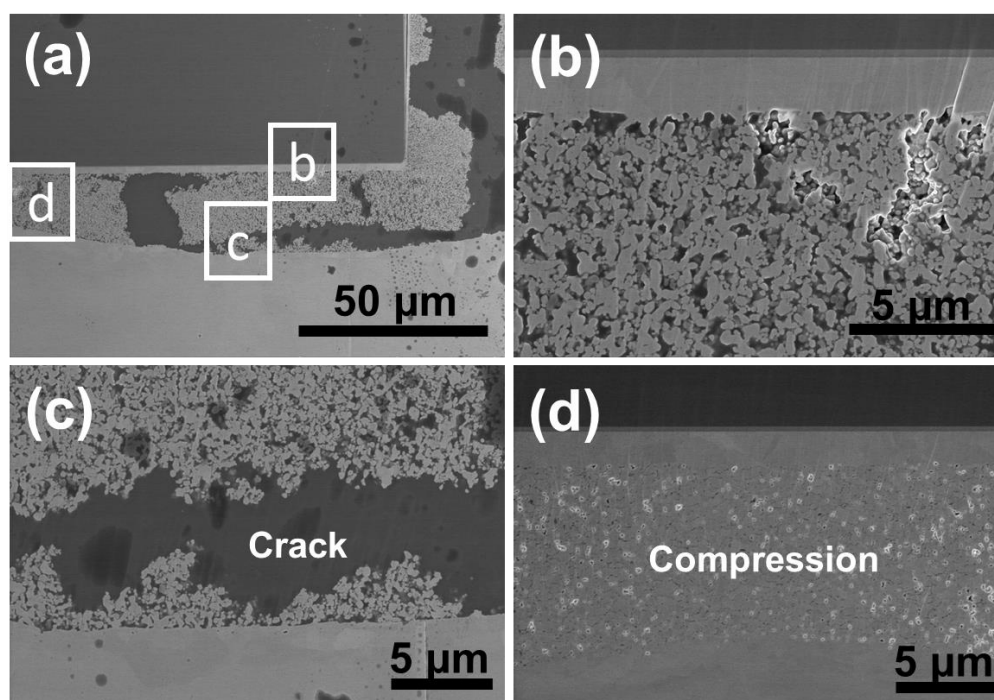


Fig. 4. 11 Cross-section observation on the edge of specimens after thermal shock test of 1000 cycles in vacuum, b, c and d are the high-resolution images of the corresponding parts in a.

To identify the reason which causes the significant difference in microstructure between specimens tested in ambient atmosphere and vacuum. EDX analysis was applied to the cross-section of specimens both tested in ambient and vacuum. The results have been shown in Fig. 4.12. It can be observed that there was an obvious O concentration in specimens after tested in ambient (Fig. 4.12b), which did not exist in as-bonded specimens (Fig. 4.12a) and specimens after tested in vacuum (Fig. 4.12c). This result indicated the similar oxidation phenomenon was also occurred during thermal shock test in ambient atmosphere. The spectrometer containing analysis also confirmed that the sintered Cu joints contained 6.22 wt% O element after 1000 thermal shock cycles in ambient (Fig. 4.12d), which is far higher than those tested in the vacuum (0.31 wt%).

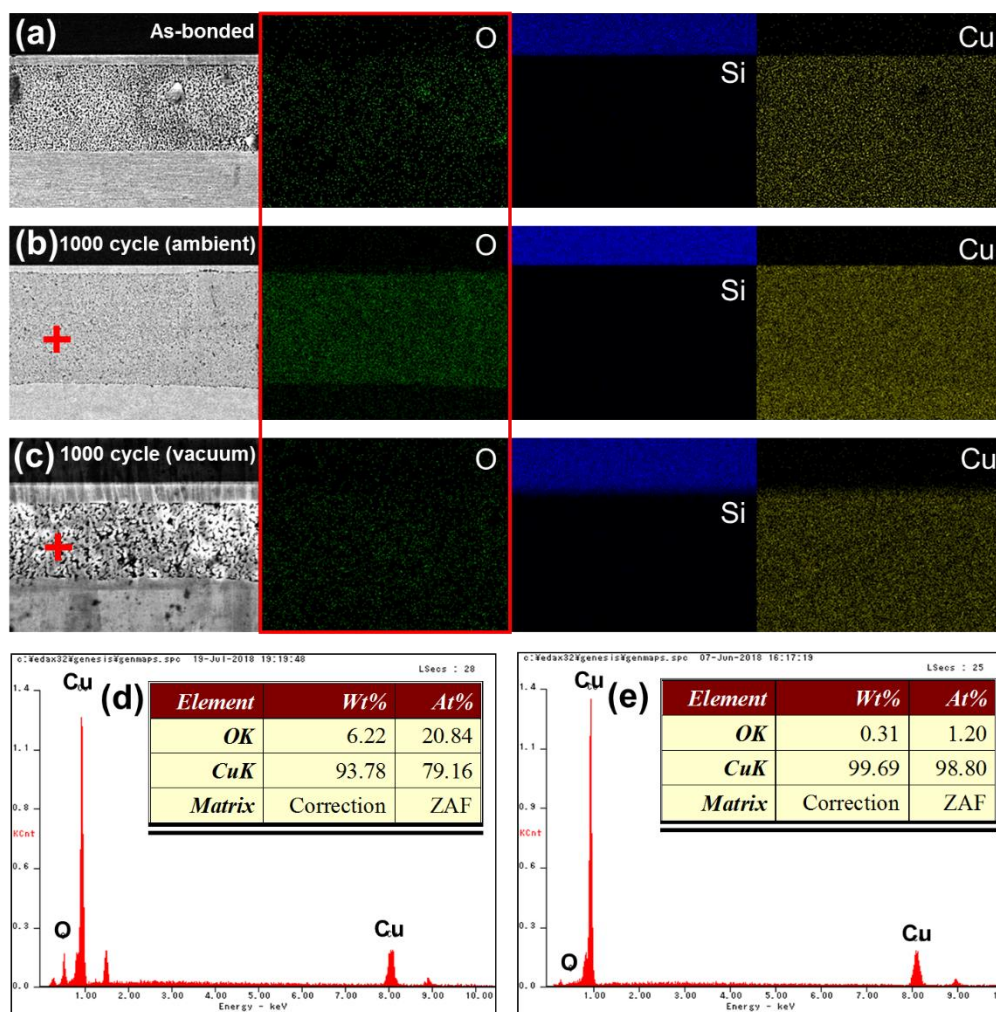


Fig. 4. 12 EDX analysis on the cross-section of specimens of as-bonded state (a), after 1000 cycles in ambient (b) and vacuum (c), d and e were point analysis spectra of b and c respectively

The XRD recorded the phase information of the joints at the as-bonded state and after 1000 cycles thermal shock test both in ambient and vacuum (Fig. 4.13). In the XRD pattern of as-bonded specimens, only three peaks attributed to Cu (bcc) were observed, suggesting the pure sintered Cu was obtained. The similar pattern was also obtained in specimens tested in vacuum. Though small peaks indicated the existence of  $\text{Cu}_2\text{O}$ , the weak peak intensity suggested the content of both types of Cu oxides is quite low, which was also proved by EDX result (0.31 wt%). In contrast, obvious oxides peaks were observed in the pattern obtained in specimens after thermal shock test in ambient,

corresponding to the 6.33 wt% in O content which showed in EDX analysis.

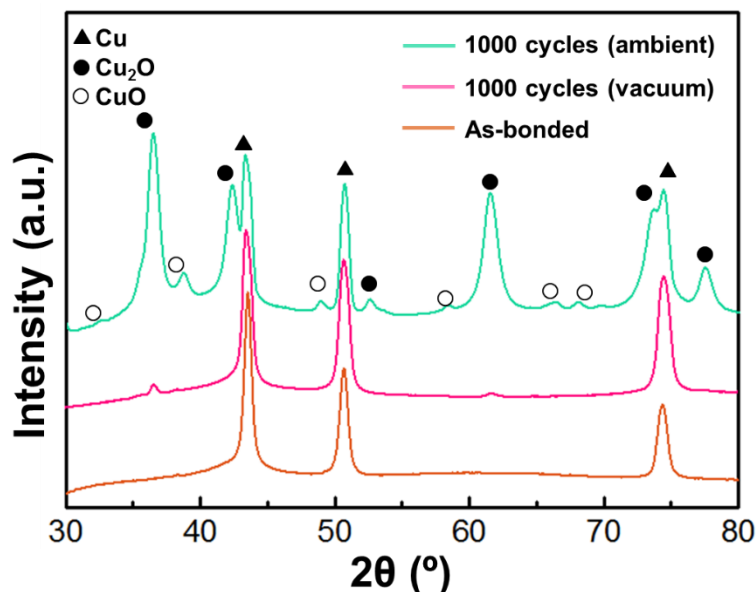


Fig. 4. 13 XRD patterns of sintered Cu joints at as-bonded state, after 1000 cycle in ambient and vacuum

In conclusion, sintered Cu joints exhibited high reliability toward thermal shock test. During the thermal shock test in ambient atmosphere, no deterioration of bonding strength in sintered Cu joints was observed during thermal shock test. This result is cheerful because the sintered Ag joints and Pb-Sn solder joints always exhibited inferior bonding strength after thermal shock test [11, 14]. It is proved that Cu can be oxidized during the thermal shock test, According to XRD result, the Cu oxides mainly consisted of Cu<sub>2</sub>O, which was similar to that during thermal storage test. Approximate 30 wt% of the joints consisted of Cu<sub>2</sub>O calculated from the EDX data. Those formed Cu oxides have low density (6 g/cm<sup>3</sup>) than Cu (8.96 g/cm<sup>3</sup>), which occupied the largest volume of the pores. Thus, denser structure was formed, and with less pores, the joint became much stronger. The obtained structure also had high resistance against the deformation in substrate, with almost no formation of compression and cracks and extended endurance against thermal shock. On the other hand, the thermal shock test in vacuum is close to the operating condition. The deformation of substrate caused by internal stress could be the main problem. Fortunately, the problem had been noticed by some researchers, solutions such

as thermal stress relaxation structure had been proposed to deal with the problem [15]

In addition, the detection of oxidation could be a problem for the industrial application of sintered Cu joints. Moreover, most power devices were operating under resin-sealed module, but in present work, samples were only exposed to air or vacuum. Considering the resin might fill the porous structure of sintered Cu joints and cause the variety in properties, further investigation should be applied on the actual devices.

\

#### **4.3.4 Power cycle test**

The existence of Cu oxides introduce some concerns such as the decrease in thermal or electrical conductivity. To identify the deterioration in thermal conductivity, the SiC MOSFET-DBC device bonded by sintered Cu joints was evaluated by power cycles test for 1000 cycles. The thermal conductivity variation was monitored by T3ster technology. The results were compared in Fig. 4.14. It can be noticed that the MOSFET devices survived after 1000 cycle's power cycle test. Moreover, the T3ster results show the sintered Cu joints have nearly no change after power cycle test, indicating no large defects occurred during power cycle test. For time being, the sintered Cu joints shows great reliability both in thermal shock test and power cycle test, suggesting its great potential as the next generation die-attach material.

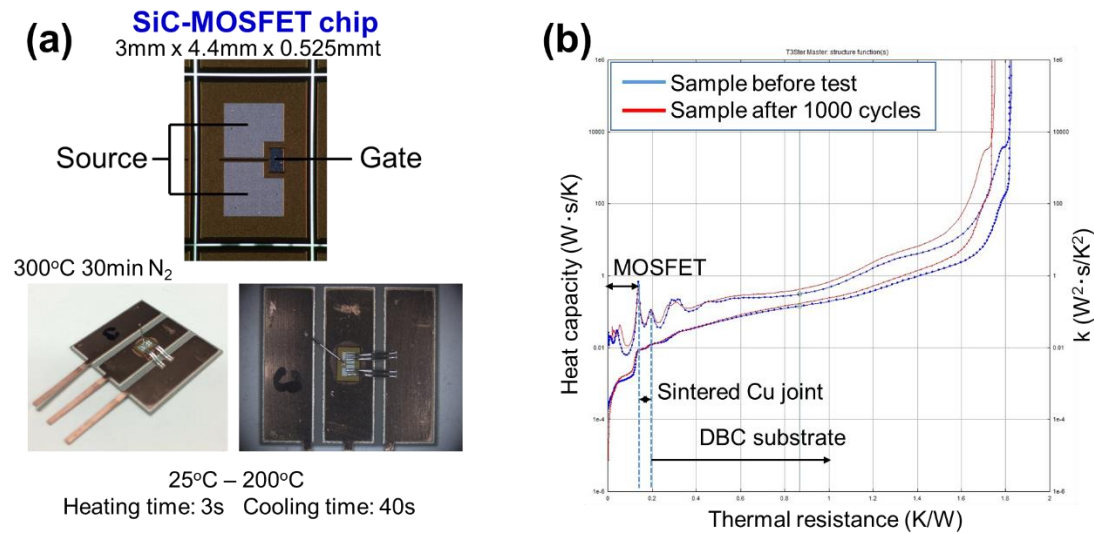


Fig. 4. 14 power cycle test of SiC MOSFET with DBC substrate (a), and T3ster result of samples before and after power cycles test of 1000 cycles

#### 4.4 Conclusion

The reliability of sintered Cu joints was evaluated by various environmental test. Firstly, High-strength sintered Cu joints were successfully achieved on SiC-DBC structure. The shear strength on SiC-DBC was 25.5 MPa, which is better than that of tradition Pb-Sn solder, suggesting the industrial applying possibility of the sintered Cu joints. The sintered Cu joints exhibited a special bonding enhancement based on oxidation, which ensured good bonding strength during both thermal storage test and humidity storage test. During the thermal shock test, the sintered Cu joints also exhibited excellent thermal shock reliability when the test condition was in ambient atmosphere, but inferior reliability was achieved when the sintered Cu joints were tested in vacuum. The reason of the difference is attributed to the formation of Cu oxides which has been proved with spectrometry analysis on the tested samples. However, the power cycle test showed that the sintered Cu joints were able to maintain a similar thermal conductivity even after 1000 cycles, suggesting the remarkable potential of the sintered Cu joints as disruptive die-attach materials for high-reliability applications.

## References

- [1] Y. Jianfeng, Z. Guisheng, H. Anming, Y.N. Zhou, Preparation of PVP coated Cu NPs and the application for low-temperature bonding, *Journal of Materials Chemistry*, 21 (2011) 15981-15986.
- [2] T. Fujimoto, T. Ogura, T. Sano, M. Takahashi, A. Hirose, Joining of Pure Copper Using Cu Nanoparticles Derived from CuO Paste, *MATERIALS TRANSACTIONS*, 56 (2015) 992-996.
- [3] X. Liu, H. Nishikawa, Low-pressure Cu-Cu bonding using in-situ surface-modified microscale Cu particles for power device packaging, *Scripta Materialia*, 120 (2016) 80-84.
- [4] J. Liu, H. Chen, H. Ji, M. Li, Highly Conductive Cu–Cu Joint Formation by Low-Temperature Sintering of Formic Acid-Treated Cu Nanoparticles, *ACS Applied Materials & Interfaces*, 8 (2016) 33289-33298.
- [5] Y.Y. Dai, M.Z. Ng, P. Anantha, Y.D. Lin, Z.G. Li, C.L. Gan, C.S. Tan, Enhanced copper micro/nano-particle mixed paste sintered at low temperature for 3D interconnects, *Applied Physics Letters*, 108 (2016) 263103.
- [6] S. Sun, Q. Guo, H. Chen, M. Li, C. Wang, Solderless bonding with nanoporous copper as interlayer for high-temperature applications, *Microelectronics Reliability*, 80 (2018) 198-204.
- [7] H. Niu, A review of power cycle driven fatigue, aging, and failure modes for semiconductor power modules, in: 2017 IEEE International Electric Machines and Drives Conference (IEMDC), IEEE, 2017, pp. 1-8.
- [8] C. Choe, C. Chen, S. Noh, K. Suganuma, Thermal Shock Performance of DBA/AMB Substrates Plated by Ni and Ni–P Layers for High-Temperature Applications of Power Device Modules, *Materials*, 11 (2018) 2394.
- [9] R. Khazaka, L. Mendizabal, D. Henry, Review on Joint Shear Strength of Nano-Silver Paste and Its Long-Term High Temperature Reliability, *Journal of Electronic Materials*, 43 (2014) 2459-2466.
- [10] H. Zhang, C. Chen, J. Jiu, S. Nagao, K. Suganuma, High-temperature reliability of

- low-temperature and pressureless micron Ag sintered joints for die attachment in high-power device, *Journal of Materials Science: Materials in Electronics*, 29 (2018) 8854-8862.
- [11] H. Zhang, S. Nagao, K. Suganuma, H.-J. Albrecht, K. Wilke, Thermostable Ag die-attach structure for high-temperature power devices, *Journal of Materials Science: Materials in Electronics*, 27 (2016) 1337-1344.
- [12] J. Kim, H. Schoeller, J. Cho, S. Park, Effect of Oxidation on Indium Solderability, *Journal of Electronic Materials*, 37 (2008) 483-489.
- [13] R.K. Shiue, L.W. Tsay, C.L. Lin, J.L. Ou, The reliability study of selected Sn–Zn based lead-free solders on Au/Ni–P/Cu substrate, *Microelectronics Reliability*, 43 (2003) 453-463.
- [14] R. Satoh, K. Arakawa, M. Harada, K. Matsui, Thermal fatigue life of Pb-Sn alloy interconnections, *IEEE Transactions on Components, Hybrids, and Manufacturing Technology*, 14 (1991) 224-232.
- [15] D. Kim, C. Chen, A. Suetake, C. Choe, T. Sugahara, S. Nagao, K. Suganuma, Development of thermal shock-resistant of GaN/DBC die-attached module by using Ag sinter paste and thermal stress relaxation structure, 2018.

## **Chapter 5**

### **Conclusions**



In this dissertation, a novel Cu particles paste was developed for high temperature die-attach application in WBG devices as a low-cost, green and reliable substitute of traditional and highly toxic Pb-based solders. The synthesis process of Cu particles with bimodal size distribution, the composition of Cu paste with high effective additives, die-attached sintering parameters and reliability of sintered Cu joint under different environment were demonstrated in detail to realize a high strength and high stability Cu joint in WBG devices. The results illuminate a promising die-attach process based on affordable Cu particles materials, which will largely contribute to the development of clean and sustainable energy in semiconductor industry.

In Chapter 1, the history of the power devices and relative package technology were briefly reviewed. With the requirement in high temperature electronic packaging, relative technology and materials were summarized. Especially, current choice of various die-attach materials were reviewed with their bonding mechanism, development trends, application fields, and technical limitation. Package technology based on Cu pastes was mainly selected and discussed to evaluate the application prospect from its characters, cost, performance, encountering problems until now. It was concluded Cu pastes is a promising package technology was taken by improving its intrinsic oxidation with suitable strategies, such as size tailor, optimizing composition, controlling sintering conditions.

In Chapter 2, bimodal Cu particles with desired size distribution were successfully synthesized by a simple and large-scale polyol process by selecting suitable Cu sources, additives. Both of soluble Cu sources and insoluble Cu sources were possible for the large-scale preparation of Cu particles with different size and size distribution. Insoluble  $\text{Cu}(\text{OH})_2$  was better to control the size distribution of Cu particles with ideal bimodal type. That related to the slow and stable dissolution process of Cu source. Moreover,  $\text{Na}_2\text{S}$  additive could largely accelerate the reduction reaction of Cu ions in Cu source, which controlled the formation of Cu nucleus resulting in the tailor of size and size distribution

of Cu particles. The Cu pastes based the synthesized bimodal Cu particles achieved a high bonding strength above 25 MPa at 350°C with a 0.4 MPa assisting pressure. The high strength was contributed to the size matching and increasing diffusion effect between particles during sintering process. And the strength was superior to many joints utilizing expensive nano-Cu pastes, and furtherly confirmed that the tailor of Cu particles was feasible strategy. However, due to the intrinsic oxidation, some small Cu particles in the Cu pastes seems hinder the sintering process and high bonding strength can only achieved in reductive formic acid atmosphere..

In Chapter 3, in order to decrease the negative effect of oxide, reducing additives was used to improve the bondability of Cu sinter joining. The AA additive endowed Cu paste self-reduction and self-protection characteristics. The oxide layer on the surface of Cu particles was reduced even at room temperature because of the efficient reduction characteristic of AA. The self-protection characteristic further suppressed Cu particles and substrate from oxidation during the sintering process. These advantages promoted the diffusion of Cu atoms and accelerated the low-temperature and low-pressure sintering of Cu particle paste. Also, AA shows excellent adaptability to various solvent, which ensuring its great potential in industrial application. Sintered Cu joints with high strength of 27.8 MPa were easily obtained with 1.3 wt.% AA at only 300 °C in N<sub>2</sub> atmosphere.

In Chapter 4, the environmental stability and thermal shock reliability of Cu sinter joining were confirmed. Thermal storage test, humidity storage test and thermal shock test were applied on sintered Cu joints. Sintered Cu joints exhibited a special oxidation property, which ensuring excellent bonding strength in storage test. Moreover, the sintered Cu joints also exhibited more excellent thermal shock reliability in ambient atmosphere than in vacuum. The reason of the difference is attributed to the formation of Cu oxides which increased the strength in ambient. Lastly, the power cycle test showed that the sintered Cu joints were able to maintain a similar thermal conductivity even after 1000 cycles, suggesting the remarkable potential of the sintered Cu joints as disruptive die-attach materials for high-reliability applications.

In conclusion, an innovatively one-step synthesis process was developed to obtain bimodal Cu particles. And highly reliable Cu particles sinter joining could be realized at a relatively mild sintering condition (300 °C, 30 min, 0.4 MPa, N<sub>2</sub>) by the AA-treated Cu paste. The established Cu sinter joining has comparable bondability to the widely applied Pb-Sn solder and Ag sinter joining technology, ensuring it is as promising a candidate as die-attach material. The reliability analysis of the present Cu sinter joining unveiled the unusual bonding enhancement based on oxidation, which could guide further investigation of Cu sinter joining technology. In this work, Cu sinter joining exhibits excellent bondability, high storage reliability and high resistance toward thermal shock, suggesting its illuminating future as die-attach material for the next generation power devices.

Chapter 5  
Conclusion

# Research achievements

## A. Papers

1. Yue Gao, Wanli Li, Chuantong Chen, Hao Zhang, Jinting Jiu, Cai-Fu Li, Shijo Nagao and Katsuaki Suganuma, “Novel copper particle paste with self-reduction and self-protection characteristics for die attachment of power semiconductor under a nitrogen atmosphere” *Materials & Design*, 160 (2018) 1265-1272.
2. Yue Gao, Wanli Li, Hao Zhang, Jinting Jiu, Dawei Hu and Katsuaki Suganuma, “Size-Controllable Synthesis of Bimodal Cu Particles by Polyol Method and Their Application in Die Bonding for Power Devices” *IEEE Transactions on Components, Packaging and Manufacturing Technology*, 8 [12] (2018) 2190-2197.
3. 高悦, 石名敏之, 丁蘇, 酒金婷, 菅原徹, 長尾至成, 菅沼克昭, 銅ナノワイヤの合成と光焼結による高性能透明導電膜の作製, *日本金属学会誌*, 2017, 81 巻, 8 号, p. 383-388.
4. Yue Gao, Hao Zhang, Wanli Li, Jinting Jiu, Shijo Nagao, Tohru Sugahara, Katsuaki Suganuma, “Die Bonding Performance Using Bimodal Cu Particle Paste Under Different Sintering Atmospheres” *Journal of Electronic Materials*, 46 [7] (2017), 4575–4581.
5. Yue.Gao, Shuhei Takata. Chuantong Chen, Shijo Nagao, Katsuaki Suganuma, Amir Sajjad Bahman, Francesco Iannuzzo, “Reliability analysis of sintered Cu joints for SiC power devices under thermal shock condition”, *Microelectronics Reliability*, **Under review**
6. Chuantong Chen, Dongjin Kim, Zhenghong Wang, Zheng Zhang, Yue Gao, Chanyang Choe and Katsuaki Suganuma, “Low temperature low pressure solid-state porous Ag bonding for large area and its high-reliability design in die-attached power modules”, *Ceramics International*, 45 [7] (2019) 9573-9579
7. Wanli Li, Lingying Li, Yue Gao, Dawei Hu, Cai-Fu Li, Hao Zhang, Jinting Jiu, Shijo Nagao, and Katsuaki Suganuma, “Highly conductive copper films based on submicron copper particles/copper complex inks for printed electronics: microstructure, resistivity, oxidation resistance, and long-term stability” *Journal of*

- Alloys and Compounds, 731 [15] (2018), 1280-1287
8. Hao Zhang, Wanli Li, Yue Gao, Hao Zhang, Jinting Jiu, and Katsuaki Suganuma, “Enhancing Low-Temperature and Pressureless Sintering of Micron Silver Paste Based on an Ether-Type Solvent” *Journal of Electronic Materials*, 46 [8] (2017), 5201–5208
  9. Wanli Li, Hao Zhang, Yue Gao, Jinting Jiu, Cai-fu Li, Chuantong Chen, Dawei Hu, Yusuke Goya, Yutao Wang, Hirotaka Koga, Shijo Nagao and Katsuaki Suganuma, “High reliable and high conductive submicron Cu particle patterns fabricated by low temperature heat-welding and subsequent flash light sinter-reinforcement” *Journal of Materials Chemistry C*, 5 (2017), 1155-1164
  10. Hao Zhang, Yue Gao, Jinting Jiu, and Katsuaki Suganuma, “In situ bridging effect of Ag<sub>2</sub>O on pressureless and low-temperature sintering of micron-scale silver paste”, *Journal of Alloys and compounds*, 696 [5] (2017), 123-129

## **B. Proceeding and presentations**

1. Yue Gao, Chuantong Chen, Shijo Nagao, Katsuaki Suganuma, Amir Sajjad Bahman, Francesco Iannuzzo, “Highly Reliable Package using Cu Particles Sinter Paste for Next Generation Power Devices”, PCIM Europe Conference 2019, Nuremburg, Germany, May 7-9. 2019
2. Yue Gao, Shijo Nagao, Akio Shimoyama, Shinichi Yamauchi, Takahiko Sakaue, Yoichi Kamikoriyama, and Katsuaki Suganuma, “Sintering Cu paste die-attach for high T<sub>J</sub> power devices” PCIM Europe Conference 2018, Nuremburg, Germany, June 5-7 2018
3. Yue Gao, Hiroki Yoshikawa, Shijo Nagao, Takahiko Sakagami, Yoichi Kamikoriyama, Takashi.Sasaki, Masako Kagami, Tohru Sugahara, and Katsuaki Suganuma, “Long-term reliability of Cu-particle-sinter die-attached SiC-SBD” International Forum on Wide Bandgap Semiconductors China (IFWS2017), Beijing, China, November 1-3, 2017
4. Yue Gao, Jinting Jiu, Chuantong Chen, Toshiyuki Ishina, Tohru Sugahara, Shijo Nagao, and Katsuaki Suganuma, “Enhancing Bonding Property of Cu Particles Paste

- by Adding Organic Acid”, MS&T2017, Pittsburgh, Pennsylvania, USA, October 8-12, 2017
5. Yue Gao, Jinting Jiu, Shijo Nagao, and Katsuaki Suganuma, “High strength Cu joints using ascorbic acid-treated copper paste and their degrade behavior during aging” 161th annual meeting of the Japan Institute of metal and materials, Hokkaido, Sapporo, Japan, September 6-8, 2017
  6. 高悦、酒金亭、菅沼克昭, “有機酸添加 Cu 粒子ペーストによる耐熱焼結接合” 第 27 回 マイクロエレクトロニクスシンポジウム 秋季大会 (MES2017), 2017 年 8 月 29 日-8 月 30 日、中京大学名古屋キャンパス
  7. 高悦、酒金亭、石名敏之、長尾至成、菅沼克昭 “” 第 31 回エレクトロニクス実装学会春季講演大会(JIEP); “有機酸処理による銅粒子ペーストの低温接合” 慶應義塾大学・矢上キャンパス, 2017 年 3 月 6 日-3 月 8 日



## Acknowledgements

I would like to appreciate continuous encouragement, help and support from many people. First, the great thanks go to my supervisor Prof. Katsuaki Suganuma. He opened the window for me to the world of high-power devices and printed electronics. I would like to express my sincere gratitude for his continuous support, patience, motivation, enthusiasm, and immense knowledge.

Besides my advisor, I would like to thank the rest of my thesis committee: Prof. Hiroshi Nishikawa, Prof. Shijo Nagao and Prof. Tohru Sugahara, for their invaluable advice and encouraging comments.

I am grateful to Dr. Jinting Jiu and Dr. Chuantong Chen, who's out of the way help and guidance helped me during research work. I also would like to thank Dr. Cai-fu Li, Dr. Hao Zhang and Dr. Yosufu Ekubara for their invaluable advices and encouragement. I am also thankful to all other laboratory members for their invaluable advice, constant help, encouragement, inspiration and blessings.

I am also indebted to my senior research colleagues, Dr. Wanli Li, Dr. Seungjun Noh, Dr. Semin Park, Dr. Hao Zhang, Dr. Su Ding, Dr. Chunhui Wu, Dr. Zhenghong Wang, and Dr. Chun Pei for their useful discussion and great friendship and for their unconditional support and constant motivation whenever needed. I am very grateful to all my fellow research colleagues as well as friends Mr. Zheng Zhang, Mr. Guiming Liu, Ms. Bowen Zhang, Ms. Haoran Ding, Mr. Dawei Hu, Ms. Linying Li and Mr. Shuhei Takata who have given me their friendship, put up with my odd hours, and provided me with lifts and practical help.

Last but not the least, I would like to thank my dear parents for their support.